Spring 5-8-2021

Role Of Endocytic Machinery Regulators in EGFR Traffic and Viral Entry

Insha Mushtaq
University of Nebraska Medical Center

ROLE OF ENDOCYTIC MACHINERY REGULATORS IN EGFR TRAFFIC AND VIRAL ENTRY

By

Insha Mushtaq

A DISSERTATION

Presented to the Faculty of

The University of Nebraska Graduate College

In Partial Fulfillment of the Requirements

For the Degree of Doctor of Philosophy

Pathology and Microbiology

Graduate Program

Under the Supervision of Professor Hamid Band, M.D., Ph.D.

University of Nebraska Medical Center

Omaha, Nebraska

May 2021

Supervisory Committee:

Rakesh Singh, Ph.D. Erika Boesen, Ph.D.

Amarnath Natarajan, Ph.D. Kaustubh Datta, Ph.D.

Additional Final Oral Examination Committee Member:

Siddappa Byrareddy, Ph.D.

Acknowledgements

I am thankful to Allah for me giving me wisdom, courage, guidance, and patience which helped me to come this far in the pursuit of learning. All praise and thanks to Allah for granting me an inquisitive nature and to his messenger Mohammed S.A.W. for presenting an ideal example to carry the life.

With immense pleasure and gratitude, I would like to thank my advisor Dr. Hamid Band for his constant guidance, mentorship, and support. I greatly appreciate him for believing in me with incredible patience, constructive criticism, and endless encouragement. Numerous interesting and thought-provoking discussions with Dr. Band have always motivated me to seek perfection and maturity in my scientific thinking and temperament. He has been everything I could have hoped for in an advisor, and more.

I would like to thank the members of my supervisory committee, Dr. Rakesh Singh, Dr. Amarnath Natarajan, Dr. Erika Boesen, Dr. Kaustubh Datta and Dr. Byrareddy (additional final oral examination committee member) for their valuable insights, suggestions, and constant support. Positive discussion and feedback from my supervisory committee is an indispensable part of my research work and has been pivotal for my development as a researcher.

I would like to thank current and former members of the Band lab for their help and support. They have always been enthusiastic whether I needed to discuss some or cheers or anything you want. Special thanks to Dr. Bhopal Mohapatra for his hand-to-hand help when I started in the lab. I appreciate his kindness and help, without which the road would have been much more difficult in the beginning. Also, I would like to thank Matthew D Storck for always being helpful.

I would like to present a humble gratitude and thanks to my family for their unconditional support and understanding for all these years. Specially, I would like to extend my heartfelt appreciation to my parents- Aamina Akhter and Mushtaq Ahmad Bandh and sisters- Navreen and Zainab, for their constant encouragement throughout my life. My family has always inspired me to follow my dreams. I would also like to thank my family in Omaha, Nebraska for making my graduate student life easier and special thanks goes to my Aunt- Vimla Band and cousin- Romana Bhat for their love and care. I would also like to thank my in-laws for their love, support, and applause. Last but not the least, I would also like to thank my husband Zahoor Ganie, for his unconditional love and support.

I dedicate my thesis to my Mom and Dad for giving me the best education they could.

Abstract

ROLE OF ENDOCYTIC MACHINERY REGULATORS IN EGFR TRAFFIC AND VIRAL ENTRY

Insha Mushtaq

University of Nebraska, 2021

Supervisor: Hamid Band, M.D., Ph.D.

STUDY 1: ROLE OF ENDOCYTIC REGULATOR EHD1 AND ITS BINDING PARTNER RUSC2 IN EGFR TRAFFIC

Abstract

Epidermal growth factor receptor (EGFR) is a prototype receptor tyrosine kinase and an oncoprotein in many solid tumors. Cell surface display of EGFR is essential for cellular responses to its ligands. While post activation endocytic trafficking of EGFR has been well elucidated, little is known about mechanisms of basal/pre-activation surface display of EGFR. Here, we identify a novel role of the endocytic regulator EHD1 and a potential EHD1 partner, RUSC2, in cell surface display of EGFR. EHD1 and RUSC2 colocalize with EGFR in vesicular/tubular structures and at the Golgi compartment. Inducible EHD1 knockdown reduced the cell surface EGFR expression with accumulation at the Golgi compartment, a phenotype rescued by exogenous EHD1. RUSC2 knockdown phenocopied the EHD1 depletion effects. EHD1 or RUSC2 depletion impaired the EGF-induced cell proliferation, demonstrating that the novel, EHD1- and RUSC2-dependent transport of unstimulated EGFR from the Golgi compartment to the cell surface that we describe is functionally important, with implications for physiologic and oncogenic roles of EGFR and targeted cancer therapies.

STUDY 2: ROLE OF CLATHRIN-MEDIATED ENDOCYTOSIS REGULATOR AAK1 IN SARS-CoV-2 ENTRY INTO HOST CELLS

Abstract

The immune system of human populations is naïve towards the newly-emerged Severe Acute Respiratory Syndrome Coronavirus-2 (SARS-CoV-2). Combined with the high transmission rate and a huge burden of morbidity and mortality among patients, Coronavirus disease (COVID-19) has led to enormous healthcare and economic emergency worldwide. SARS-CoV-2 uses its spike (S) protein to bind to the cell surface receptor Angiotensin-Converting Enzyme 2 (ACE2). The first step in subsequent viral infection is the entry of the virus-receptor complex into the target cell through endocytosis. Most viruses use the endocytic pathways to deliver viral contents into the host cell. Among them, the most used pathway is clathrin-mediated endocytosis. It has been shown that SARS-CoV, a close relative of SARS-CoV-2, uses the clathrin-mediated endocytosis for entry into acidic endosomes where viral envelope to cell membrane fusion takes place. Thus, we posited that SARS-CoV-2 also utilizes the same mechanism to enter the host cells. Studies of non-coronavirus systems have shown that AP2 adaptor-associated kinase AAK1 functions as a key positive regulator of clathrin-mediated viral endocytosis by phosphorylating the mu subunit of Adaptor protein 2 complex (AP2M1). Here, we modeled the SARS-CoV-2 entry into host cells using the receptor-binding domain of the viral Spike protein (S-RBD) and used a combination of genetic and pharmacological approaches to test a hypothesis that AAK1 is required for the endocytosis of SARS-CoV-2. We found that genetic knockdown of AAK1 with siRNA reduced the internalization of S-RBD, suggesting a role for AAK1 in the entry of SARS-CoV-2 into host cells. Towards a chemical inhibitor approach to determine the role of AAK1 in SARS-CoV-2 entry into host cells, we employed AAK1 specific inhibitors and clinically-used drugs that have emerged to have an AAK1 inhibitory activity. In all analyses of chemical inhibitors, we used their

ability to reduce the AP2M1 phosphorylation as a readout of AAK1 inhibitory activity to build dose responses. The dose-response analyses showed that while all the inhibitors tested had AAK1 inhibitory activity, only the specific AAK1 inhibitors LP-935509 and LP-922761 and the anticancer agent Sunitinib among the clinically-used drugs displayed AAK1 inhibitory activity at low concentrations. Accordingly, Sunitinib, and the AAK1 specific inhibitors LP-935509 and LP-922761 exhibited a dose-dependent inhibition of the SARS-CoV-2 S-RBD internalization into host cells. These genetic and pharmacological approaches suggest the requirement of AAK1 in the entry of SARS-CoV-2 and provide an insight into the mechanism of viral entry by regulating the clathrin-mediated endocytic machinery. These studies support the potential of AAK1 inhibition as an approach to thwart SARS-CoV-2 infection.

Table of Contents

Acknowledgements i
Abstract iii
Table of Contents vi
List of Abbreviations viii
Chapter 1: Introduction 1
1.1. Modes of endocytosis 27
1.2. Endocytic trafficking and membrane receptors 28
1.3. The EHD family of endocytic traffic regulators 29
1.4. Viruses and endocytic trafficking 37
1.5. Regulators of clathrin-mediated endocytosis of viruses 39
1.6. SARS-CoV-2: A novel coronavirus 43
1.7. Figures 50
Chapter 2: Role of endocytic regulator EHD1 and its binding partner RUSC2 in EGFR traffic (Published Paper) 38
2.1. Introduction 41
2.2. Materials and Methods 46
2.3. Results 54
EHD1 KD reduces the total EGFR levels on 16A5 MECs both under steady-state and ligand-free culture. 54
EHD1 knockdown reduces the cell surface EGFR levels on 16A5 mammary epithelial cells under ligand-free culture. 56
EHD1 and EGFR colocalize in intracellular vesicular structure. 57
EHD1 knockdown results in EGFR retention in the Golgi apparatus. 59
EHD1 knockdown reduces the EGF-dependent cell proliferation. 60
RUSC2 is a novel potential EHD1 partner that colocalizes with EGFR at the Golgi compartment. 61
RUSC2 knockdown phenocopies the effects of EHD1 depletion on basal, unstimulated EGFR expression. 62
2.4. Figures 63
2.5. Discussion 82
Chapter 3: Role of clathrin-mediated endocytosis regulator AAK1 in SARS-CoV-2 entry into cells 89
3.1. Introduction 90
3.2. Material and Methods 91
3.3. Results 98

The system for studying SARS-CoV-2 internalization in Biosafety level I/II Lab..... 98
Characterization of endogenous or ectopically-expressed ACE2 expression levels in various cell lines. 100
Specific surface binding of S-RBD to ACE2 on target cells. 100
Surface-bound SARS-CoV-2 S-RBD is internalized in a time-dependent manner. 101
AAK1 plays a role in SARS-CoV-2 internalization. 102
Pharmacological inhibition of AAK1 reduced or inhibited internalization of S-RBD. 104
3.4. Figures 106
3.5. Discussion 139
Chapter 4: Bibliography..... 145

List of Abbreviations

AAK1	Adaptor-associate protein kinase 1
ACE2	Angiotensin converting enzyme 2
AP2	Adaptor protein 2
CCP	Clathrin-coated pits
CCV	Clathrin-coated vesicles
CME	Clathrin-mediated wndocytosis
COVID-19	Coronavirus disease-19
Dox	Doxycycline
EE	Early endosome
EGF	Epidermal growth factor
EGFR	Epidermal growth factor receptor
EHD	EPS15 homology domain containing proteins
EH-Domain	EPS15 homology domain
ERC	Endocytic recylcing compartment
FP	Fusion peptide
GAK	Cyclin G associate kinase
GFP	Green fluorescent protein
HCV	Hepatitis C virus
HR	Heptapeptide repeats
KD	Knockdown
LE	Late endosome
MERS-CoV	Middle East respiratory syndrome coronavirus
MHC-1	Major histocompatibility complex class
ORF	Open reading frame

PDGF	Platelet derived growth factor
RBD	Receptor Binding Domain
RME-1	Receptor-mediated endocytosis
RTK	Receptor tyrosine kinase
SARS	Severe acute respiratory syndrome
SARS-CoV-2	Severe acute respiratory syndrome coronavirus-2
S-RBD	Spike receptor binding domain
TGF	Transforming growth factor
TM	Transmembrane domain
TNG	Trans-Golgi network
UTR	Untranslated region

Chapter 1: Introduction

Overview of endocytosis and endocytic trafficking

Endocytosis is the cellular process that brings materials from outside to inside the cell in vesicles which after budding off from the cell membrane are transported to various intracellular locations to help in the intracellular traffic of the cargo components.

1.1. Modes of endocytosis

The major forms of endocytosis include phagocytosis, pinocytosis, macropinocytosis, caveolae-mediated endocytosis, clathrin-mediated endocytosis, and caveolae and clathrin-independent endocytosis (Doherty, McMahon 2009) (Fig. 1.1).

Phagocytosis is the process by which larger extracellular particles are engulfed and brought into the cell. For example, this process is used by macrophages to bring in and degrade bacteria and various other microbes (Flannagan, Jaumouille et al. 2012).

Macropinocytosis is like phagocytosis, but it is non-specific in cargo selection. It helps bring in large quantities of extracellular fluid and membrane (Lim, Gleeson 2011).

Caveolae-mediated endocytosis helps in the internalization process by forming inward bulb-like invaginations called caveolae (or little caves) enriched in glycosphingolipids (Pelkmans, Helenius 2002).

Clathrin-mediated endocytosis (CME) is the well-characterized mode of entry of molecules into the cells. In CME, clathrin serves as the major protein which makes the lattice-like coat around the vesicles (McMahon, Boucrot 2011). Clathrin forms a triskelion structure that is composed of three heavy chains and three light chains. Clathrin itself cannot bind to cargo, instead, it uses a wide variety of adaptor protein complexes (e.g., Adaptor protein 2 (AP2)) and accessory proteins, which recognize specific sequences in cytoplasmic domains of plasma membrane proteins. The adaptor protein complexes and

clathrin make a polyhedral lattice around the vesicles, which are thus known as clathrin-coated vesicles (CCVs). CCVs are present in almost all cells and start as plasma membrane domains known as clathrin-coated pits (CCPs). During CME, the cargo is translocated into CCPs, followed by invagination, and pinching off the CCVs from the plasma membrane, mediated by the recruitment of GTPase protein dynamin (Mukherjee, Ghosh et al. 1997). After pinching off, the clathrin coat is disassembled, and cargo is transported to other locations by various molecular motors. For example, CME helps in the endocytosis of ligand-occupied growth factor receptors and antibodies bound to cell surface antigens (Marsh, McMahon 1999) (Fig. 1.2).

Regardless of the mode of entry, endocytosed cargo is delivered to the early endosome/sorting endosome, where the cargos are further sorted for traffic to different destinations. From the early endosome/sorting endosome, the cargo can go to the late endosomes, or lysosomes for degradation, the trans-Golgi network (retrograde transport), or recycling endosomes where from the cargo is recycled back to the plasma membrane. The recycling takes either a fast route back or a slow route through the endocytic recycling compartment (ERC) (Fig. 1.3).

1.2. Endocytic trafficking and membrane receptors

Many cellular activities are controlled by cell surface receptors, such as transporters, growth factor receptors, surface-associated enzymes, cell adhesion proteins, etc. Their levels at the cell surface are regulated by endocytic traffic. These receptors, either basally or after binding to ligands, undergo internalization and traffic through a series of vesicular compartments. The endosomal delivery of cargo to the lysosome typically destines such materials for degradation by lysosomal enzymes. The endosomal recycling pathways return the internalized components back to the plasma membrane and help maintain the cell type-specific levels of receptors and membrane

components on the cell surface. The plasma membrane composition is maintained by a balance between endocytic uptake, degradation, and recycling. Besides the role of endocytosis in the internalization of cargo and maintenance of cell surface receptor levels, it is also important to maintain the lipid composition of intracellular compartments and plasma membrane. Endocytic trafficking is crucial for growth factor-mediated cellular activation, neurotransmission, and other cell-cell and cell-environment communications (Guichet, Wucherpfennig et al. 2002, Oved, Yarden 2002, Sorkin, Von Zastrow 2002). Given the fundamental roles of endocytic traffic in intracellular transport processes, especially the trafficking of materials from the plasma membrane to the inside of cells, it is no surprise that endocytic traffic has emerged as a key target of research in many areas of cell biology, including drug delivery and mechanisms of viral entry into host cells.

Traffic along the different routes is regulated by several protein families, a major one being the Rab-GTPases. For example, early/sorting endosome traffic is regulated by Rab5, fast recycling involves Rab4, slow recycling involves Rab11, and late endosome/lysosome traffic involves Rab7 (Vanlandingham, Ceresa 2009, Meresse, Gorvel et al. 1995, Ullrich, Reinsch et al. 1996, Daro, van der Sluijs et al. 1996, van der Sluijs, Hull et al. 1992, Bucci, Parton et al. 1992, Gorvel, Chavrier et al. 1991). Many other families of endocytic traffic regulators have also been characterized (Salminen, Novick 1987, Schmitt, Wagner et al. 1986, Touchot, Chardin et al. 1987). The two protein families which are the interest of our lab are EHD1 protein family and AAK1 kinase protein family.

1.3. The EHD family of endocytic traffic regulators

The EPS15 Homology Domain-containing (EHD) proteins, are a conserved family of four highly homologous members having an EH domain at their C-termini in contrast to the N-terminal domain organization of typical EH domain proteins (EPS15, Intersectin,

Reps1 and 2, and others) (Miliaras, Wendland 2004). One of the study about EHD1 showed it is involved in the recycling of transferrin in mammalian cells, and shares nearly 70% identity with its lone *Ceanorhabditis elegans* ortholog Receptor-Mediated Endocytosis (RME-1) whose knockdown or in isolated mutants showed yolk protein uptake defects into oocytes from endocytic vesicles which suggested its role in regulating membrane trafficking (Grant, Zhang et al. 2001, Lin, S. X., Grant et al. 2001). The members of EHD family in mammals share 67% or more homology with each other having an N-terminal helical region and nucleotide binding G-domain, followed by a linker region, a lipid binding coiled-coil domain and the C-terminal EH domain (Fig. 1.4). Each EHD family member has a single module of proline-phenylalanine following a variant residue (X-P-F) situated within the G-domain, with the exception of EHD2 which has two. Mutagenesis studies revealed a critical role for this motif in regulating the hetero-dimerization, protein-protein interactions, and intracellular localization of the various EHDs (Naslavsky, Caplan 2011, Bahl, Naslavsky et al. 2015). The EHD G-domain structurally resembles the GTPase dynamin but exhibits a preference for ATP binding. It has been shown that the intrinsic ATPase activity allows EHD1 to function in a manner similar to dynamin and coordinates dynamin-dependent budding of synaptic vesicles in cooperation with amphiphysin (Daumke, Lundmark et al. 2007, Jakobsson, Ackermann et al. 2011).

The EH domain was identified as an evolutionary conserved domain in eukaryotes in the EGFR pathway substrate 15 (EPS15) (Wong, Schumacher et al. 1995). The EH domain is typically 70-100 amino acids in length and comprised of two helix-loop-helix 'EF hands' connected by an antiparallel βsheet. This motif forms a conserved binding pocket for the tripeptide asparagine-proline-phenylalanine (NPF). Many EH-domain containing proteins are shown to interact with key components of endocytosis including dynamin, the clathrin adapter AP-2, actin and ubiquitin (Santolini, Salcini et al. 1999). Thus, a network

of EH proteins are thought to act as molecular scaffolds involved in protein sorting and transport (Miliaras, Wendland 2004). Eps15 is known for localizing to clathrin-associated endocytic pits after receptor tyrosine kinase (RTK) stimulation but is not seen at early endosomes. Recent data indicates it has a function in regulating formation of the clathrin coat and through its ubiquitin-interacting motif, has a role in regulating internalization of surface proteins, among them: Connexin43, AMPA-type glutamate receptors and EGFR (Girao, Catarino et al. 2009, Lin, A., Man 2014, Carbone, Fre et al. 1997). EPS15 was found to be phosphorylated after stimulating cells with epidermal growth factor (EGF) or transforming growth factor- α (TGF-α), but not after platelet derived growth factor (PDGF) or insulin, although in each case it redistributed to clathrin pits following stimulation. Its overexpression was shown to be sufficient to transform NIH 3T3 fibroblasts further suggesting a role in mediating signal transduction (van Delft, Schumacher et al. 1997, Fazioli, Minichiello et al. 1993). Roles in clathrin-independent internalization and the recycling of EGFR have also been identified (Sigismund, Woelk et al. 2005, Chi, Cao et al. 2011).

***In-vitro* roles of EHDs:** EHDs localize to tubular-membranes and vesicular compartments. In case of EHD1 the tubular distribution requires the EH domain for mediating an interaction with phosphotidylinositols (Naslavsky, Rahajeng et al. 2007). EHDs have been shown to play a critical role in the regulation of endocytic recycling of a number of surface proteins. The best characterized member is EHD1, which has a role in mediating transport from the ERC back to the plasma membrane for the transferrin receptor and integrins and its knockdown leads to phenotypes of intracellular accumulation of cargo (Rotem-Yehudar, Galperin et al. 2001, Jovic, Naslavsky et al. 2007).

A role for EHD1 in mediating endosomal transit from early endosomes to the ERC has been suggested based on findings of impaired recruitment to enlarged early endosomes upon ablation of Connecdenn, a Rab35 guanine exchange factor whose knockdown interfered in the normal recycling of MHCI (Allaire, Marat et al. 2010), and II (Walseng, Bakke et al. 2008). Finally, similarity in phenotypic defects observed in Caenorhabditis elegans for yolk protein uptake in mutants of an orthologous DENN domain-containing regulator of Rab35 closely resembles loss of RME-1 (Sato, Sato et al. 2008).

A role for EHD members has also been described in retrograde traffic. EHD1 was shown to colocalize with vacuolar protein sorting (Vps) 26 and 35, members of the retromer cargo recognition sub-complex, part of a critical evolutionarily conserved hub for sorting molecules bound for transit back to the Golgi. The retromer sorting nexin complex forms SNX-1 positive tubules during the early endosome to late endosome transition, an activity required for the diversion of substrate fate away from lysosomal degradation and into recycling (Mari, Bujny et al. 2008). EHD1 is required for the cation-independent mannose-6-phosphate receptor trafficking from the recycling endosome to the Trans Golgi Network through an interaction required for the stabilization of SNX1-positive tubule formation (Gokool, Tattersall et al. 2007, Zhang, Reiling et al. 2012). A recent report from another group saw no such requirement using a chimeric CI-M6PR featuring the ectodomain of CD8 and the cytoplasmic tail of the CI-M6PR (McKenzie, Raisley et al. 2012).

EHD2, like the other EHD family members has a role in regulating the surface presentation of proteins on the plasma membrane. Similar to EHD1, EDH2 interacts with clathrin adapter proteins. In cultured adipocytes, EHD2 couples the endocytosis to actin cytoskeleton through binding to NPF motif of EHD2-binding protein 1 (EHBP1), which

contains an actin-binding calponin homology domain. This interaction is required for endocytosis of transferrin and GLUT4 into EEA1-positive endosomes. Further insulin treatment significantly increased the co-immunoprecipitation of EHD2 with GLUT4 suggesting a role in the mobilization of glucose transporters to the plasma membrane (Guilherme, Soriano, Bose et al. 2004, Park, Ha et al. 2004). EHD1 was shown to interact with IGF1 receptor and colocalized with activated IGF1R in endocytic vesicles (Rotem-Yehudar, Galperin et al. 2001).

EPS15 and CALM both undergo nuclear-cytoplasmic shuttling and all four EHD family members were identified as containing a bipartite nuclear localization signal. Inhibition of nuclear exit with leptomycin B was only successful at demonstrating accumulation of EHD2, where it displayed activity as a co-repressor of the p21WAF1/Cip1 gene. EHD2 was shown to co-immunoprecipitate with Sumo1 and mutagenesis of a sumoylation consensus site (also present in all EHD members) caused nuclear accumulation. A putative nuclear export signal present in all EHD members was seen as a partial contributor (Pekar, Benjamin et al. 2012). EHD3 has been shown by the same group to undergo sumoylation and this modification is required for its localization to tubular membranes but not for its dimerization, and a sumoylation defective mutant delayed transferrin recycling from the ERC (Cabasso, Pekar et al. 2015). Interestingly EHD3 is the closest EHD1 homolog and binds similar effectors Rabenosyn-5, RCP and MICAL-L1 through their NPF motifs, however, EHD3 had not previously been implicated as having a role in regulating the exit of recycling cargo back to the plasma membrane. EHD3 knockdown instead displayed an impaired exit of transferrin from early endosomes and caused a redistribution of both Rab11 and RCP from the interior to the cell periphery (Naslavsky, Rahajeng et al. 2006).

EHD3 was demonstrated as necessary for transport of cargo to the Golgi and required for the maintenance and function of this organelle. The retrograde trafficking of mannose-6- phosphate receptor is essential for the export of lysosomal hydrolases. Knockdown of EHD3 or its effector Rabenosyn-5 caused mannose 6-phosphate receptor to remain in peripheral endosomes, resulting in accumulation of lysosomal hydrolase Cathepsin D. An impairment of endosome-to-Golgi movement was also seen for ShigaToxin B, SNX1, and AP-1 gamma adaptin (a mediator of mannose 6-phosphate receptor retrieval). Overall, the disruption of return traffic caused Golgi morphology to appear dispersed and fragmented; however, no defects in secretion were detected upon transfection of VSV-G-GFP

EHD4, like the other EHDs, requires its EH domain for localization to the tubular endosomal system. EHD4 colocalizes with markers for the early endosome, sorting nexins and newly internalized transferrin. Its knockdown caused the formation of enlarged early endosomes and prevented the transport of MHCI to the perinuclear ERC and prevented the exogenous low-density-lipoprotein from reaching the lysosomal compartment. An overexpressed Rab5-binding domain from Rabaptin-5, which binds preferentially to the active conformation of GTP–Rab5, demonstrated the enlarged endosomal structures are enriched for GTP-loaded activated Rab5. This may suggest a defect in the ability to recruit the next sequential component required for GTP hydrolysis and vesicle budding or transit out of the early endosome (Sharma, Naslavsky et al. 2008).

The nerve growth factor NGF binds its RTK TrkA at the nerve terminal and is unique in the sense that it avoids the typical itineraries of recycling and degradation and instead undergoes long-distance retrograde transport to the nerve cell body, and the signaling events that occur en-route are necessary for the growth and survival of the cell. It was immediately suggested signaling events generated intracellularly within endosomes

have the capacity to be qualitatively different than those signals generated at the plasma membrane (Watson, Heerssen et al. 2001). Indeed, in the PC12 cell model, NGF acting through TrkA effectors, including Ras, Rap, and the Erk/MAP kinases mediate sustained signaling events, while the EGFR acting through the same MapK pathway generates only transient signals and may explain the inability of EGFR to mediate differentiation of neuronal phenotype and survival (Valdez, Philippidou et al. 2007). The Trk signaling endosome is formed by concentrating the receptor within membrane ruffles, a process termed 'macro-endocytosis', and mediated by the Rho-GTPase, Rac, as well as EHD4 (referred to in the neuronal system literature as Pincher) (Shao, Akmentin et al. 2002). EHD4 is shown to be essential for the retrograde traffic of activated TrkA and is a transcriptional target of neurotrophin signaling through this receptor (Valdez, Akmentin et al. 2005). In contrast to Trk, the EGFR is not internalized by the same EHD4-dependent mechanism in this system. Further, TrkA endosomes were seen to remain Rab5 positive for longer whereas EGFR endosomes rapidly exchange Rab5 for Rab7, thereby moving into late-endosomes/lysosomes for degradation. Therefore, one mechanistic determinant of EHD4-mediated retrograde traffic is the ability to maintain 'immature' early endosomal character whereby the transition to Rab7 positive late endosomes/early lysosomes is prevented. This is consistent with data where EHD4 knockdown was seen to result in enlarged early endosomes and indicates EHD4 may be required to chaperone early endosomal cargos in the transition towards divergent character (Sharma, Naslavsky et al. 2008).

***In-vivo* roles of EHDs:** Ehd1-null mice are born at sub-Mendelian ratios exhibiting embryonic lethality, in part due to defects in the closure of the neural tube. Surviving pups are smaller in size through adulthood, infertile, and display a range of spermatogenic defects resulting from disruption of spermatogenesis with abnormal acrosomal

development with clumping of acrosomes, and round, misaligned spermatids missing normal elongation (Rainey, George et al. 2010). Over half of surviving Ehd1-null mice display ocular abnormalities, including anophthalmia, aphakia, microphthalmia and congenital cataracts. These phenotypes appear to be the result of reduced lens epithelial proliferation, survival, defects in corneal endothelial differentiation and impaired maintenance of cell junctions (Arya, Rainey et al. 2015).

EHD2 knockout mouse has only recently been developed and is currently undergoing characterization in the laboratory. A previous report has indicated expression in the mouse brain, heart, lungs, mammary gland, and spleen (George, Ying et al. 2007). Future studies will focus on the developmental role of EHD2 and its characterization in these organs. It has been shown loss of EHD2 leads to disregulation of the lipid storage capacity (Matthaeus, Lahmann et al. 2020). The detachment of caveolae due to EHD2 removal results in reduced calcium entry and lack of activated eNOS and NO generation in endothelial cells which leads to reduced blood vessel relaxation in EHD2 knockout mice and reduced running wheel endurance (Matthaeus, Lian et al. 2019).

EHD3 is expressed in cardiac muscle and participates in the trafficking of the sodium calcium ion exchanger (NCX1) to the cell membrane, and thus it has a role in regulating electrical potentiation of the heart. Both EHD3 and NCX1 have elevated expression levels in models of heart failure (Gudmundsson, Curran et al. 2012, Curran, Makara et al. 2014). EHD3 is also predominantly expressed in the glomerular endothelial cells of the kidney but its deletion had no obvious effect on function. Interestingly EHD3-knock out cells see an increase of the expression of EHD4, and a double EHD3/4 knock out results in death between 3-24 weeks of age. These mice display small pale kidneys, proteinuria, thrombotic lesions, thickening and duplication of glomerular basement membrane, endothelial swelling and loss of fenestrations (George, Rainey et al. 2011).

Knockouts of EHD4 display a 50% reduced testis size and feature increased germ cell proliferation and apoptosis. A reduction in seminiferous tubule diameter, and dysregulation of seminiferous epithelium was observed. Like EHD1, EHD4-knockout mice display similar defects in elongated spermatids and reduced fertility. EHD4 deletion altered the expression profile of other 3 EHD members indicating a role for regulatory balance or functional redundancy (George, Rainey et al. 2010).

1.4. Viruses and endocytic trafficking

A variety of pathogens infect humans and animals. Viruses are responsible for numerous devastating acute and chronic diseases in humans. Viruses have no metabolic systems of their own and thus act as obligate intracellular pathogens, using the host cells for replication, viral assembly, and budding and other aspects of viral pathogenesis. They use the host endocytic machinery to reach the intracellular sites where they introduce their genomes into the cytosol for replication in specific subcellular sites. They commonly exploit the endocytic organelle network for assembly following replication of their genomes and expression of structural genes (Cossart, Helenius 2014).

The entry of a viral particle into the host cell occurs in a stepwise manner. It first attaches to the cell surface typically by binding to cell surface receptors, leading to the activation of signaling pathways. In most cases, virus-receptor complexes are incorporated into endocytic vesicles and delivered to early endosomal compartments where sorting occurs to direct the virus to a location where virus material is finally released into the cytosol. Within the endocytic system, viruses are exposed to changing conditions, including a drop in pH during the maturation process of endocytic compartments/viral vacuoles, which in many cases provide a cue to activate penetration (Helenius, Kartenbeck et al. 1980). The protease exposure and processing of viral proteins are

important for some viruses because it helps them in penetration and uncoating mechanisms (Danthi, Guglielmi et al. 2010, Hunt, Lennemann et al. 2012, Kubo, Hayashi et al. 2012). The enveloped viruses fuse their envelope with membranes of internal organelles and avoid exposure of their glycoproteins on the cell surface which helps them to delay detection by immune surveillance.

The endocytosis of viruses occurs at variable rates and with different degrees of efficiency. The internalization process can take from a few minutes to several hours after binding to the cell surface. Viruses take advantage of the host machinery by binding directly or indirectly to host factors and leading to either activation or modification of the host system for their specific purposes.

The endocytic processes by which viruses are internalized include micropinocytosis, clathrin-mediated endocytosis, caveolae-mediated endocytosis, and clathrin- and caveolin-independent mechanisms (Gilbert, Goldberg et al. 2003, Damm, Pelkmans et al. 2005, Anderson, Chen et al. 1996, Stang, Bakke 1997, Swanson, Watts 1995). The widely studied and most common trafficking process in the case of small and medium-sized viruses is clathrin-mediated endocytosis (Helenius, Kartenbeck et al. 1980, Matlin, Reggio et al. 1981, DeTulleo, Kirchhausen 1998, Sun, He et al. 2013). Clathrin-mediated internalization of the virus is so prevalent that viruses fused with fluorescent tags are often used as one of the tools to study key factors of CME, such as cargo size (Ehrlich, Boll et al. 2004). Upon the virus binding to its receptor, clathrin-mediated endocytosis is activated and induces the binding of an adaptor protein complex to the cytoplasmic domain of the receptor. During this early process, the AP2M1 component of the AP2 complex is phosphorylated by adaptor-associated kinase AAK1 (Ricotta, Conner et al. 2002) (Fig. 1.5). AP2M1 phosphorylation enhances the adaptor protein binding to clathrin, and together with other accessory machinery, the clathrin-coated pits are formed. AAK1

thus functions as a key positive regulator of clathrin-mediated endocytosis. The CCVs are pinched off from the plasma membrane with the help of scission proteins leading to the release of endocytic vesicles from the plasma membrane (Mukherjee, Ghosh et al. 1997) (Fig. 1.5). From the endocytic vesicle, the viral content gets delivered to early endosomes. Structural modifications of the viral surface proteins are induced by the endosomal pH and/or binding to the receptor, leading to genome penetration into the cytoplasm to carry forward the further steps in the life cycle of a virus.

1.5. Regulators of clathrin-mediated endocytosis of viruses

Adaptor Proteins: Clathrin-mediated endocytosis depends on oligomeric clathrin and adaptor protein complexes (Conner, Schmid 2003a, Conner, Schmid 2003b), coordinating the specific recruitment and assembly of clathrin into a polyhedral lattice at the plasma membrane, as well as its coupling to endocytic cargo (Brodsky 2012). One of the well-studied adaptor protein complexes, a major component of clathrin-coated vesicles at the plasma membrane, is the multimeric adaptor protein 2 complex (Owen, Collins et al. 2004). AP2 is a hetero-tetrameric complex consisting of two large subunits, the alpha (AP2A1) and beta (AP2B1) adaptins, a medium subunit mu (AP2M1), and the small sigma adaptin (AP2S1). The mu and beta subunits mediate cargo binding, the sigma subunit helps in membrane binding, and the alpha subunit binds to accessory proteins (Owen, Collins et al. 2004, Ohno 2006, Ohno, Stewart et al. 1995, Pearse 1988, Boll, Ohno et al. 1996). The mu subunit is essential for clathrin-mediated endocytosis. AP2M1 recognizes tyrosine- or dileucine-based sorting signals, also known as internalization signals, within the cytoplasmic domains of transmembrane receptors to facilitate the internalization of cargo (Owen, Collins et al. 2004, Ohno 2006, Ohno, Stewart et al. 1995, Pearse 1988, Boll, Ohno et al. 1996)

AAK1 kinase Protein family of endocytic regulators: The Prk/Ark family of Ser/Thr protein kinases functions during receptor-mediated endocytosis. This family consists of four mammalian homologs: cyclin-G-associated kinase (GAK), adaptor-associated kinase 1 (AAK1), BMP-2-inducible kinase (BIKE), and myristoylated and palmitoylated serine/threonine kinase 1 (MPSK1; also referred to as STK16). Members of this family are known to regulate endocytosis through phosphorylation of endocytic pathway components. The family members are quite diverse in their function and structure, with only 30% sequence identity in their kinase domain and only a little conservation in their other domains (Smythe, Ayscough 2003).

AP-2-Associated protein kinase 1 (AAK1) is encoded by the *AAK1* gene located on human chromosome 2 and mouse chromosome 6. The major forms of AAK1 are a 961 amino acid full-length polypeptide and an 863 amino acid isoform generated by alternative splicing. Both isoforms are similar in their kinase activity (Henderson, Conner 2007). AAK1 consists of the N terminal kinase domain and a clathrin-binding domain near the C terminus. AAK1 has been well established to play a positive role in clathrin-mediated endocytosis (Conner, Schmid 2002) by promoting clathrin assembly and interaction with the membrane-bound receptors and facilitating the recruitment of endocytic factors like adaptor proteins and various other accessory factors. AAK1 interacts with and phosphorylates AP2M1 at T156 residue, promoting the binding of AP-2 complex to sorting signals found in membrane receptors and leads to receptor endocytosis (Ricotta, Conner et al. 2002). Its kinase activity is stimulated by clathrin which ensures that AP-2 binds with high affinity to the cargo during the internalization process (Ricotta, Conner et al. 2002, Henderson, Conner 2007).

Functional roles of AAK1: Previous studies have found AAK1 to be broadly expressed in different cell types and participate in numerous functions. Inhibition of the

yeast homolog of AAK1 (Prk1p) impaired the pheromone receptor endocytosis (Sekiya-Kawasaki, Groen et al. 2003). AAK1, by promoting the endocytosis of the active Notch receptor into endosomes, was found to enhance Notch signaling (Gupta-Rossi, Ortica et al. 2011). AAK1 phosphorylates numb which is thought to be important for promoting the maturation of coated pits (Sorensen, Conner 2008). AAK1 function modulates the distribution of numb within the cells (Sorensen, Conner 2008). AAK1 promotes the recycling of alphav-beta3 integrin from endosomes to the cell surface and its depletion impaired cell adhesion (Waxmonsky, Conner 2013). An alkaloid K252a which targets AAK1, inhibits neuregulin-1/Erythroblastic leukemia viral oncogene homology 4 (Nrg1/ErbB4) dependent neurotrophic signaling and neuritogenesis. Loss of AAK1 alters ErbB4 expression and trafficking (Kuai, Ong et al. 2011). AAK1 is a downstream effector of nuclear dbf2-related (NDR) kinases in a pathway that reduces neuronal dendrite formation (Ultanir, Hertz et al. 2012). A recent study showed that AAK1 knockout mice had reduced response to persistent pain, apparently promoting alpha2 adrenergic signals (Kostich, Hamman et al. 2016). In Alzheimer's disease (AD) model mice it has been shown the increased levels of AAK1 are significantly associated with the decline in cognitive function. An interaction between AAK1 and CME might be involved in the production and clearance of Amyloid β. The inhibition of clathrin-mediated endocytosis was found to prevent amyloid β-induced axonal damage suggesting that AAK1 could be a viable therapeutic target for AD (Fu, Ke et al. 2018). A single nucleotide polymorphism in an intron of the AAK1 gene has been associated with the age of onset of Parkinson's disease (Abdel-Magid 2017, Latourelle, Pankratz et al. 2009). AAK1 negatively regulates β-catenin-dependent WNT signaling through clathrin-mediated endocytosis of the receptor LRP6 (Agajanian, Walker et al. 2019). AAK1 overexpression has been shown to reduce the endocytosis of membrane proteins, such as transferrin receptors and low-density lipoprotein receptor–related protein (Conner, Schmid 2003b). It has been shown that

AAK1 not only leads to the acquisition of Adriamycin resistance in yeast cells but also leads to Adriamycin resistance in mammalian cells when overexpressed in HEK293T and HeLa cells (Takahashi, Furuchi et al. 2006).

Functional role of AAK1 at different steps of virus life cycle: AAK1 has been shown to regulate the endocytic traffic of multiple viruses. Targeting the kinase activity of AAK1 by some clinically approved anticancer drugs reduces the internalization, assembly, and release of various viruses (Pu, Xiao et al. 2018). AAK1 regulates the clathrin-mediated entry of Hepatitis C virus (HCV) into target cells. In one of the studies, it was shown that the entry of HCV was inhibited when AAK1 kinase activity was targeted with sunitinib (which is a multi-kinase inhibitor) or Erlotinib (an EGFR kinase inhibitor). The combination of these inhibitors had a synergistic effect. Genetic silencing of AAK1 reduced the epidermal growth factor receptor-mediated HCV entry (Neveu, Ziv-Av et al. 2015). Independent of entry, AAK1 was also shown to play a role in the assembly of the HCV. In the case of HCV AAK1 phosphorylates the mu subunit of AP2 which stimulates the interaction of AP2 with the cargo proteins and regulates the binding of AP2-HCV core protein required for the assembly of the virus. The kinase inhibitors targeting AAK1 disrupted the core-AP2 binding and significantly inhibited HCV assembly and virus production (Neveu, Barouch-Bentov et al. 2012). It has been shown that AAK1 not only has a role to play in entry and assembly of HCV but also plays a role in release and cell-to-cell spread of HCV. The selective inhibitors of AAK1, Sunitinib and Erlotinib disrupted the temporal distinct steps in the life cycle of HCV (Xiao, Wang et al. 2018). Rabies virus, upon receptor binding, enters cells via clathrin-mediated endocytosis, which is regulated by phosphorylation of AP2M1 subunit on T156 residue by AAK1 (Wang, C., Wang et al. 2019). In a high-throughput RNA silencing analysis, it was shown that AAK1 knockdown significantly inhibited rabies virus entry (Wang, C., Wang et al. 2019). Also, the inhibition

of AAK1 by Sunitinib reduced the infection by blocking AP2M1 phosphorylation (Wang, C., Wang et al. 2019). Ebola and Dengue exploit AAK1 for entry and infection purposes. Inhibition of AAK1 with Sunitinib or Erlotinib inhibited the intracellular trafficking of these viruses (Bekerman, Neveu et al. 2017). In the case of IFN-alpha/beta and INF-gamma deficient mice infected with dengue virus, it was shown that targeting the kinase activity of AAK1 with a combination of Sunitinib and Erlotinib reduced systemic infection. The infection-induced expression of AAK1 transcripts further supports the potential that AAK1 can be a molecular target of these anticancer drugs as broad-spectrum antiviral agents (Bekerman, Neveu et al. 2017). AAK1 promotes clathrin-mediated internalization of MHC-I and its lysosomal degradation. Downregulation of AAK1 increased the surface MHC-I levels and anti-viral immune response (Loi, Muller et al. 2016).

1.6. SARS-CoV-2: A novel coronavirus

Coronaviruses are large, enveloped, positive-stranded RNA viruses responsible for infections of a wide variety of mammalian and avian species (Li 2016). Coronaviruses are classified under the family *Coronaviridae* and the subfamily Coronavirinae by The International Committee on Taxonomy of viruses. The genotypic and serological characterization subdivides Coronavirinae further into 4 genera, alpha, beta, gamma, and delta coronaviruses (Woo, Lau et al. 2012, Cui, Li et al. 2019, Fouchier, Hartwig et al. 2004, van der Hoek, Pyrc et al. 2004). Until 2019 only 6 human coronaviruses were known, of which 4 are known to cause only mild symptoms. The other two viruses, which include the Severe Acute Respiratory Syndrome Corona Virus (SARS-CoV) and the Middle East Respiratory Syndrome Corona Virus (MERS-CoV) cause fatal illnesses (Holmes 2003, Zaki, van Boheemen et al. 2012).

A novel coronavirus, the Severe Acute Respiratory Syndrome Coronavirus-2 (SARS-CoV-2), was detected in 2019 (Zhou, Yang et al. 2020, Chan, J. F., Kok et al.

2020, Lu, R., Zhao et al. 2020). Viruses were isolated and deep sequencing was carried out to analyze the genome (Zhou, Yang et al. 2020, Chan, J. F., Kok et al. 2020, Lu, R., Zhao et al. 2020). These analyses revealed that SARS-CoV-2 showed 96% sequence identity with the bat SARS-like coronavirus RaTG13 and, therefore, it has been categorized under Beta coronavirus genera (Zhou, Yang et al. 2020, Chan, J. F., Kok et al. 2020, Lu, R., Zhao et al. 2020).

SARS-CoV-2 has emerged as a highly transmissible and pathogenic coronavirus in humans that has caused global public health emergencies and economic crises. In the beginning, the virus was named 2019-nCoV and on Feb 11, 2020 the International Committee on Taxonomy of Viruses changed it to SARS-CoV-2. (WHO. https://www.who.int/emergencies/diseases/novel-coronavirus-2019/technical-guidance/naming-the-coronavirus-disease-(covid-2019)-and-the-virus-that-causes-it). However, SARS-CoV-2 is far more contagious than related SARS-CoV and MERS-CoV and has caused a global pandemic. As of April 28, 2021, there have been more than 150M confirmed cases worldwide, with a death toll of 3.15 Million. The United States ranks first in the number of confirmed cases and a total number of deaths reported by WHO. The evolutionary mechanisms like recombination and mutations make coronaviruses capable of expanding their host ranges, with some posing more threat than the original strains (Peck, Burch et al. 2015). Evidence for this scenario with SARS-CoV-2 has emerged with variants recently identified in the U.K., South Africa, Brazil, and New York (US) already beginning to become dominant in certain parts of the world. The emergence of such variants, with enhanced transmissibility and potential evasion of natural and vaccine-mediated immunity, is a further threat to global health. Therefore, understanding viral biology right from the structural level to its interaction with the host for multiplication and infectivity is of utmost importance.

Structure of SARS-CoV-2

Coronaviruses are single-stranded RNA (ssRNA), non-segmented, and enveloped viruses with lengths ranging between 26 to 32 kb. Among RNA viruses, their genome is the largest. SARS-CoV-2 is spherical in shape (Fig. 1.6A) with a diameter ranging from 60-140 nm and having long spikes on the outer surface, which are 9-12-nm long, as revealed by the microscopic studies (Li 2016) (Fig. 1.6A). These spikes give SARS-CoV-2 the shape of the solar corona (Fig. 1.6A). The SARS-CoV-2 morphology resembles other viruses of the corona family (Zhu, Zhang et al. 2020, Lu, R., Zhao et al. 2020). To characterize the entire genome, metagenomics next-generation sequencing, which is RNA-based, has been applied (Lu, R., Zhao et al. 2020).

The SARS-CoV-2 genome is 29 Kb long (9860 amino acids) (Chen, Liu et al. 2020) (Fig. 1.6C upper panel). The genome is capped at 5' end, has 3' polyadenylation with two untranslated regions (UTRs) and several open reading frames (ORFs) which code for structural as well as non-structural genes. The genome order is non-coding 5' UTR, replicase genes, orf1ab genes- non-structural and structural genes (S, E, M, and N) and non-coding 3' UTR (Wang, C., Liu et al. 2020). SARS-CoV-2 lacks the common hemagglutinin-esterase gene found in the Beta coronaviruses lineage (Chan, J. F., Kok et al. 2020). The largest ORF of the genome is orf1a/b which is at the 5' end and codes for 15 non-structural proteins (nsps) (nsp1–10 and nsp12–nsp16) (Wu, Peng et al. 2020). The orf1a/b consist of overlapping ORFs, which code for 2 polypeptides. There are two cysteine proteases encoded by the genome of the virus: a papain-like protease (PL2pro) or nsp3 and a 3C-like protease (3CLpro) or nsp5. The two polypeptides are cleaved into 15 nsps by these proteases. The nsp1|2, nsp2|3, and nsp3|4 sites are cleaved by PL2pro, and LQ↓SAG sites are cleaved by 3CLpro to produce nsp4 through nsp16 (Chan, J. F., Kok et al. 2020, Harcourt, Jukneliene et al. 2004). RNA-dependent RNA polymerase

(nsp12) is a critical enzyme required for viral transcription and replication. The other players involved in this process are nsp7/8, helicase (nsps13), and exonuclease (nsp14). The four structural proteins are encoded by the 3' end of the SARS-CoV-2, which play a role in virus-host cell receptor binding, virus assembly, morphogenesis, and release of virus particles from the host cell. The smallest structural protein found in the viral membrane is E, and in the host cells, it localizes to the endoplasmic reticulum and Golgi complex (Nieto-Torres, Dediego et al. 2011). The virus-like particle formation requires E protein, along with M and N (Siu, Teoh et al. 2008). The most abundant structural protein, a transmembrane glycoprotein in the virion, is the M protein. In the viral assembly, the M protein, together with E and N proteins, plays an important role (Siu, Teoh et al. 2008, Vennema, Godeke et al. 1996, Voss, Kern et al. 2006). The N protein plays a role, in the packaging of viral genome RNA into a helical ribonucleocapsid. The SARS-CoV-2 also encodes for eight accessory proteins (3a, 3b, 6, 7a, 7b, 8b, 9b, and orf14), which are distributed among structural genes are derived from sub-genomic RNA (based on the National Center for Biotechnology Information [NCBI] annotation NC_045512.2) (Wu, Peng et al. 2020, Wang, C., Liu et al. 2020).

Structure of S protein

The S protein of coronaviruses is 180-200 kDa in size; it consists of an extracellular N-terminus domain followed by a transmembrane (TM) domain anchored in the viral membrane and a small intracellular C-terminal domain (Bosch, van der Zee et al. 2003) (Fig. 1.6B). Before binding to a host cell receptor, the S protein is in metastable conformation. The interaction of the virus with the host cell leads to structural changes in the S protein that allow the virus to bind to the host cell. The spike proteins use a polysaccharide coating due to extensive glycosylation to evade the host's immune surveillance (Watanabe, Allen et al. 2020). The total length of the SARS-Cov-2 S protein

is 1273 aa, with a short signal peptide (amino acids 1–13) at the N-terminus, the S1 subunit (14–685 residues), and the S2 subunit (686–1273 residues) (Fig. 1.6C lower panel). The S1 and S2 subunits play a role in receptor binding and membrane fusion, respectively. The S1 subunit consists of an N-terminal domain (NTD) (14–305 residues) and a receptor-binding domain (RBD, 319–541 residues); the S2 subunit contains a fusion peptide (FP) (788–806 residues), heptapeptide repeat sequence 1 (HR1) (912–984 residues), HR2 (1163–1213 residues), a Transmembrane domain (TM) (1213–1237 residues), and a cytoplasmic domain (1237–1273 residues) (Xia, Zhu et al. 2020).

The cryo-electron microscopy determined the SARS-CoV-2 trimeric S protein structure, which showed the opened and closed conformations of the receptor-binding domain and the corresponding functions (Wrapp, Wang et al. 2020, Walls, Park et al. 2020). The S1 and S2 subunits form the bulbous head and stalk region, respectively. The S protein is in inactive precursor form when coronavirus is in the native state. During the infection process, the host proteases (like TMPRSS2) activate the S protein by cleaving it into S1 and S2 subunits which are required for the activation of the membrane fusion domain after the virus enters into the target cells (Bertram, Dijkman et al. 2013, Hoffmann, Kleine-Weber et al. 2020).

S1 subunit

The initiation of viral infection begins when the virus binds to the host cell surface receptors. Therefore, the recognition and binding process in which the S1 subunit plays a role is an important determinant in viral entry and a step that the drugs may target. The S1 subunit is comprised of the NTD and RBD. The important substitutions in SARS-CoV-2-CTD are: that more residues directly interact with the human receptor ACE2 than as seen in SARS-RBD. Studies have shown that the mutations of important residues of RBD

of SARS-CoV-2 play a role in enhancing the interaction with ACE2 and higher affinity for RBD than RBD of SARS-CoV (Wrapp, Wang et al. 2020, Walls, Park et al. 2020, Wang, Q., Zhang et al. 2020, Lan, Ge et al. 2020). he RBDs of SARS-CoV-2 and SARS-CoV have 73-77% sequence similarity. The receptor-binding motif analysis of SARS-CoV and SARS-CoV-2 has shown that the essential ACE2 binding residues are conserved. Some studies showed that even when the residues which are essential for ACE2 binding are conserved, the murine monoclonal antibodies (mAbs) and polyclonal antibodies against SARS-CoV-S RBD are unable to interact with the SARS-CoV-2 S protein, which suggests that there is a difference in antigenicity between SARS-CoV and SARS-CoV-2 (Wang, Q., Zhang et al. 2020).

S2 subunit

The S2 subunit, consisting of FP, HR1, HR2, TM domain, and cytoplasmic domain fusion (CT), is responsible for the fusion and entry of the virus. The short part of the S2 subunit is FP which is composed of 15–20 conserved, mainly hydrophobic, amino acid residues such as glycine (G) or alanine (A), which get anchored to the target membrane (Millet, Whittaker 2018) When the S protein changes to pre-hairpin conformation the FP gets anchored to the target membrane. FP disrupts and connects the lipid bilayer of the target cell, which helps in membrane fusion with the host cell (Millet, Whittaker 2018). HR1 and HR2 are composed of polar hydrophilic, hydrophobic, and charged repetitive heptapeptide. HR1 (at the C-terminus of a hydrophobic FP) and HR2 (at the N-terminus of the TM domain) form a six helical bundle required for the viral fusion and entry function of the S2 subunit (Xia, Zhu et al. 2020, Robson 2020). The TM domain helps anchor the S protein to the viral membrane, and the CT tail completes the S2 subunit (Tang, Bidon et al. 2020). The conformation of S2 changes when RBD binds to ACE2 receptors on target cells due to FP insertion into the target cell membrane, a process that is dependent on the

proteolytic cleavage at the S1/S2 site separating S1 and S2 and at the S2 site to generate a mature FP. HR1 domain is exposed, which triggers HR1 and HR2 trimer interaction to form the helical bundle, thus bringing the envelope of the virus and cell membrane into proximity for viral fusion and entry (Xia, Xu et al. 2018).

Despite high sequence similarities with SARS-CoV, there are variations in the novel SARS-CoV-2 virus-like (a) mutations in the host cell RBD (b) a polybasic furin-like protease site at the S1/S2 subunits rather than a single arginine observed in SARS-CoV and (c) the addition of O-linked glycans (Coutard, Valle et al. 2020, Andersen, Rambaut et al. 2020). All these variations are thought to interact with host ACE2 receptor and with high affinity.

ACE2- A primary receptor for SARS-CoV-2

ACE2 is a type I transmembrane metallocarboxypeptidase present in the membranes of cells located in the lungs, arteries, heart, kidney, and intestines (Hamming, Timens et al. 2004, Donoghue, Hsieh et al. 2000). ACE2 is an enzyme long-known to be a main player in the Renin-Angiotensin system (RAS) and is a target for the treatment of hypertension (Riordan 2003). The major substrate of ACE2 is Angiotensin II. ACE2 cleaves Angiotensin II to form a vasodilator Angiotensin (1-7) thereby negatively regulating RAS system (Kuba, Imai et al. 2010, Tikellis, Thomas 2012).

PCR analysis revealed that ACE2 is also expressed in the lung, kidney, and gastrointestinal tract, tissues shown to harbor SARS-CoV (Ksiazek, Erdman et al. 2003, Harmer, Gilbert et al. 2002, Leung, To et al. 2003). Based on the sequence similarities between SARS-CoV-2 and SARS-CoV, several independent research groups investigated if SARS-CoV-2 also utilizes ACE2 as a cellular entry receptor. Zhou *et*

al. showed that SARS-CoV-2 could use ACE2 from humans, Chinese horseshoe bats, civet cats, and pigs to enter ACE2-expressing HeLa cells. Hoffmann *et al.* reported similar findings for human and bat ACE2. Additionally, Hoffmann *et al.* showed that treating Vero-E6 cells, a monkey kidney cell line known to permit SARS-CoV replication, with an Anti-ACE2 Antibody (R&D Systems, Catalog # AF933) blocked entry of VSV pseudotypes expressing the SARS-CoV-2 spike protein.

1.7. Figures

Figure 1.1

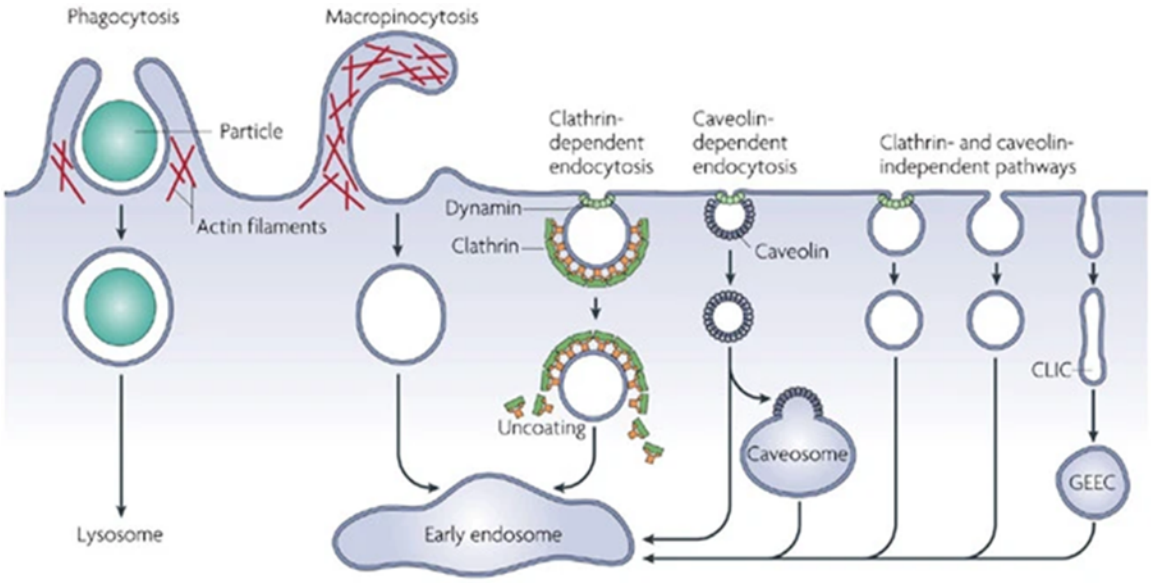
Phagocytosis
Macropinocytosis
Particle
Actin filaments
Clathrin-dependent endocytosis
Caveolin-dependent endocytosis
Clathrin- and caveolin-independent pathways
Dynamin
Clathrin
Caveolin
CLIC
Uncoating
Caveosome
GEEC
Lysosome
Early endosome

Figure 1.1. Routes of Internalization.

Several mechanisms for entry into the cell have been described. Clathrin-mediated endocytosis is best characterized, and internalization pathways are frequently classified upon their dependence for clathrin and dynamin. Image used with permission from (Mayor 2007. Pathways of clathrin-independent endocytosis).

Figure 1.2

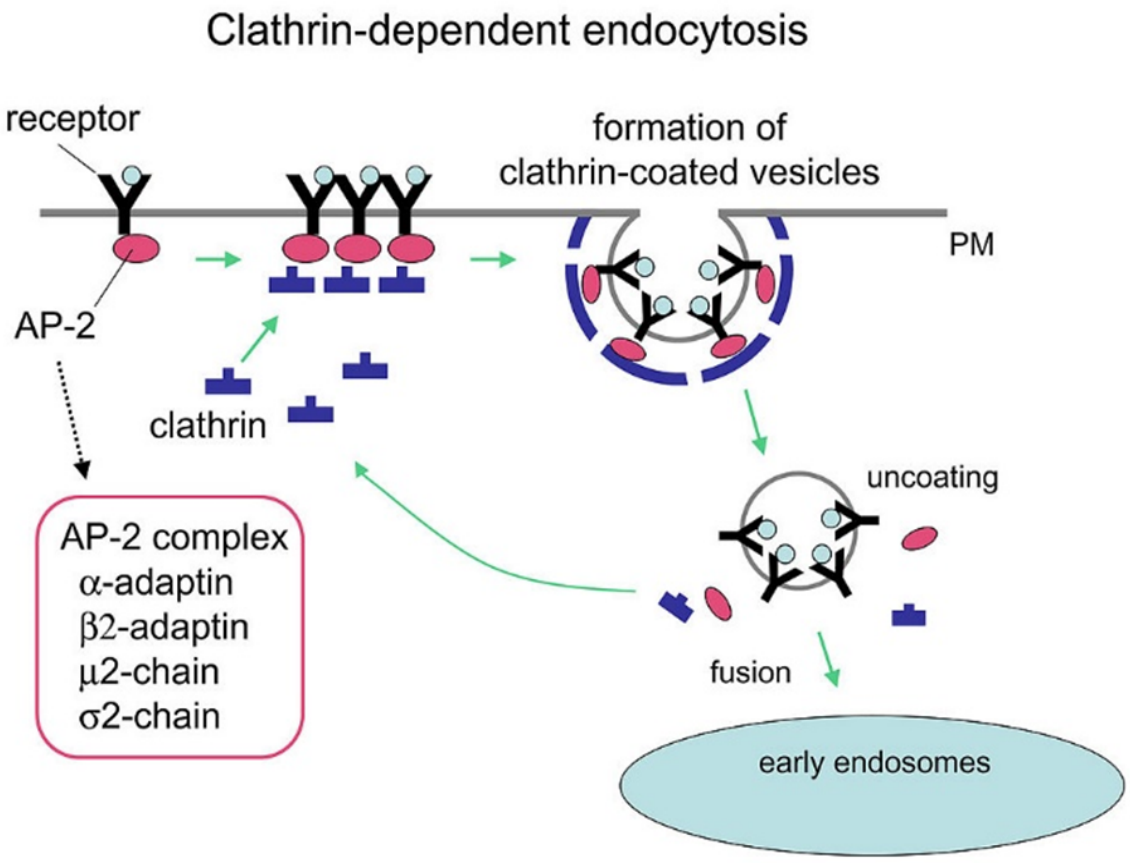
Clathrin-dependent endocytosis
receptor
formation of
clathrin-coated vesicles
PM
AP-2
clathrin
uncoating
AP-2 complex
α-adaptin
β2-adaptin
μ2-chain
σ2-chain
fusion
early endosomes

Figure 1.2. Mechanism of clathrin-dependent endocytosis.

Clathrin and cargo molecules are assembled into clathrin-coated pits on the plasma membrane together with an adaptor complex called AP-2 that links clathrin with transmembrane receptors, concluding in the formation of mature clathrin-coated vesicles (CCVs). CCVs are then actively uncoated and transported to early/sorting endosomes. Image used with permission and modified from (Grant, B. D. and Sato, M. via Wikimedia Commons)

Figure 1.3

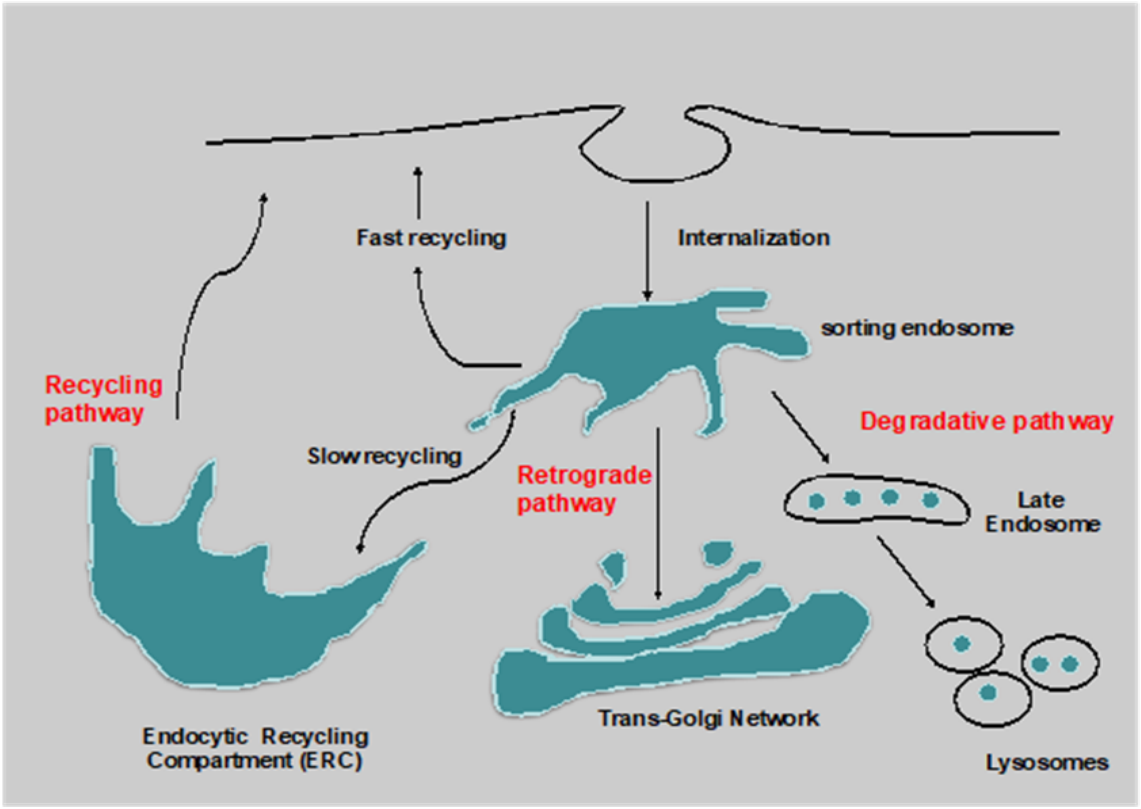
Fast recycling
Internalization
sorting endosome
Recycling pathway
Slow recycling
Retrograde pathway
Degradative pathway
Late Endosome
Endocytic Recycling Compartment (ERC)
Trans-Golgi Network
Lysosomes

Figure 1.3. Pathways of endocytic trafficking.

When the cargo is internalized, its components merge at a common location known as the early endosomal (EE) compartment. Trafficking routes from the EE include cargo recycling back to the plasma membrane via fast recycling or through a slow recycling pathway that involves an endocytic recycling compartment (ERC), lysosomal degradation of cargo by delivery to the late endosome (LE), or retrograde transport to the trans-Golgi network (TNG).

Figure 1.4

A

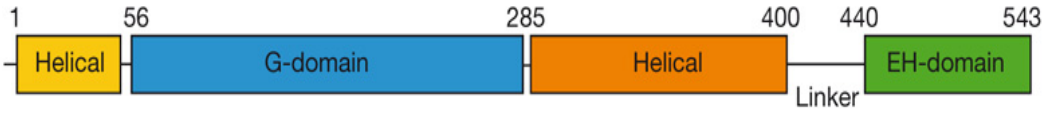
1
56
285
400
440
543
Helical
G-domain
Helical
EH-domain
Linker

B

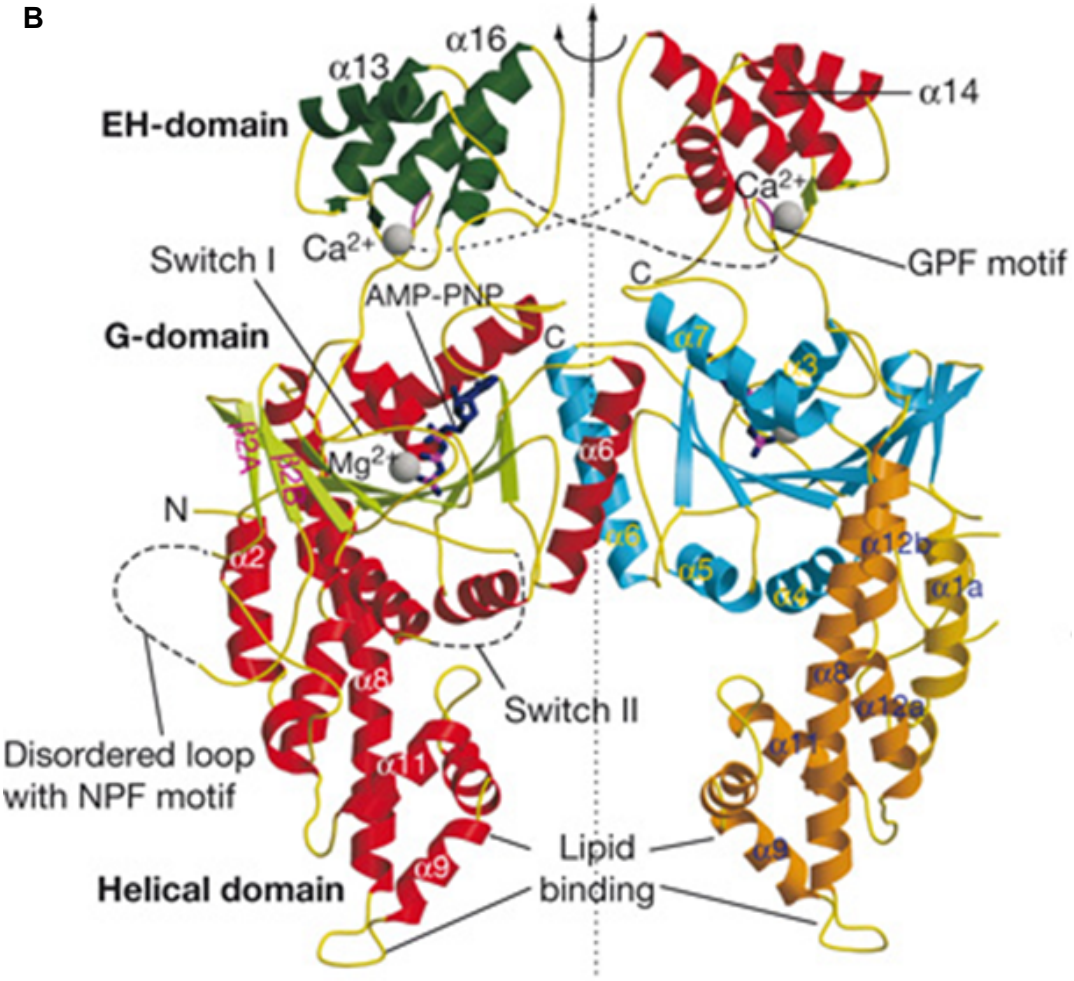
α16
α13
α14
EH-domain
Ca2+
Ca2+
Switch I
GPF motif
AMP-PNP
C
G-domain
C
α7
α3
β2A
β2B
Mg2+
α6
N
α2
α6
α12b
α5
α4
α1a
α8
α12a
α11
Switch II
Disordered loop
with NPF motif
α11
α9
Lipid
binding
Helical domain
α9

Figure 1.4. Domain Structure of EHDS.

A. (numbering from mouse EHD2 amino acids). All four EHD proteins consist of an N-terminal helical domain, an ATP-binding dynamin-like G-domain, a central helical domain followed by a linker-region and a characteristic EH domain at the C-terminus.

B. Ribbon-type presentation of the EHD2 dimer. One molecule is coloured according to the secondary structure (helices in red, -strands in green) and the other according to the domain structure. GPF and NPF motifs are indicated. Image used with permission and modified from (Daumke et al., 2007).

Figure 1.5

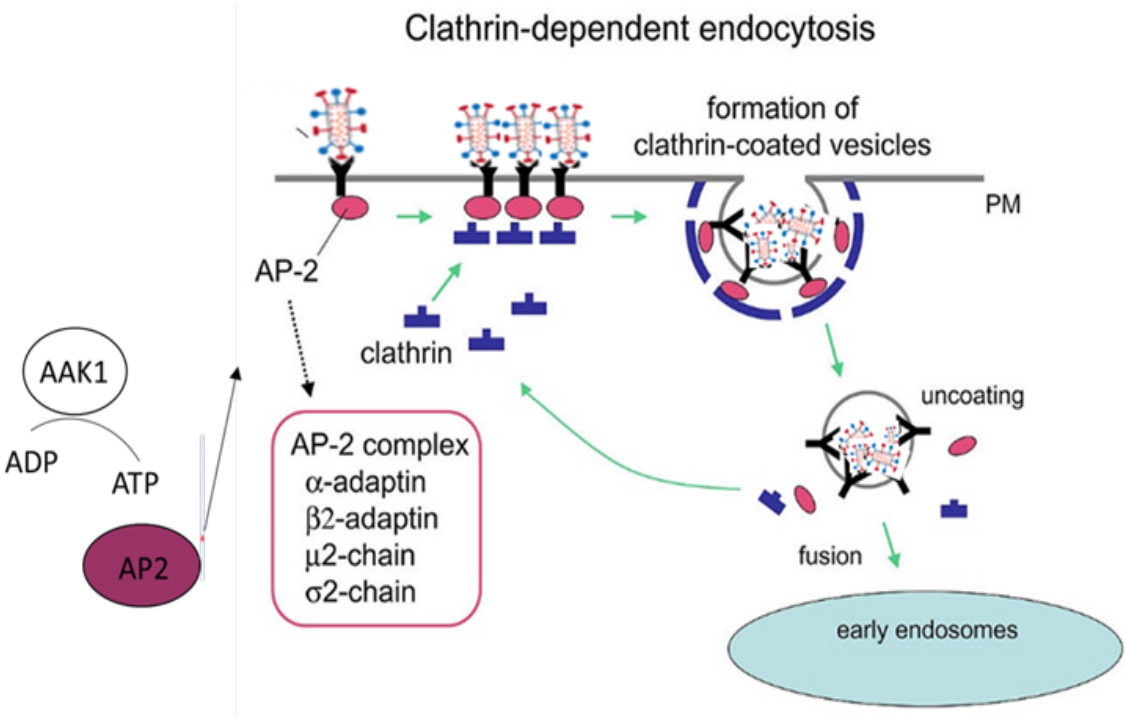
Clathrin-dependent endocytosis
formation of
clathrin-coated vesicles
PM
AP-2
clathrin
AAK1
ADP
ATP
AP2
AP-2 complex
α-adaptin
β2-adaptin
μ2-chain
σ2-chain
uncoating
fusion
early endosomes

Figure 1.5. AAK1 mediated clathrin-dependent endocytosis.

Clathrin and cargo molecules are assembled into clathrin-coated pits on the plasma membrane together with an adaptor complex called AP-2 which after getting phosphorylated by AAK1 links clathrin with transmembrane receptors, concluding in the formation of mature clathrin-coated vesicles (CCVs). CCVs are then actively uncoated and transported to early/sorting endosomes. Image used with permission and modified from (Grant, B. D. and Sato, M. via Wikimedia Commons)

Figure 1.5

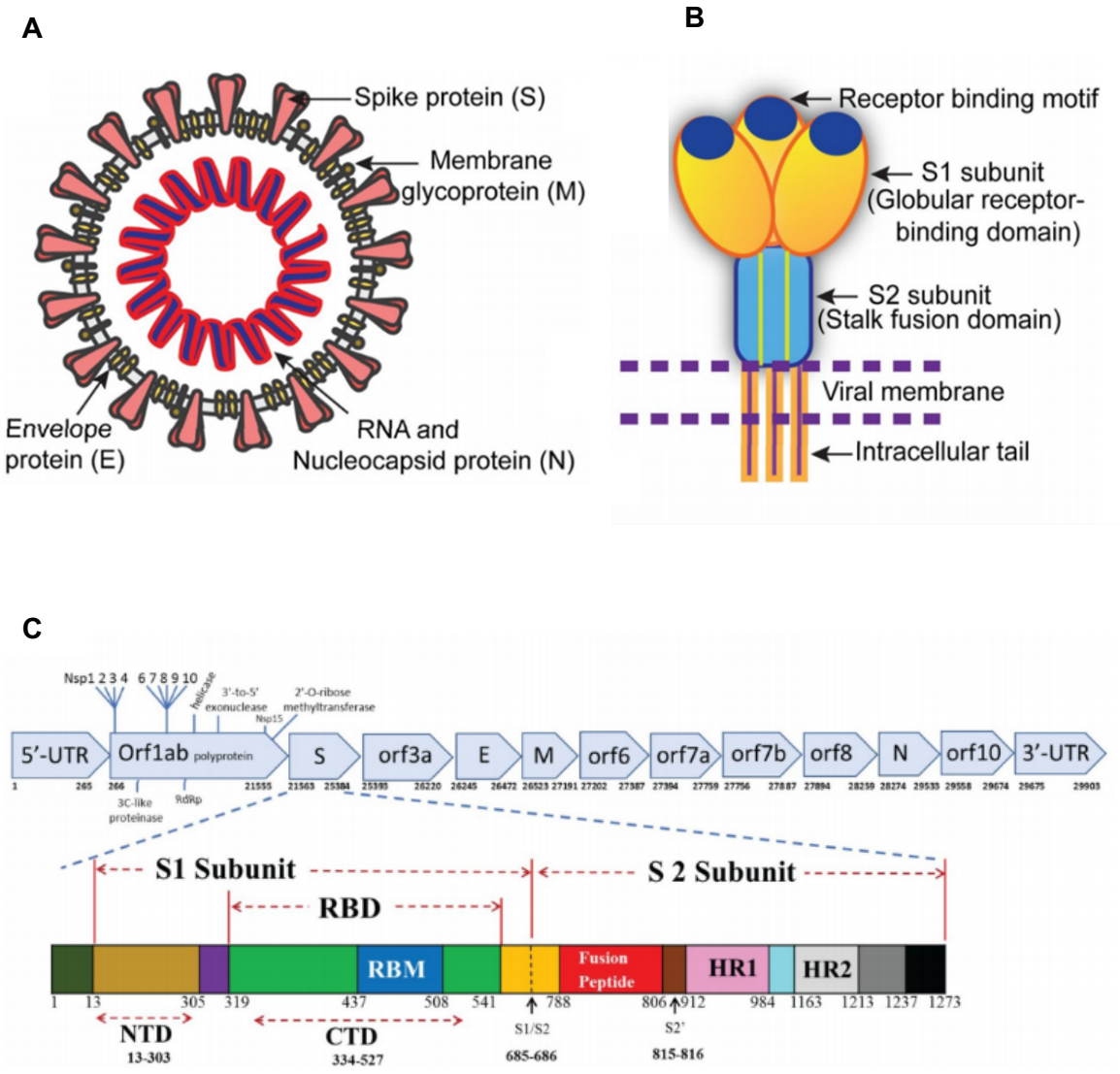
A
Spike protein (S)
Membrane glycoprotein (M)
Envelope protein (E)
RNA and Nucleocapsid protein (N)
B
Receptor binding motif
S1 subunit (Globular receptor-binding domain)
S2 subunit (Stalk fusion domain)
Viral membrane
Intracellular tail
C
5'-UTR
Orf1ab polyprotein
S
orf3a
E
M
orf6
orf7a
orf7b
orf8
N
orf10
3'-UTR
S1 Subunit
S 2 Subunit
RBD
RBM
Fusion Peptide
HR1
HR2
NTD
13-303
CTD
334-527
S1/S2
685-686
S2'
815-816

Figure 1.6. Structure of coronavirus.

A. Simplified structure of SARS-CoV-2

B. The cartoon depicts key features and the trimeric structure of the SARS-CoV-2 S protein.

C. Schematic of SARS-CoV-2 genome (top) and S protein (bottom).

https://doi.org/10.1371/journal.ppat.1008762 images used with permission and modified from (COVID-19 pandemic: Insights into structure, function, and hACE2 receptor recognition by SARS-CoV-2. Anshumali Mitta and Vikash Verma, 2020

Chapter 2: Role of endocytic regulator EHD1 and its binding partner RUSC2 in EGFR traffic

(Published Paper)

(Based on the Following Published Paper)

EHD1 and RUSC2 Control Basal Epidermal Growth Factor Receptor Cell Surface Expression and Recycling

Eric C. Tom,[#a,b] Insha Mushtaq,[#a,c] Bhopal C. Mohapatra,[a,d] Haitao Luan,[a] Aaqib M. Bhat,[a,d] Neha Zutshi,[a,c] Sukanya Chakraborty,[a,d] Namista Islam,[a,d] Priyanka Arya,[a,d,*] Timothy A. Bielecki,[a] Fany M. Iseka,[a,d,*] Sohinee Bhattacharyya,[a,c] Luke R. Cypher,[a,*] Benjamin T. Goetz,[a] Simarjeet K. Negi,[d,*] Matthew D. Storck,[a] Sandeep Rana,[a] Angelika Barnekow,[f] Pankaj K. Singh,[a,b,c,d,e] Guoguang Ying,[g] Chittibabu Guda,[d,e] Amarnath Natarajan,[a,e] Vimla Band,[a,d,e] and Hamid Band[a,b,c,d,e]

[#]Contributed equally. Eric C. Tom and Insha Mushtaq are co-first authors. Eric C. Tom initiated the project and performed the majority of the studies. Insha Mushtaq completed the project and carried out studies for manuscript revision.

Corresponding author.

a. Eppley Institute for Research in Cancer and Allied Diseases, University of Nebraska Medical Center, Omaha, Nebraska, USA. **b**. Department of Biochemistry and Molecular Biology, University of Nebraska Medical Center, Omaha, Nebraska, USA. **c**. Department of Pathology and Microbiology, University of Nebraska Medical Center, Omaha, Nebraska, USA. **d.** Department of Genetics, Cell Biology and Anatomy, College of Medicine, University of Nebraska Medical Center, Omaha, Nebraska, USA. **e.** Fred and Pamela Buffett Cancer Center, University of Nebraska Medical Center, Omaha, Nebraska, USA. **f.** Department of Experimental Tumorbiology, Westfälische Wilhelms University Muenster, Muenster, Germany. **g**. Laboratory of Cancer Cell Biology, National Clinical Research Center for Cancer, Tianjin Key Laboratory of Cancer Prevention and Therapy, Tianjin Medical University Cancer Institute and Hospital, Tianjin, China

2.1. Introduction

The plasma membrane of metazoan cells provides a fundamental interface for cell-to-cell and cell-to-environment communication. Understanding how the cell surface levels of receptors that recognize and communicate changes in a cell's environment into alterations of a cell's biochemical machinery are regulated is therefore of fundamental interest in cell biology. RTKs are a particularly important class of surface receptors as they provide a pervasive mechanism of signal transduction in higher eukaryotes (Regad 2015). The surface expression of RTKs and their compartmentalization are key determinants of the spatial-temporal signaling output of their ligand-induced activation and dictate the magnitude, duration, and potentially the type of physiological responses (Sigismund, Confalonieri et al. 2012, Sorkin, Goh 2009). Aberrant overexpression or mutational activation of RTKs is a widespread mechanism to drive oncogenesis, and many targeted therapeutics are directed at RTKs or their signaling cascades (Mishra, Hanker et al. 2017).

EGFR, the founding member of the ErbB receptor family, is a prototype RTK with critical roles in development and maintenance of epithelial and other tissues by generating cell proliferation, survival, differentiation, and migration cues in response to members of the EGF family of growth factors (Herbst, R. S. 2004). Activation of ErbB receptors is linked to the initiation and progression of human cancers, and the levels of their expression are often significantly elevated in many solid tumors (e.g., breast, colon, ovary, pancreas, and glial) (Rowinsky 2004, Gschwind, Fischer et al. 2004, Santarius, Shipley et al. 2010). EGFR expression is a feature of the basal-like breast cancer subtype, which has an especially poor prognosis (Rakha, Reis-Filho et al. 2008).

Given key physiological and oncogenic roles of EGFR, many previous investigations have elucidated mechanisms that control the endocytic trafficking of ligand-activated EGFR, including the ligand-induced activation of both clathrin-dependent and clathrin-independent endocytosis and differential transport into lysosomal degradation or

endocytic recycling based on the nature of activating ligands and their concentrations (Roepstorff, Grandal et al. 2009, Sigismund, Woelk et al. 2005). Accordingly, impaired endocytosis or diminished lysosomal targeting of EGFR or other RTKs has emerged as a mechanism by which RTKs become oncogenic (Mosesson, Mills et al. 2008, Tomas, Futter et al. 2014, Chung, Tom et al. 2014). The Cbl family of ubiquitin ligases are key to sorting EGFR and other RTKs for lysosomal degradation and attenuation of their signaling (Mohapatra, Ahmad et al. 2013). Indeed, mutations in Cbl are now known to drive a small subset of myeloid leukemia (Nadeau, An et al. 2017).

In contrast to the mechanisms of ligand-activated EGFR trafficking through the endocytic pathway, mechanisms that help maintain the optimal activation-ready pool of cell surface EGFR prior to ligand binding are much less clear. In the absence of a ligand, EGFR is constitutively internalized at a slow rate and thought to primarily recycle (Waterman, Sabanai et al. 1998). It is estimated that 2 to 3% of unoccupied EGFRs on typical cultured cells are endocytosed per minute and rapidly recycle to the plasma membrane (Wiley 2003, Herbst, J. J., Opresko et al. 1994). However, few studies have sought to characterize mechanisms that regulate the cell surface levels, endocytosis, or recycling of EGFR or other RTKs under their basal unstimulated state. A recent study of EGFR on mouse embryonic fibroblasts (MEFs) in which the Arp2/3-activator Wiskott-Aldrich syndrome protein and Scar homologue (WASH) was deleted showed reduced basal EGFR levels at the cell surface, apparently due to increased diversion to the lysosome (Gomez, Gorman et al. 2012). As WASH serves as an actin-nucleating component of the retromer complex, which is involved in retrograde trafficking of receptors from endosomes to the Golgi compartment (Seaman, Gautreau et al. 2013), this study suggested that retrograde transport into the Golgi compartment may in part regulate the cell surface EGFR levels. Notably, sorting nexins 1 and 2, which are included in the

retromer complex, have been primarily characterized as regulators of ligand-induced lysosomal traffic of EGFR and other RTKs (Gullapalli, Garrett et al. 2004).

Members of the highly homologous and evolutionarily conserved EPS-15 homology (EH) domain-containing (EHD) protein family localize to tubular and vesicular endocytic compartments and regulate trafficking of a number of non-signaling receptors, such as transferrin receptor, major histocompatibility complex class I (MHC-I), and β1 integrin, from the endocytic recycling compartment (ERC) to the cell surface (Caplan, Naslavsky et al. 2002, Braun, Pinyol et al. 2005, Jovic, Naslavsky et al. 2007). A role for EHD proteins has also emerged in retrograde trafficking from endosomes to the Golgi compartment. Expression of a dominant negative EHD1 mutant in Chinese hamster ovary cells was shown to slow down the transport from the cell surface to the Golgi compartment of TGN38, a marker of endocytic recycling compartment-mediated retrograde transport, but not that of furin, which is transported through the lysosomal route (Lin, S. X., Grant et al. 2001). EHD1 binds to vacuolar protein sorting 26 (Vps26) and Vps35, members of the retromer cargo recognition complex, and these interactions were shown to be required for endosome-to-Golgi retrieval of the cation-independent mannose-6-phosphate receptor (Gokool, Tattersall et al. 2007). EHD3 was shown to be necessary for the maintenance of Golgi morphology and transport of endocytosed Shiga toxin B to this organelle (Naslavsky, McKenzie et al. 2009).

Previous studies in primary neurons and a neuronal cell line showed that neurotrophin activation of TrkA, an RTK, transcriptionally upregulated the expression of EHD4 (referred to as “pincher” in that study) and that EHD4 in turn facilitated the retrograde trafficking of activated TrkA from dendrites to the neuronal body, thereby promoting neurotrophin signaling through this receptor (Valdez, Akmentin et al. 2005). Notably, ligand-induced retrograde trafficking of EGFR in the same system was not dependent on EHD4 (Philippidou, Valdez et al. 2011). EHD1 and its binding partner

SNAP29 were found to be associated with insulin-like growth factor (IGF)-activated IGF1 receptor (IGF1R) and to colocalize with it in endosomes, with EHD1 overexpression resulting in reduced IGF1-induced signaling (Rotem-Yehudar, Galperin et al. 2001). One study reported that EHD2 interacts with glucose transporter 4 (GLUT4) and colocalizes with it on endosomes, with intracellular application of anti-EHD2 antibody or a peptide blocker, resulting in reduced GLUT4 exocytosis to the plasma membrane (Park, Ha et al. 2004). Another study found no role of EHD2 in GLUT4 localization in the perinuclear region or in its insulin-stimulated surface transport; instead, the study showed that EHD1 and its interacting partner EHBP1 regulate the perinuclear localization of GLUT4 and its surface transport upon insulin stimulation (Guilherme, Soriano, Furcinitti et al. 2004). Neither study reported any role of EHD proteins in the trafficking of insulin receptor. Notably, we observed reduced expression of vascular endothelial growth factor receptor 2 (VEGFR2, an RTK) in glomerular endothelial cells of EHD3/EHD4 (EHD3/4) knockout (KO) mice, which display thrombotic renal glomerular angiopathy, suggesting a potential role of EHD3/4 in VEGFR2 trafficking (George, Rainey et al. 2011).

More recently, mouse models of EHD deficiency or cells derived from these animals have provided support for the role of EHD proteins in regulating the surface display of non-RTK receptors. EHD1-null MEFs or MEFs with small interfering RNA (siRNA)-mediated EHD1 depletion were reported to show reduced overall but increased activated β1 integrin levels at the cell surface, with impaired focal adhesion disassembly and cell migration reflecting aberrant β1 integrin trafficking (Jovic, Naslavsky et al. 2007). We have shown that EHD family members participate in cell surface trafficking of sodium/calcium (Ca^{2+}) exchanger (Gudmundsson, Hund et al. 2010, Gudmundsson, Curran et al. 2012), L-type Ca^{2+} channel type 1.2 (Curran, Makara et al. 2014), and voltage-gated T-type Ca^{2+} channels CaV3.1 and CaV3.2 (Curran, Musa et al. 2015) in cardiomyocytes and of the ferlin protein Fer1L1 (Posey, Pytel et al. 2011, Posey, Swanson

et al. 2014) in skeletal muscle cells. These findings raised the possibility that EHD proteins also function in the surface expression of RTKs. Recently, using wild-type and EHD1-null bone marrow-derived macrophages, we found that EHD1 is required for the basal surface expression of the RTK colony-stimulating factor 1 (CSF1) receptor (Cypher, Bielecki et al. 2016). In previous work investigating the subcellular organelles where constitutively active non-small cell lung cancer (NSCLC)-associated EGFR mutants traffic, we observed the colocalization of EHD1 and mutant EGFR in the endocytic recycling compartment (Chung, Raja et al. 2009). Expression of EHD1 in NSCLC patients was found to correlate with high levels of EGFR and the Rab11 interactor RAB11-FIP3 as well as with shorter survival (Lu, H., Meng et al. 2013, Gao, Wang et al. 2014). A similar analysis in breast cancer showed a positive correlation between EHD1 and RAB11-FIP3 expression, and the expression of these markers correlated with phospho-EGFR levels in tumors; EHD1-positive (EHD1+) patients had a shorter overall and disease-free survival, and a patient status of EHD1+ plus phospho-EGFR+ was even more predictive of shorter survival (Tong, Liang et al. 2017). EHD1 and EGFR expression levels were also reported to be increased in human papillary thyroid cancer, and levels of EHD1 protein were significantly associated with tumor size, lymph node metastasis, and EGFR expression (Liu, Liang et al. 2018). EHD1 levels in NSCLC also showed a negative correlation with sensitivity to EGFR-targeted kinase inhibitor therapy (Wang, X., Yin et al. 2018). How EHD1 may be involved in regulating EGFR biology, however, is not known. A recent study suggested that EHD3 may function in targeting the ligand-stimulated EGFR to lysosomal degradation by diverting it from endocytic recycling (Amessou, Ebrahim et al. 2016), consistent with EHD3 deletion in glioblastoma (Chukkapalli, Amessou et al. 2014), although doxycycline (Dox)-inducible EHD3 expression in EHD3-deleted glioblastoma cell lines increased the basal levels of EGFR (Amessou, Ebrahim et al. 2016). Studies presented here reveal a novel role of EHD1, in conjunction with a new potential interacting partner, RUN and SH3

domain-containing protein 2 (RUSC2) (Bayer, Fischer et al. 2005), in the transport of EGFR from the Golgi compartment to the surface.

RUSC2/iporin contains a RUN domain (named based on its presence in RPIP8, UNC-14, and NESCA proteins) that interacts with Rab1 and Rab35 small GTPases (Fukuda, Kobayashi et al. 2011, Chi, Cao et al. 2011). RUSC2 has also been reported to interact with the Golgi protein GM130 and has been proposed as a potential regulator of endosomal targeting of vesicles derived from the endoplasmic reticulum (ER) (Bayer, Fischer et al. 2005). We noted RUSC2 as an uncharacterized protein identified in an EGFR-associated protein complex isolated from cells in the absence of ligand stimulation (Deribe, Wild et al. 2009). Here, we show that EHD1 and RUSC2 show an overlapping subcellular localization and function as positive regulators of the transport of unstimulated EGFR from the Golgi compartment to the cell surface to help maintain an activation-ready cell surface pool of EGFR on the plasma membrane.

2.2. Materials and Methods

Biochemical reagents

The reagents and their sources are as follows: puromycin, hygromycin, G418, doxycycline (Dox), enzyme immunoassay-grade bovine serum albumin (BSA), paraformaldehyde (PFA), monensin, propidium iodide, DMSO, GTPγS (catalog number G8634), and Triton X-100 were from Sigma-Aldrich (St. Louis, MO). EGF was from PeproTech (Rocky Hill, NJ). Halt protease and phosphatase inhibitor cocktail were from Life Technologies. Normal goat serum (catalog no. 005-000-121) was from Jackson ImmunoResearch Laboratories. 35S-labeled methionine-cysteine (EXPRE35S35S protein labeling mix; NEG072) was from Perkin Elmer. Vectashield mounting medium was from Vector Laboratories (Burlingame, CA). NeutrAvidin Protein Dylight 488 conjugate

(catalog no. 22832) was from Thermo Scientific. Glutathione-Sepharose 4B beads were from GE Healthcare. Protein G-Sepharose beads were from Invitrogen.

Antibodies

Anti-EGFR mouse monoclonal 528 (catalog no. Grol1) was from Calbiochem or purified from hybridoma supernatants in-house; anti-EGFR rabbit polyclonal (SC-03) and anti-HSC-70 (B-6; 7298) were from Santa Cruz Biotechnology; anti-EHD1 (ab109311) was from Abcam; anti-β-actin (A5316) was from Sigma-Aldrich; anti-Turbo-GFP (PA5-22688) was from Thermo Scientific; anti-p-Erk (9101), anti-Erk (9102), and anti-p-EGFR (Tyr-1068;2234) were from Cell Signaling Technology; anti-GM130 (610822) was from BD Biosciences; anti-mouse IgG2a–allophycocyanin (APC) conjugate was from BioLegend (407109); and a nonspecific mouse IgG2a control (34950) was from BD Biosciences. APC–anti-human EGFR (clone Ay13; catalog no. 352906) and APC–mouse IgG2a isotype control (clone MOPC-173; 400220) were from BioLegend. Brilliant Violet 605 anti-human HLA-A, -B, -C (clone W6/32; 311432) and Brilliant Violet 605 mouse IgG2a isotype control (clone MOPC-173; 400269) were from BioLegend. In-house generated rabbit antibodies recognizing EHD1/EHD4, EHD2, EHD3 or EHD4 have been described previously (87). A rabbit polyclonal antibody against human RUSC2/iporin was generated against an internal peptide sequence (amino acid residues 532 to 553) through a commercial vendor (Pacific Immunology, Ramona, CA) and validated using epitope-tagged RUSC2 expressed in 293T cells and shRNA knockdown of endogenous RUSC2. HA tag antibody (catalog no. 901503) was from BioLegend. Anti-Myc epitope antibody (9E10; ATCC) was protein G purified in-house from hybridoma supernatants.

Transfection reagents and plasmids

The Dox-inducible EHD1 expression construct (pRevTRE-EHD1-GFP) was generated by cloning the full-length, PCR-amplified, human EHD1 cDNA sequences into pDest47-GFP vector in frame with GFP and subsequently subcloning the EHD1-GFP

insert into pRev-Tre vector (Clontech Laboratories Inc./TaKaRa Bio) at the AgeI/ClaI sites. The PCR primers were as follows: 5′-GATCGATCaccggtTCACCATGTTCAGCTGGGTCA-3′ (forward) and 3′-GATCGATCatcgaTCATTATTTGTAGAGCTCATCCATG-5′ (reverse). The pCDNA3-based EHD1-DsRed and EHD1-myc constructs (George, Ying et al. 2007) and the N-terminally HA-tagged human RUSC2 construct in pSV-HA vector (Bayer, Fischer et al. 2005) have been described previously. Individual siRNAs or SMARTpools and Dharmafect I transfection reagent were from the Dharmacon division of ThermoFisher (Pittsburg, PA). An individual custom siRNA sequence for EHD1 (#2006) was 5′-GACAUUGGGCAUCUCUUUCUU-3′ (Lu, H., Meng et al. 2013). The control siRNA 5 (catalog no. D-00210-05-50), the 3′ UTR (D-019022-20), and SMARTpool (M-019022-02) siRNAs targeting EHD1 were from ThermoFisher. XtremeGENE 9 transfection reagent was from Roche Applied Science (Indianapolis, IN). siRNA transfections were performed in Opti-MEM (Life Technologies).

The following Dox-inducible lentiviral shRNA constructs were obtained from GE Healthcare: control shRNA (VSC6580), EHD1 shRNA sequence 1 (source clone, V2IHSPGG_388688; target sequence, GCTAGTTTCTGTTCTGTAA), EHD1 shRNA sequence 2 (source clone, V2IHSPGG_908952; target sequence, AAGGTCCATAAAGACTGAG); RUSC2 shRNA sequence 1 (source clone, V2IHSPGG_463376; target sequence, GCCTAGACCGAAGATCACA); RUSC2 shRNA sequence 2 (source clone, V2IHSPGG_463384; target sequence, GCTCACCAGTCATACCATG).

Cell culture

Media and supplements were from Life Technologies. Fetal bovine serum (FBS) and tetracycline-free FBS were from HyClone.

16A5 is an HPV16 E6/E7-immortalized derivative of the reduction-mammoplasty-derived 76N normal mammary epithelial cell (MEC) line (Band, Sager 1989) and was grown in DFCI medium containing 2 nM EGF (Band, Sager 1989) in a humidified atmosphere of 95% air and 5% CO2 at 37°C. For growth factor stimulation experiments, 16A5 cells were cultured in growth factor-free D3 medium (Band, Sager 1989) for the time periods indicated in the figure legends.

Wild-type control and EHD1−/− mouse embryonic fibroblast (MEF) cell lines established by in vitro infection of NIH 3T3 protocol-immortalized Ehd1flox/flox MEFs using adeno-GFP (control) and adeno-Cre-GFP viruses, respectively, have been described previously (Bhattacharyya, Rainey et al. 2016). The MEFs and the triple-negative breast cancer cell line MDA-MB-231 (ATCC) were maintained in Dulbecco's modified Eagle's medium (DMEM) containing 10% FBS and supplements (Zhao, Goswami et al. 2008).

Generation of 16A5 cell lines with Dox-inducible ectopic EHD1 expression or EHD1/RUSC2 knockdown

To generate a 16A5 cell line with Dox-inducible EHD1 expression, cells were first stably transfected with pRevTet-On plasmid containing a Tet-responsive transcriptional activator (Clontech/TaKaRa) using Lipofectamine 2000 (Life Technologies), selected in medium containing 100 µg/ml G418, and individual G418-resistant, Tet-on clones were screened for inducible expression by transient transfection of pRevTRE-GFP and assessment of Dox-inducible GFP expression. A tightly inducible clone was used for stable transfection with pRevTRE-EHD1-GFP or the empty vector (pRevTRE-GFP) using Lipofectamine 2000 and selected in 50 µg/ml hygromycin, and clones were analyzed for inducible EHD1-GFP or GFP (vector only clones) after 7-day culture with 1 µg/ml Dox using Western blot analysis.

Dox-inducible lentiviral shRNA knockdown and control 16A5 cell lines (or 16A5 cells stably expressing Dox-inducible EHD1-GFP) were generated using lentiviral constructs (GE Healthcare) against EHD1 or RUSC2 (listed above). Viral transduction was performed according to the manufacturer's protocol using 14 μg/ml of Polybrene, and transductants were selected with a predetermined (2 μg/ml) concentration of puromycin for 7 days and subsequently maintained in the same concentration of puromycin.

Quantification of cell surface EGFR and MHC-1 using FACS analysis

16A5 cells were seeded at 105 cells per well of six-well plates (five replicates per condition) and grown in regular medium in the presence of Dox for 48 h. Cells were then either maintained in Dox-containing regular medium (steady state) or serum- and EGF-free D3 medium for 24 h, rinsed with ice-cold PBS, and released from dishes with trypsin-EDTA (Life Technologies). Trypsinization was stopped by adding trypsin inhibitor (Gibco). Cell suspensions were transferred to Eppendorf tubes and washed three times in ice-cold FACS buffer (1% bovine serum albumin in PBS) (Ahmad, Mohapatra et al. 2014). Live cells were stained with APC–anti-human EGFR antibody or anti-mouse IgG2a–APC control or with Brilliant Violet 605–anti-human HLA-A, -B, and -C or Brilliant Violet 605-mouse IgG2a isotype control. FACS analyses were performed on a Becton Dickinson LSRII instrument, and data were analyzed using FlowJo software.

Confocal immunofluorescence microscopy

Cells were grown on coverslips, transfected where indicated, and fixed with 4% paraformaldehyde in PBS. Fixed cells were permeabilized in 0.05% Triton X-100, blocked with 10% goat serum in PBS, and incubated with primary antibodies in 1% goat serum-PBS at 4°C overnight. After washes in PBS, the cells were incubated with the appropriate fluorochrome-conjugated secondary antibody for 1 h at room temperature. All images were acquired using a Zeiss 710 Meta confocal laser scanning microscope (Carl Zeiss) using a 40× or 63× objective with a numerical aperture of 1.0 and appropriate filters.

Merged fluorescence pictures were generated and analyzed using ZEN 2012 software from Carl Zeiss.

Western blotting

Following cell culture and the indicated treatments, cells were rinsed twice with ice-cold PBS, and dish-attached cells were directly lysed in ice-cold Triton X-100 lysis buffer (0.5% Triton X-100, 50 mM Tris [pH 7.5], 150 mM sodium chloride) (Fisher) containing Halt EDTA-free protease inhibitor cocktail and rotated overnight. The lysates were transferred to Eppendorf tubes and spun at 13,000 rpm for 30 min at 4°C, and supernatants were collected and quantified for protein using a Pierce bicinchoninic acid (BCA) assay reagent according to the manufacturer's directions (Thermo Scientific). Forty micrograms of protein lysates was resolved by 8% sodium dodecyl sulfate-polyacrylamide gel electrophoresis (SDS-PAGE), transferred to polyvinylidene fluoride (PVDF) membrane, and immunoblotted with the indicated antibodies.

Cell proliferation and viability assay

A CellTiter-Glo assay was performed according to the manufacturer's specifications (Promega).

Metabolic labeling and pulse-chase with [35S] methionine-cysteine

Cells pretreated with Dox were washed with and kept in methionine-cysteine-free medium (catalog no. 21013-024; Life Technologies) for 30 min and pulse-labeled with 100 μCi of [35S] methionine-cysteine (EXPRE35S35S protein labeling mix) for 20 min. The cells were then washed in medium without radioactive label and either immediately lysed (0-min chase) or incubated in regular medium with a 100-fold excess of unlabeled methionine-cysteine for a 30-, 90- or 270-min chase time before lysis. The lysates (500 μg protein) were subjected to immunoprecipitation with anti-EGFR antibody (clone 528), and the samples were resolved by SDS-PAGE. The gel was fixed, dried, and incubated with Auto-Fluor (LS-315; National Diagnostics) before drying, and signals were visualized by

autoradiography. For control cells, the above-mentioned steps were the same except that the Dox pretreatment was omitted.

FP competition assays

All fluorescence polarization (FP) measurements were performed in 384-well, low-volume, black round-bottom polystyrene NBS microplates (Corning). Assays were set up in a total volume of 20 µl, with 1× PBS as the assay buffer. To each well, increasing concentrations (0 to 1 mM) of 10 µl of unlabeled RUSC2 peptides (amino acids 43-NPFCPPELG-51 or 101-NPFLLQEGV-109) and 10 µl of a mixture of GST-EHD1 EH domain fusion protein (at a final concentration of 15 µM) and FITC-labeled competing peptide derived from MICAL-like 1 protein (amino acids 425-NPFEEEEED-433) (at a final concentration of 100 nM) were added. The polarization values were measured at an excitation wavelength of 485 nm and emission wavelength of 538 nm using a Spectramax M5 plate reader (Molecular Devices, Sunnyvale, CA).

GST fusion protein pulldown assays

For glutathione S-transferase (GST) pulldown assays, HEK293 cells were transiently transfected with GFP- or HA-tagged constructs in 10-cm dishes. Cells were grown for 48 h and lysed overnight at 4°C in 600 µl of lysis buffer containing 50 mM Tris (pH 7.5), 150 mM NaCl, and 0.5% Triton X-100 (wt/vol), 1 mM sodium orthovanadate, 10 mM sodium fluoride, and 0.5 mM phenylmethylsulfonyl fluoride (PMSF). Cell lysate was centrifuged at 13,000 rpm to pellet the insoluble material, and protein concentration in the cleared lysate was determined using BCA reagent. One milligram of total cell lysate was incubated with 25 µg of GST fusion proteins [GST-Ctrl, GST–EHD1-(399–534), and GST–EHD1-(399–534)-W485A, representing a GST control, a GST fusion with a truncated EHD1 consisting of residues 399 to 534, and a fusion with the truncated EHD1 with a point mutation, respectively] bound to glutathione-Sepharose beads. After 3 h of incubation at 4°C, the pulldown beads were washed six times in lysis buffer (described above) and

eluted in boiling sample buffer. Proteins were resolved by SDS–9% PAGE, transferred onto polyvinylidene difluoride (PVDF) membranes (IPVH00010; Millipore, Billerica, MA), and immunoblotted with anti-GFP (overnight at 4°C) or anti-HA (2 h at room temperature) antibodies. Bound antibodies were visualized using horseradish peroxidase (HRP)-conjugated protein A (10-1023; Life Technologies, Grand Island, NY) and enhanced chemiluminescence (ECL) detection (PI-32106; Thermo Scientific, Rockford, IL).

Coimmunoprecipitation analyses

For coimmunoprecipitation (co-IP) analyses, 1-mg aliquots of cleared lysate protein were incubated with optimized amounts of the indicated antibodies and rocked overnight at 4°C. Thirty microliters of protein G- or A-Sepharose beads (washed with PBS and blocked in 1% BSA) was added to each IP sample and rocked at 4°C for 3 h. The beads were washed six times with TX-100 lysis buffer, and bound proteins were resolved by SDS–9% PAGE, transferred to polyvinylidene difluoride (PVDF) membrane, and immunoblotted with anti-HA, anti-Myc, anti-EHD1, and anti-EGFR antibodies. Prior to washing protein G- or A-Sepharose beads, aliquots of supernatant (equal to 5% of the amount used for IP) were saved and run alongside the IP samples.

Statistical analyses

The results of densitometry analyses of Western blots, CellTiter-Glo assay of proliferation (as relative light units [RLU]), and flow cytometry analyses (as median mean fluorescence intensities [MFI]) were quantified and compared between groups using Student's t test, and data are presented as means ± standard errors of the means (SEM) of multiple experiments, with a P value of ≤0.05 deemed significant. Prism, version 4.0c (GraphPad), was used to perform the statistical analysis and graphical representations of the data.

2.3. Results

While a substantial body of literature has focused on mechanisms involved in the trafficking itinerary of ligand-activated EGFR and the impact of receptor activation on subsequent signaling and biological outcomes (Roepstorff, Grandal et al. 2009, Sigismund, Woelk et al. 2005, Goh, Huang et al. 2010), relatively little is known about the regulatory mechanisms that control the trafficking of unstimulated EGFR to ensure a cell-optimal display of activation-ready EGFR at the cell surface. Given the role of EHD family proteins, in particular EHD1, in the surface expression of non-RTK receptors and our previous observation that EHD1 colocalized with the oncogenic mutant EGFR in the endocytic recycling compartment (Chung, Raja et al. 2009), we examined the role of EHD1 in the surface display of EGFR under unstimulated conditions.

EHD1 KD reduces the total EGFR levels on 16A5 MECs both under steady-state and ligand-free culture.

16A5 is a nontumorigenic, human papillomavirus 16 (HPV16) E6/E7-immortalized and EGF-dependent human mammary epithelial cell (MEC) line (Band, Sager 1989) that displays the expected ligand-induced EGFR degradation kinetics (Fukazawa, Miyake et al. 1996, Duan, Miura et al. 2003, Duan, Chen et al. 2010, Dimri, Naramura et al. 2007, Duan, Raja et al. 2011) (Fig. 2.1A). 16A5 as well as other cell lines, including the triple-negative breast cancer cell line MDA-MB-231 and the pancreatic cancer cell line S2013 used in this work, express EHD1 as well as other EHD proteins (Fig. 2.1B); mouse embryonic fibroblasts (MEFs), the other cell type we use, are known to express EHD1 and other family members as well, and EHD1 was critical for primary cilium biogenesis in these cells (Bhattacharyya, Rainey et al. 2016). To examine the impact of EHD1 knockdown (KD) on total EGFR levels, we transduced 16A5 cells with doxycycline (Dox)-inducible lentiviral constructs expressing a control non-targeting short hairpin RNA (shRNA) or an

shRNA directed against the 3′ untranslated region (UTR) of EHD1. Cells were kept at steady state in EGF-containing DFCI medium (Band, Sager 1989) and pretreated with Dox for 3 days to induce sufficient EHD1 KD; cells were then re-plated in Dox, and lysates were prepared over a 5-day time course and analyzed by Western blotting. Under conditions of EHD1 KD, we observed a steady reduction in total EGFR levels over the course of the experiment (Fig. 2.1C and D). We then sought to determine whether the observed depletion was dependent on ligand stimulation. Absence of EGF is known to lead to accumulation of EGFR in an inactive state (unphosphorylated) and increased localization at the cell surface as the receptor is not subject to ligand-induced lysosomal degradation (Alexander 1998). To determine the impact of EHD1 KD under basal ligand-free conditions, we used the 16A5 cell lines engineered with two distinct shRNA sequences targeting EHD1 or a non-targeting control. The cells were pretreated with Dox for 3 days under steady-state conditions and re-plated in Dox. After 24 h, cells were subjected to EGF deprivation in conjunction with continued Dox treatment and assayed at the indicated time points (0, 6, 12, and 24 h). Total EGFR levels measured by Western blotting were reduced in EHD1 KD cells relative to levels in controls, as seen in representative blots and quantified data from three independent experiments (Fig. 2.1E and F). To further validate this finding, we carried out overnight transfection of 16A5 cells with distinct siRNAs directed against EHD1 in low-serum Opti-MEM and allowed the cells to recover in regular culture medium for 24 h. Cells were then switched to EGF-free medium for 24 h, followed by Western blotting of lysates. We observed a moderate depletion of total EGFR levels in EHD1 KD cells relative to levels in controls (Fig. 2.1G and H).

Although the use of multiple distinct siRNAs or shRNAs and analysis of knockout MEFs (see below) make any off-target effects of the knockdown approach remote, we carried out rescue analyses to rigorously validate our findings. We generated 16A5 cell

lines that coexpress an exogenous Dox-inducible EHD1-green fluorescent protein (GFP) fusion construct lacking the 3′ UTR of EHD1, and thus resistant to the EHD1 3′ UTR-targeted shRNAs, together with the EHD1-directed shRNA or a control shRNA. Cells were pretreated with Dox for 2 days prior to initiating serum and EGF deprivation. Cells coexpressing the shRNA-resistant EHD1-GFP together with EHD1-specific shRNA displayed total EGFR levels comparable to those in the EHD1-GFP-expressing cell line coexpressing a control shRNA. In contrast, cells transduced with only a control empty vector in conjunction with the EHD1 shRNA displayed reduced EGFR levels (Fig. 2.1I and J).

EHD1 knockdown reduces the cell surface EGFR levels on 16A5 mammary epithelial cells under ligand-free culture.

To assess if EHD1 KD impacted the surface EGFR expression, we examined the cell surface levels of EGFR in control and EHD1 KD 16A5 cells using fluorescence-activated cell sorter (FACS) analysis. Correlating with the depletion of total levels of EGFR, the surface EGFR levels were reduced in EHD1 KD cells relative to levels of the controls (Fig. 2.2A and B). To assess if non-RTK receptor expression is impacted by EHD1 depletion under the conditions where we observe an impairment of EGFR expression, we carried out FACS analysis of MHC class I (MHC-I) expression in control and EHD1 KD 16A5 cells cultured under conditions similar to those used for EGFR analyses (growth in serum- and EGF-deprived medium). Previous studies in which MHC-I internalized from the cell surface was tracked showed that EHD1 is required for exit of MHC-I from the endocytic recycling compartment back to the cell surface (Fig. 2.2C and D). However, MHC-I cell surface levels were comparable in EHD1 KD and control cells.

EHD1 knockout or knockdown in other cell systems reduces the total EGFR levels under ligand-free culture.

To determine whether the reduction in total EGFR levels upon EHD1 depletion could be seen in cell types other than the 16A5 MECs, we used an isogenic pair of EHD1-floxed and EHD1-null mouse embryonic fibroblasts (MEFs) (Bhattacharyya, Rainey et al. 2016). MEFs were plated in regular medium (without supplemental EGF) for 2 days, followed by treatment with 2 nM EGF for 4.5 h to promote EGFR degradation, and the cells were then subjected to serum and EGF deprivation. As in 16A5 cells, we observed a diminished capacity for the recovery of total EGFR levels over time in EHD1-null MEFs compared to levels in control MEFs although the impact was modest (Fig. 2.3A and B). Moderate EHD1 dependence of the accumulation of EGFR after serum and EGF deprivation was also seen when we compared control shRNA and EHD1 shRNA-expressing versions of a triple-negative breast cancer cell line, MDA-MB-231 (Fig. 2.3C and D), or a pancreatic adenocarcinoma cell line, S2013 (Fig. 2.3E).

Based on these findings, we conclude that EHD1 plays a key positive role in the maintenance of total and cell surface levels of EGFR under basal, ligand-unstimulated conditions.

EHD1 and EGFR colocalize in intracellular vesicular structure.

Given the impact of EHD1 depletion on the total and cell surface levels of unstimulated EGFR, we considered the possibility that EHD1 regulates the intracellular trafficking of EGFR. To determine whether EHD1 colocalizes with EGFR, 16A5 cells were deprived of serum and EGF for 6 h in the presence of either dimethyl sulfoxide (DMSO) or 10 μM monensin and subjected to immunofluorescence costaining of endogenous EGFR and EHD1. Monensin treatment was included as we previously found it to enhance the colocalization of lung cancer-associated EGFR mutants with EHD1 in the endocytic recycling compartment (Chung, Raja et al. 2009). Consistent with previous reports using other cell types (Barzilay, Ben-Califa et al. 2005), monensin treatment of 16A5 cells

increased the accumulation of EGFR in perinuclear vesicles, indicating an effective inhibition of cargo exit from endocytic compartments. EHD1+/EGFR+ vesicles were observed as sparse puncta in DMSO-treated cells (Fig. 2.4A); however, a clear perinuclear EHD1 and EGFR colocalization was observed in monensin-treated cells (Fig. 2.4B). When an exogenous EHD1-DsRed construct was expressed via transient transfection, the colocalization with endogenous EGFR became obvious even in the absence of monensin treatment (Fig. 2.4C) and was more robust in monensin-treated cells (Fig. 2.4D). Since cells in regular culture (in EGF-containing medium) showed little surface and intracellular staining and barely detectable EGFR by blotting (Fig. 2.1C), the accumulation of cell surface EGFR upon removal of EGF is likely to be largely dependent on transport from the Golgi compartment to the cell surface of newly synthesized EGFR. Thus, we reasoned that EHD1 may function in part by regulating EGFR trafficking at the Golgi apparatus. Three-color confocal immunofluorescence staining of endogenous EGFR and the Golgi marker GM130 with ectopically expressed EHD1-DsRed demonstrated that a pool of EHD1 and EGFR was colocalized at the Golgi compartment (Fig. 2.4E and F). In view of the colocalization of EHD1 and EGFR, we asked if the two proteins physically associate with each other. To this end, we carried out anti-EHD1 or anti-EGFR immunoprecipitations (IPs) from lysates of EGF-deprived 16A5 cells, followed by immunoblotting for EGFR or EHD1, respectively. In each case, efficient IP of EHD1 or EGFR was established by immunoblotting for the cognate protein and by its depletion in the supernatants remaining after IP (Fig. 2.4G). No co-IP between EHD1 and EGFR, however, was observed. Thus, while EHD1 and EGFR do not appear to physically interact, they colocalize in intracellular compartments, consistent with a role of EHD1 in the intracellular traffic of EGFR.

EHD1 knockdown results in EGFR retention in the Golgi apparatus.

Given the EGFR and EHD1 colocalization at the Golgi apparatus, we asked if EHD1 functions in EGFR trafficking out of the Golgi compartment, using the inducible knockdown and EHD1-GFP rescue 16A5 cell lines. Cells were switched from regular, EGF-containing medium to a serum- and EGF-free medium and analyzed for EGFR localization at various time points up to 24 h using confocal imaging. Under steady-state conditions, weak EGFR (green) signals seen at time zero were predominantly intracellular, partly localizing to the perinuclear area (Fig. 2.5A). In EHD1-GFP-expressing rescue cells, some perinuclear EGFR colocalized with EHD1 (pseudocolored red). Upon EGF removal from the medium, EGFR in the control cell line (no Dox treatment) and in the EHD1-GFP rescue cell line (treated with Dox) progressively localized to the cell surface, as expected. In contrast, cells with EHD1 KD but without EHD1 rescue exhibited strong perinuclear EGFR accumulation with correspondingly lower surface EGFR signals (Fig. 2.5A). This perinuclear compartment was identified as the Golgi compartment, based on GM130+ costaining (Fig. 2.5B).

IPs with an antibody that recognizes the mature EGFR (clone 528) (Johns, Mellman et al. 2005) from lysates of cells that were metabolically pulse-labeled with [35S] methionine-cysteine and chased in label-free medium for the indicated times (0, 30, 90, or 270 min) revealed that a smaller fraction of the newly synthesized EGFR was converted to the mature form in EHD1 KD 16A5 cells and with a delay (Fig. 2.5C). The increase in radiolabel during the 4-h chase in control cells (Fig. 2.5C) is consistent with the EGFR becoming more antibody reactive as the receptor undergoes posttranslational modification, as shown previously (Franovic, Gunaratnam et al. 2007, Gamou, Shimizu 1987).

The Golgi retention of EGFR in EHD1-depleted cells following a switch to EGF-free medium and the results of metabolic pulse-chase analyses support a role of EHD1 in

anterograde trafficking of EGFR out of the Golgi compartment. However, given the recently identified roles of EHD proteins in retrograde trafficking of endocytic cargo, we assessed if EGFR undergoes retrograde trafficking from the cell surface in the absence of ligand stimulation and whether this process is defective in EHD1 KD cells. Previous studies of nuclear localization of EGFR have concluded that EGFR traffics via a retrograde endocytic route, but such studies were done in the presence of ligands (Wang, Y. N., Wang et al. 2010). Cells cultured with or without Dox were subjected to serum and EGF deprivation for 6 h and chilled on ice for 20 min, and live cells on ice were stained with a biotinylated anti-EGFR antibody to visualize the internalized EGFR with fluorescein isothiocyanate (FITC)-conjugated NeutrAvidin (Fig. 2.5D, pulsed). Cells were then rinsed with ice-cold phosphate-buffered saline (PBS) and incubated at 37°C for 18 h in serum- and EGF-free medium before fixation. Cells without prestaining of the surface EGFR were processed in parallel (Fig. 2.5D, not pulsed). Fixed cells were permeabilized and stained for GM130 and the recycling endosome marker Rab11 (Calhoun, Goldenring 1996). Control cells that were not prestained with anti-EGFR–biotin were also stained for EGFR. Under these conditions, we observed that EGFR prelabeled at the cell surface accumulated in a GM130/Rab11 double-positive, perinuclear compartment in EHD1 KD cells, as also seen in cells that were not prelabeled on the cell surface (Fig. 2.5D). Very little surface-labeled EGFR was seen to accumulate in the same compartment in control cells (Fig. 2.5D). This result indicates that EHD1 also regulates the exit of the EGFR pool that enters the Golgi compartment after endocytosis and retrograde transport from the cell surface.

EHD1 knockdown reduces the EGF-dependent cell proliferation.

To assess the functional consequences of EHD1 KD in MECs, we first examined if the reduction in EGFR levels upon EHD1 KD was accompanied by reduced downstream

signaling output. Indeed, EHD1 KD 16A5 cells exhibited substantially reduced EGFR phosphorylation upon stimulation with EGF, as visualized by phosphotyrosine immunoblotting of cell lysates (Fig. 2.6A and B). In view of reduced ligand-induced EGFR phosphorylation seen upon EHD1 depletion, we compared the time course of EGF-induced proliferation of 16A5 cells with or without EHD1 KD, using a CellTiter-Glo assay. Cells engineered with two distinct Dox-inducible EHD1 shRNAs or a control shRNA were kept in Dox for the duration of the experiment. Both EHD1 KD 16A5 lines displayed significantly reduced proliferation relative to that of control shRNA-expressing cells (Fig. 2.6C). These results were confirmed by assessing the proliferation of Dox-inducible EHD1 KD 16A5 cells upon culture with and without Dox (Fig. 2.6D).

RUSC2 is a novel potential EHD1 partner that colocalizes with EGFR at the Golgi compartment.

In view of our findings that EHD1 plays a key positive role in the cell surface expression of unstimulated EGFR, we were intrigued by a proteomics analysis of unstimulated EGFR-associated protein complex in which RUSC2 was reported as an uncharacterized component (Deribe, Wild et al. 2009). We noted two potential EHD1 EH domain-binding NPF motifs in RUSC2 (amino acids 43-NPFCPPELG-51 and 101-NPFLLQEGV-109) which bound with moderate affinity to the EH domain of EHD1 in an in vitro fluorescence polarization-based competition assay using a labeled peptide derived from MICAL-like 1 protein (amino acids 425-NPFEEEEED-433) as a probe (Fig. 2.7A). Using an antibody generated against a human RUSC2 peptide (see Materials and Methods), we found that RUSC2 was expressed in 16A5 cells. However, we could not detect the binding of full-length RUSC2 with the EHD1 EH domain, nor could we detect co-IP of ectopically cotransfected EHD1 and RUSC2, either when immunoprecipitated

hemagglutinin (HA)-RUSC2 was incubated with lysates of cells transfected with Myc-EHD1 or when HA-RUSC2 and Myc-EHD1 were cotransfected in HEK293T cells (Fig. 2.7B and C).

To determine if RUSC2 and EHD1 colocalize in intracellular vesicles, we first assessed the colocalization of endogenous EHD1 and RUSC2; the anti-RUSC2 antibody, however, proved suboptimal for imaging of endogenous RUSC2. We therefore cotransfected the EHD1-DsRed and HA-RUSC2 constructs into 16A5 cells to assess their colocalization by confocal imaging. Colocalization was observed when either endogenous EHD1 was immunostained along with exogenous HA-RUSC2 (Fig. 2.7D, top panel) or when HA-RUSC2 and EHD1-DsRed were examined (Fig. 2.7D, bottom panel). Vesicular and tubular HA-RUSC2 displayed a tight correlation with DsRed-EHD1 localized to similar structures (Fig. 2.7D, bottom panel).

Given the previous reports that RUSC2 directly interacts with GM130 as well as with Golgi-associated Rab1 (Bayer, Fischer et al. 2005), the prominent colocalization of RUSC2 with EHD1 led us to hypothesize that RUSC2, similar to EHD1, may function to promote the EGFR trafficking out of the Golgi compartment. We first assessed whether RUSC2 localizes in the Golgi compartment where EGFR accumulates upon EHD1 KD. Indeed, we observed significant three-color colocalization between EGFR, RUSC2, and GM130 upon EHD1 KD (Fig. 2.7E).

RUSC2 knockdown phenocopies the effects of EHD1 depletion on basal, unstimulated EGFR expression.

Given the above results, the reported RUSC2 interaction with GM130 (Bayer, Fischer et al. 2005) and the role of RUSC2-interacting small G-protein Rab1a in regulating trafficking from the Golgi compartment to the plasma membrane (Bayer, Fischer et al. 2005, Allan, Moyer et al. 2000, Mukhopadhyay, Quiroz et al. 2014) we reasoned that

RUSC2 may also function in EHD1-dependent EGFR trafficking out of the Golgi compartment. To test this idea, 16A5 cell lines expressing Dox-inducible shRNAs targeting RUSC2 were cultured in regular EGF-containing medium in the presence of Dox for 3 days to achieve RUSC2 KD. The cells were then cultured in serum- and EGF-free medium, and the accumulation of total EGFR levels over a 24-h time course was monitored using Western blotting. RUSC2 KD, using two independent shRNAs, led to a substantial impairment of the accumulation of total EGFR protein upon EGF withdrawal compared to levels in control cells; this effect was even more robust than that seen with EHD1 KD (Fig. 2.8A and B). Flow cytometry analyses of cells treated with Dox for 48 h in EGF-containing medium followed by Dox in serum and EGF deprivation medium for 24 h revealed a significant decrease in the cell surface EGFR levels in RUSC2 KD cells compared to levels in control cells, mimicking the impact of EHD1 KD (Fig. 2.8C and D).

To determine the functional consequences of the reduced cell surface EGFR expression upon RUSC2 KD, we cultured 16A5 cell lines expressing two distinct Dox-inducible RUSC2 shRNAs in the presence of Dox for 5 days and assessed the impact of RUSC2 depletion on cell proliferation. Indeed, RUSC2 KD led to a significant reduction in EGF-induced cell proliferation relative to the level in control shRNA cells (Fig. 2.8E).

Collectively, these results support our conclusion that RUSC2 and EHD1 function in a common pathway to positively regulate the basal traffic of EGFR from the Golgi compartment to the cell surface to ensure optimal surface receptor levels for subsequent ligand-mediated activation and cellular responses.

2.4. Figures

Figure 2.1

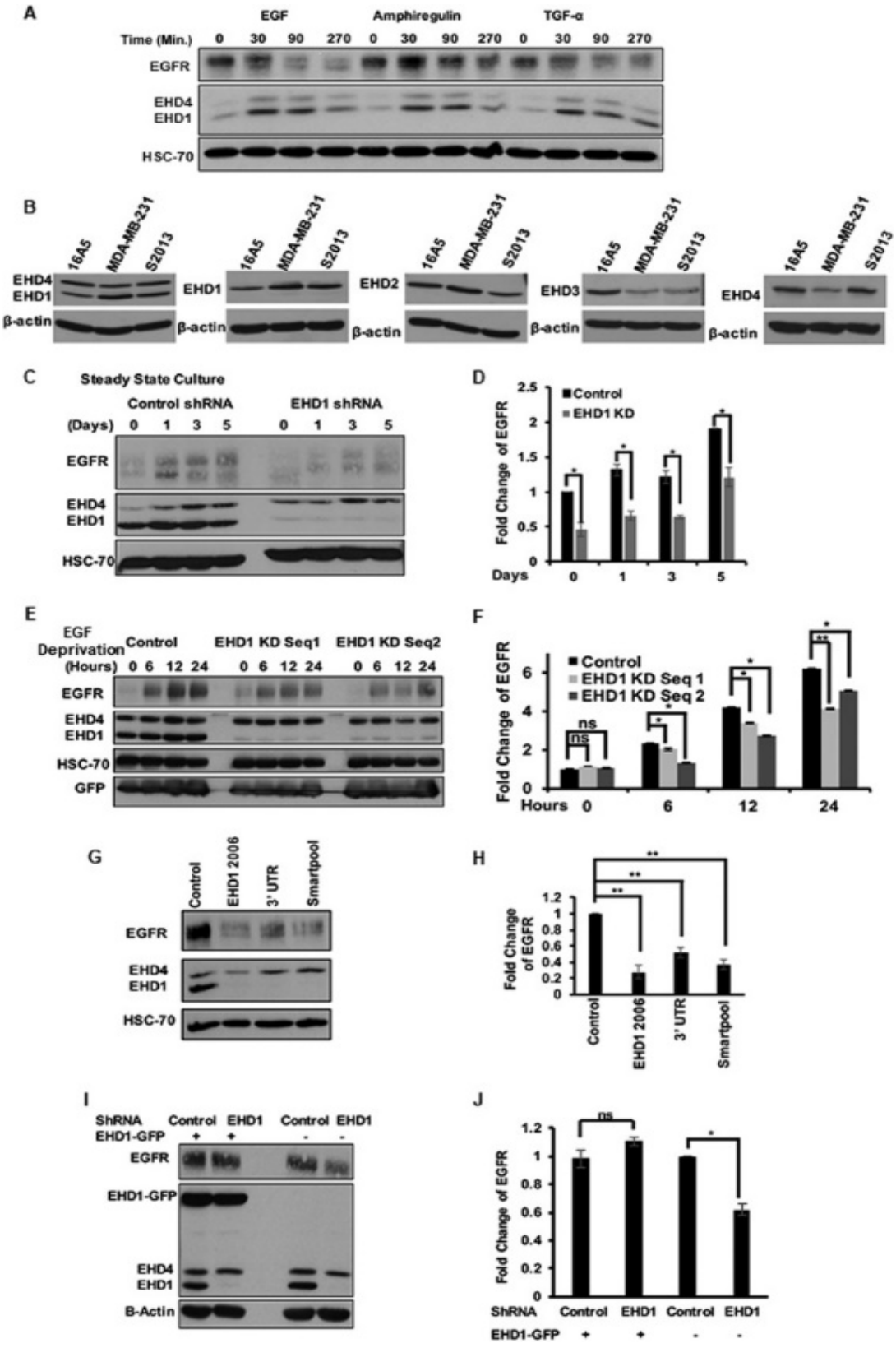
A
EGF
Amphiregulin
TGF-α
Time (Min.)
0 30 90 270 0 30 90 270 0 30 90 270
EGFR
EHD4
EHD1
HSC-70
B
16A5
MDA-MB-231
S2013
EHD4
EHD1
β-actin
EHD1
EHD2
EHD3
EHD4
C
Steady State Culture
Control shRNA
EHD1 shRNA
(Days) 0 1 3 5 0 1 3 5
EGFR
EHD4
EHD1
HSC-70
D
Control
EHD1 KD
Fold Change of EGFR
Days 0 1 3 5
E
EGF Deprivation
Control
EHD1 KD Seq1
EHD1 KD Seq2
(Hours) 0 6 12 24 0 6 12 24 0 6 12 24
EGFR
EHD4
EHD1
HSC-70
GFP
F
Control
EHD1 KD Seq 1
EHD1 KD Seq 2
Fold Change of EGFR
ns
Hours 0 6 12 24
G
Control
EHD1 2006
3' UTR
Smartpool
EGFR
EHD4
EHD1
HSC-70
H
Fold Change of EGFR
Control
EHD1 2006
3' UTR
Smartpool
I
ShRNA Control EHD1 Control EHD1
EHD1-GFP + + - -
EGFR
EHD1-GFP
EHD4
EHD1
B-Actin
J
Fold Change of EGFR
ns
ShRNA Control EHD1 Control EHD1
EHD1-GFP + + - -

Figure 2.1. EHD1 knockdown in 16A5 mammary epithelial cells leads to reduced total and cell surface EGFR levels.

(A) 16A5 cells respond to EGF ligands. The 16A5 immortalized human mammary epithelial cells were deprived of serum and EGF for 48 h and then treated with 2 nM EGF, amphiregulin, or transforming growth factor alpha (TGF-α) for the indicated times. Cell lysates were immunoblotted for EGFR, EHD1/4, and HSC-70 (loading control). Note that all ligands reduce the EGFR levels at late time points, more pronounced with EGF. **(B)** Relative expression of all four EHD proteins in cell lines examined in this work. Whole-cell lysates of the 16A5 MEC line, MDA-MB-231 breast cancer cell line, and S2013 pancreatic cancer cell line were immunoblotted with anti-EHD1/4, anti-EHD1, anti-EHD2, anti-EHD3, or anti-EHD4 antibodies as well as β-actin (loading control). **(C)** EHD1 knockdown reduces EGFR levels in 16A5 cells under steady-state culture. 16A5 cells stably transduced with Dox-inducible nontargeting or EHD1-targeted shRNA (EHD1 shRNA without specification indicates sequence 1 [Seq. 1] directed at the 3' region and refers to clone V2IHSPGG_388688; in other panels where Seq. 1 and 2 are specified, Seq. 2 refers to clone V2IHSPGG_908952) were treated with Dox over 5 days. Cells were maintained in regular medium (steady state), and lysates were collected at the indicated time points and blotted for EGFR and HSC-70 (loading control). **(D)** Densitometric quantification of EGFR results from the experiment shown in panel B (n = 3), normalized to the level for the HSC-70 control. *, $P < 0.05$. **(E)** EHD1 knockdown reduces EGFR levels in 16A5 cells under ligand-free culture. Stably transduced 16A5 cells expressing Dox-inducible nontargeting or EHD1-targeted shRNA sequences were cultured with Dox for 3 days before serum and EGF deprivation for the indicated times, and lysates were blotted for EGFR and HSC-70 (loading control). **(F)** Densitometric quantification of EGFR results from the experiment shown in panel D normalized to the level of HSC-70 (n = 3). *, $P < 0.05$; **, $P < 0.02$; ns, not significant. **(G)** Reduction in EGFR levels in 16A5 cells after transient siRNA

knockdown of EHD1. 16A5 cells were transiently transfected with the indicated control or EHD1-targeted siRNA oligonucleotides. Lysates of cells deprived of EGF and serum for 24 h were blotted for EGFR, EHD1/4, and HSC-70. **(H)** Quantification of results presented in panel G normalized to the level for HSC-70 ($n = 3$). *, $P < 0.05$; **, $P < 0.02$. **(I and J)** Rescue of the effect of EHD1 knockdown on EGFR levels by exogenous, shRNA-resistant EHD1. 16A5 cells stably transduced with nontargeting control or EHD1 3′-UTR-targeted shRNA (Seq. 1) were cotransduced with either Dox-inducible EHD1-GFP or empty vector. Cells pretreated with Dox were EGF and serum starved for 24 h, and lysates were blotted for EGFR and β-actin (loading control). Densitometric quantification of EGFR levels presented in panel H were normalized to the level for β-actin ($n = 3$). *, $P < 0.05$, **, $P < 0.02$; ns, not significant.

Figure 2.2

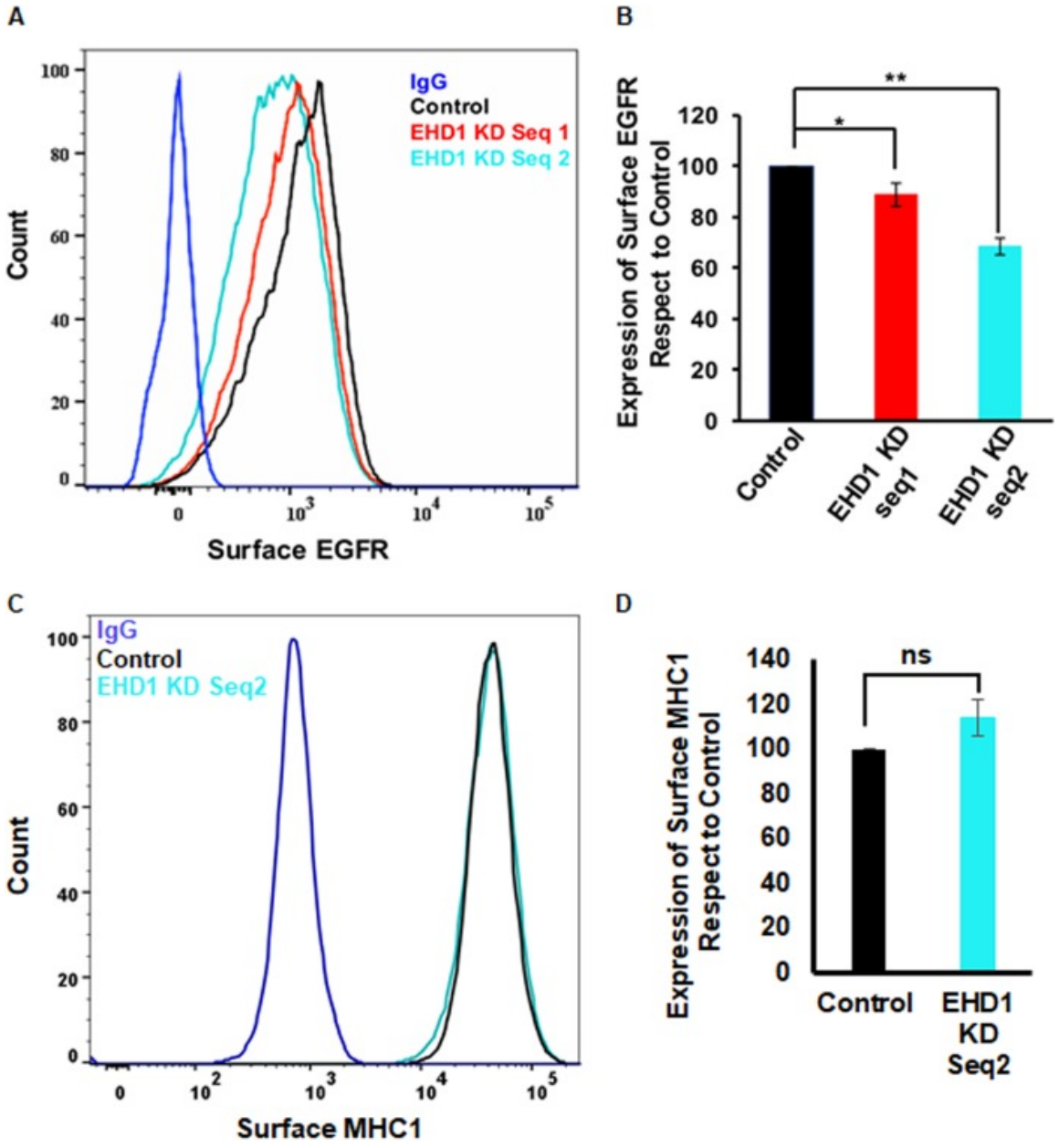
A
IgG
Control
EHD1 KD Seq 1
EHD1 KD Seq 2
Count
Surface EGFR
B
Expression of Surface EGFR Respect to Control
**
*
Control
EHD1 KD seq1
EHD1 KD seq2
C
IgG
Control
EHD1 KD Seq2
Count
Surface MHC1
D
Expression of Surface MHC1 Respect to Control
ns
Control
EHD1 KD Seq2

Figure 2.2. EHD1 knockdown leads to reduction in the cell surface EGFR levels in 16A5 cells.

(A) Reduction in cell surface EGFR upon EHD1 KD in 16A5 cells analyzed by FACS. 16A5 cells stably transduced with Dox-inducible nontargeting or EHD1-targeted shRNA (Seq. 1 or Seq. 2) were cultured under steady-state for 2 days prior to a 24-h EGF and serum deprivation with Dox present all the time. Live cells were analyzed by FACS for surface expression of EGFR. **(B)** Quantification of mean fluorescence intensities of results presented in panel A. Values are means plus standard errors of the means for $n = 4$. *, $P < 0.05$; **, $P < 0.02$; ns, not significant. **(C)** EHD1 KD did not reduce surface MHC class I (MHC-I) levels on 16A5 cells. 16A5 cells stably transduced with Dox-inducible nontargeting or EHD1-targeted shRNAs (Seq. 2) were cultured as described for panel A and analyzed by FACS for cell surface levels of MHC-I. **(D)** Quantification of mean fluorescence intensities of results presented in panel C. Values are means plus standard errors of the means for $n = 3$.

Figure 2.3

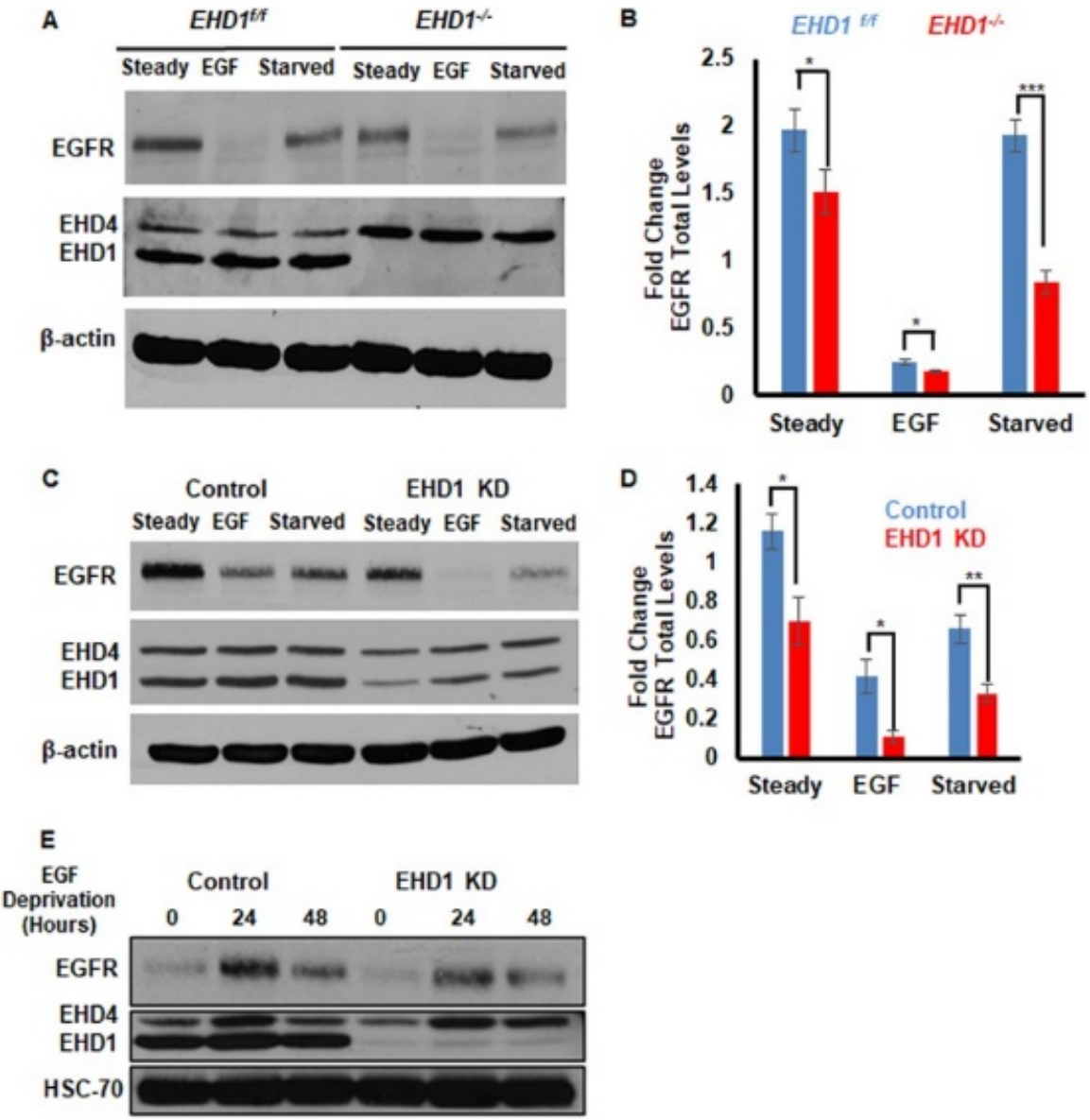
A
EHD1f/f
EHD1-/-
Steady EGF Starved Steady EGF Starved
EGFR
EHD4
EHD1
β-actin
B
EHD1 f/f
EHD1-/-
Fold Change EGFR Total Levels
2.5
2
1.5
1
0.5
0
*
*
***
Steady
EGF
Starved
C
Control
EHD1 KD
Steady EGF Starved Steady EGF Starved
EGFR
EHD4
EHD1
β-actin
D
Fold Change EGFR Total Levels
1.4
1.2
1
0.8
0.6
0.4
0.2
0
Control
EHD1 KD
*
*
**
Steady
EGF
Starved
E
EGF Deprivation (Hours)
Control
EHD1 KD
0 24 48 0 24 48
EGFR
EHD4
EHD1
HSC-70

Figure 2.3. EHD1 knockout or knockdown in additional cell types leads to reduced EGFR levels under ligand-free culture.

(A) Reduction in EGFR level in EHD1 knockout MEFs. EHD1flox/flox (EHD1f/f) and EHD1−/− MEFs were cultured in the presence of 2 nM EGF for 4.5 h to promote EGFR degradation and switched to serum starvation medium to assess the accumulation of EGFR. Lysates were blotted for EGFR, EHD1/4 and β-actin. **(B)** Densitometric quantification of EGFR signals presented in panel A normalized to the value of the β-actin loading control (n = 3). *, $P < 0.05$; ***, $P < 0.001$. **(C)** Reduction in EGFR level by EHD1 KD in MDA-MB-231 breast cancer cell line. MDA-MB-231 triple-negative breast cancer cells stably expressing nontargeting control or EHD1-targeted (Seq. 1) Dox-inducible shRNAs were pretreated with Dox for 2 days, stimulated with 2 nM EGF for 4.5 h to deplete the EGFR protein, and switched to low-serum medium without EGF to assess the EGFR accumulation by Western blotting of lysates. **(D)** Densitometric quantification of EGFR signals presented in panel C normalized to the level of the β-actin loading control (n = 3). *, $P < 0.05$; **, $P < 0.02$. **(E)** Reduction in EGFR levels by EHD1 KD in the S2013 pancreatic cancer cell line. S2013 pancreatic adenocarcinoma cells were transiently transfected with a nontargeting (control) or EHD1-targeted siRNA, and cells were treated as described for MDA-MB-231 cells in panel C, followed by Western blotting of lysates for EGFR, EHD1/4, and HSC-7

Figure 2.4

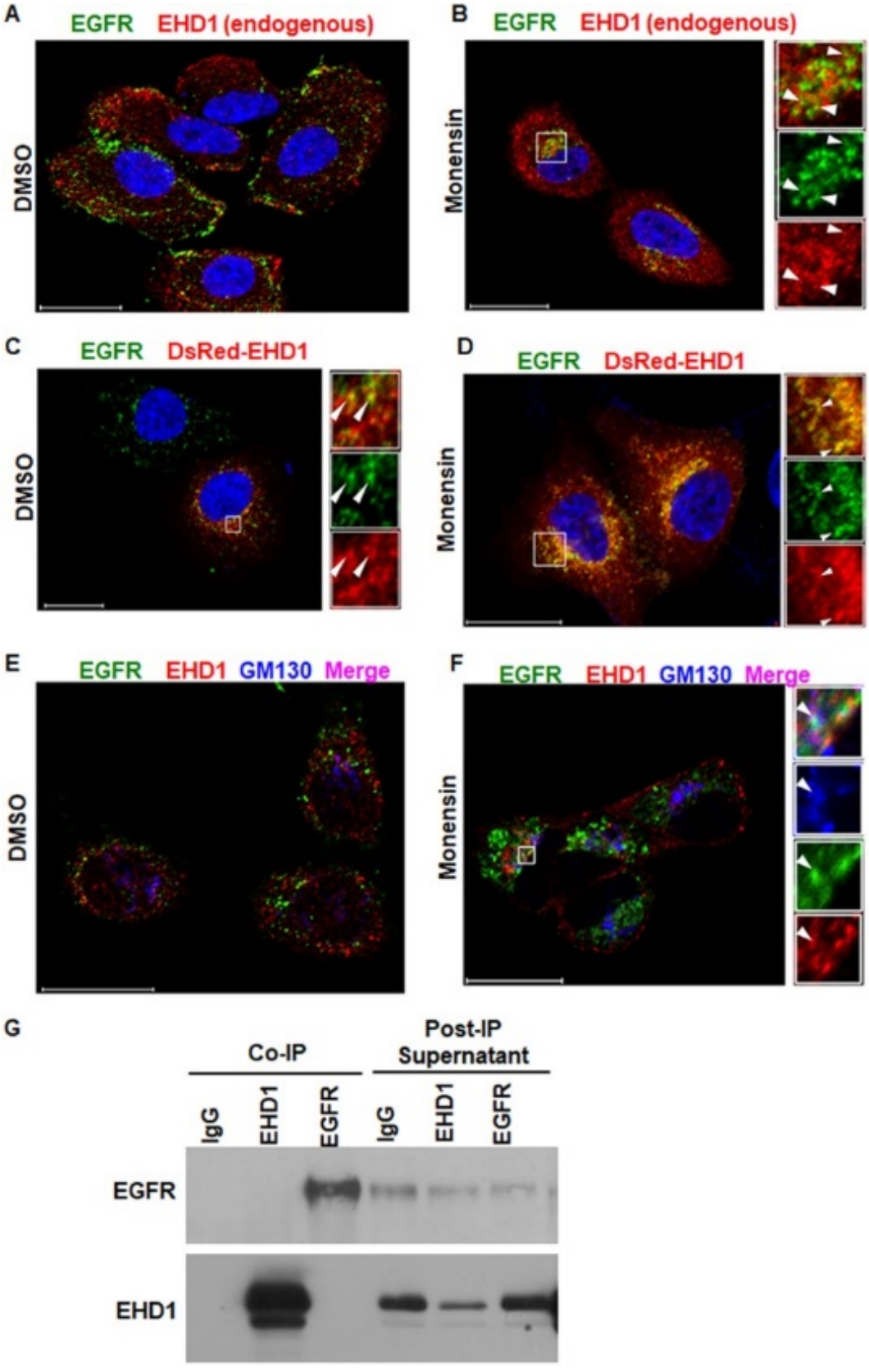
A
EGFR EHD1 (endogenous)
DMSO
B
EGFR EHD1 (endogenous)
Monensin
C
EGFR DsRed-EHD1
DMSO
D
EGFR DsRed-EHD1
Monensin
E
EGFR EHD1 GM130 Merge
DMSO
F
EGFR EHD1 GM130 Merge
Monensin
G
Co-IP
Post-IP Supernatant
IgG
EHD1
EGFR
IgG
EHD1
EGFR
EGFR
EHD1

Figure 2.4. EHD1 and EGFR colocalization in intracellular vesicular structures.

Non-transfected or transiently DsRed-EHD1-transfected 16A5 cells were subjected to serum and EGFR deprivation for 6 h and concurrently treated with DMSO or monensin (10 μM), followed by immunofluorescence staining of fixed and permeabilized cells for EGFR (green) or GM130 (blue). Colocalization is indicated by arrowheads in the insets on the right. **(A and B)** Localization of endogenous EHD1 and EGFR in DMSO- and monensin-treated non-transfected 16A5 cells. Nuclei were stained with 4′,6′-diamidino-2-phenylindole (blue). **(C and D)** Localization of transfected DsRed-EHD1 and endogenous EGFR in DMSO-treated and monensin-treated 16A5 cells. Nuclei are stained with 4′,6′-diamidino-2-phenylindole (blue). **(E and F)** Localization of transfected DsRed-EHD1 and endogenous EGFR and GM130 (blue) in 16A5 cells treated with 4′,6′-diamidino-2-phenylindole and monensin treated. Serial z-sections were obtained to validate the colocalization, which is shown in an orthogonal view. Scale bars, 5 μm. **(G)** Lack of coimmunoprecipitation between EHD1 and EGFR. 16A5 cells were serum and EGF deprived for 24 h, and 1-mg aliquots of protein lysate were subjected to immunoprecipitation with control antibody, anti-EGFR antibody, or anti-EHD1 antibody. Prior to washing the protein G- or A-Sepharose beads used for capture of IPs, aliquots of the supernatant equivalent to 5% of the lysate used for IPs were saved and concurrently run alongside the IPs and immunoblotting for EGFR or EHD1 was performed. Note a lack of co-IP between EHD1 and EGFR; supernatants indicate effective depletion of the cognate proteins during IP, as expected. The remnant of the band in the IP next to the last lane is due to cropping out a positive-control band for EHD1.

Figure 2.5

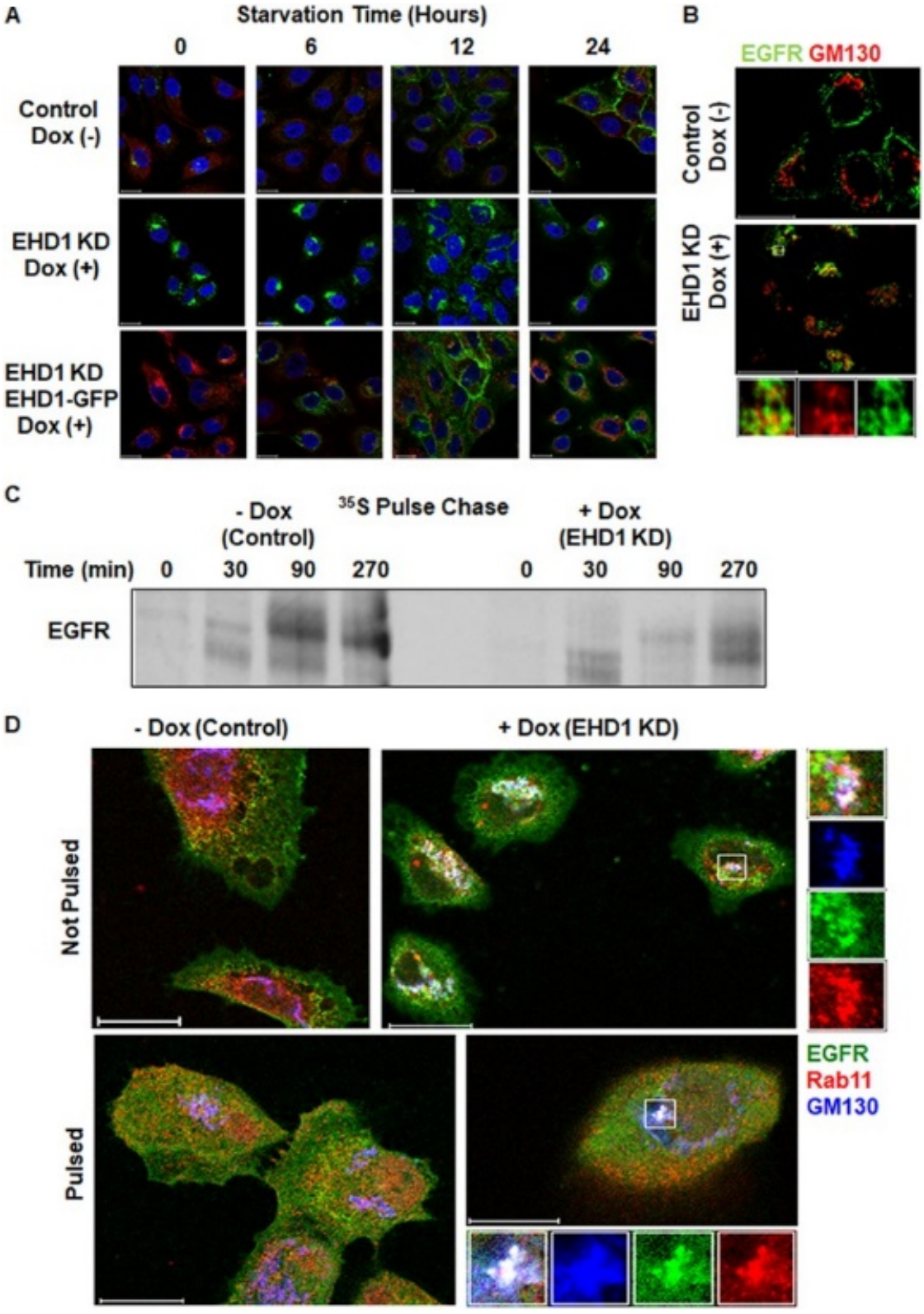
A
Starvation Time (Hours)
0
6
12
24
Control Dox (-)
EHD1 KD Dox (+)
EHD1 KD EHD1-GFP Dox (+)
B
EGFR GM130
Control Dox (-)
EHD1 KD Dox (+)
C
- Dox (Control)
35S Pulse Chase
+ Dox (EHD1 KD)
Time (min) 0 30 90 270 0 30 90 270
EGFR
D
- Dox (Control)
+ Dox (EHD1 KD)
Not Pulsed
Pulsed
EGFR
Rab11
GM130

Figure 2.5. EHD1 knockdown leads to EGFR retention in the Golgi apparatus. **(A)** Perinuclear accumulation of EGFR upon EHD1 KD in 16A5 cells and rescue of the defect by exogenous EHD1. 16A5 cells expressing Dox-inducible EHD1 shRNA (Seq. 1) were cultured without [Control Dox (−)] or with [EHD1 KD Dox (+)] Dox, or the same cells stably expressing Dox-inducible EHD1-GFP were cultured with Dox, as indicated. Cells were then switched to Dox with or without serum and EGF deprivation medium (starvation) for the indicated times, followed by staining for EGFR (green in the top and middle panels; red, pseudocolored green, in the bottom panel), EHD1 (red; top and middle panels), GFP (bottom panel; pseudocolored red), and nuclei (4′,6′-diamidino-2-phenylindole; blue) and subjected to confocal imaging. Note the accumulation of EGFR (green) in an intracellular compartment upon starvation under the EHD1 KD condition (middle panel; reduced red staining) and rescue of this phenotype by EHD-1 GFP (pseudocolored red; bottom panel). **(B)** Perinuclear EGFR in EHD1 KD 16A5 cells colocalizes with Golgi marker GM130. Intracellular EGFR colocalizes with GM130 upon EHD1 KD [Dox (+)] in contrast to results for the control [Dox (−)]. Dox treatment and serum and EGF deprivation for 24 h were performed as described for panel A. **(C)** Delayed maturation of newly synthesized EGFR upon EHD1 knockdown. 16A5 cells stably expressing a Dox-inducible EHD1 shRNA and cultured without (−Dox) or with (+Dox) Dox were metabolically pulse-labeled with [35S] methionine-cysteine, followed by chase for the indicated times. Anti-EGFR immunoprecipitates using antibody 528 were imaged by fluorography. A representative of three experiments is shown. **(D)** EHD1 KD in 16A5 cells impairs the retrograde trafficking of surface EGFR to the Golgi compartment Cells cultured with or without Dox were subjected to serum and EGF deprivation for 6 h and chilled on ice for 20 min, and live cells were stained with a biotinylated anti-EGFR antibody on ice (pulsed). Cells were rinsed with ice-cold PBS and incubated at 37°C for 18 h in serum- and EGF-free medium before

fixation. Cells without surface EGFR staining were processed in parallel (not pulsed). Cells were fixed, permeabilized, and stained as before for GM130 and Rab11 and for EGFR in cells that were not previously stained with anti-EGFR–biotin. Biotinylated antibody against EGFR was visualized with FITC-conjugated NeutrAvidin.

Figure 2.6

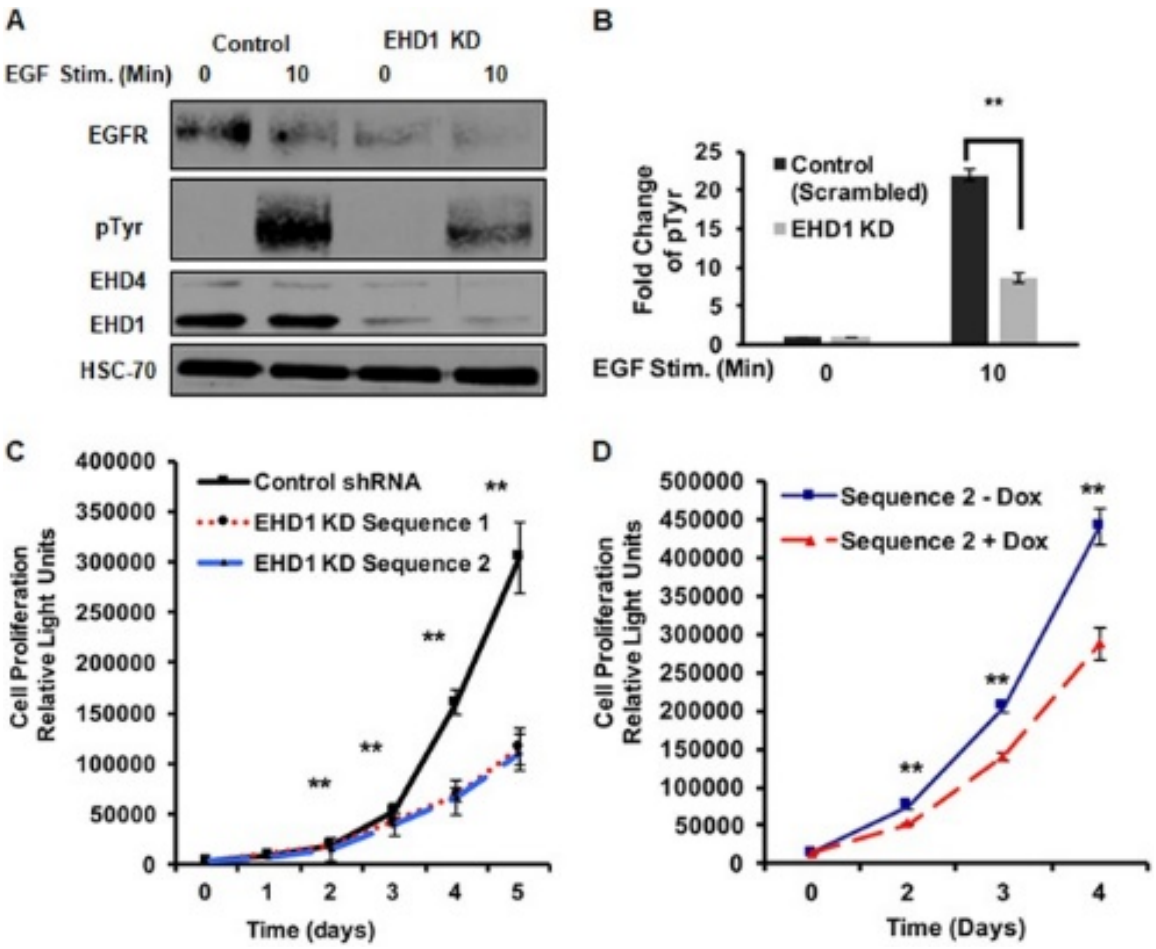
A
Control
EHD1 KD
EGF Stim. (Min) 0 10 0 10
EGFR
pTyr
EHD4
EHD1
HSC-70
B
Fold Change of pTyr
Control (Scrambled)
EHD1 KD
EGF Stim. (Min) 0 10
C
Cell Proliferation Relative Light Units
Control shRNA
EHD1 KD Sequence 1
EHD1 KD Sequence 2
Time (days)
D
Cell Proliferation Relative Light Units
Sequence 2 - Dox
Sequence 2 + Dox
Time (Days)

Figure 2.6. EHD1 knockdown reduces EGF-dependent cell signaling and cell proliferation.

(A) EHD1 KD impairs the EGF-induced tyrosine phosphorylation of EGFR. 16A5 cells were transiently transfected with a control or EHD1 3′ UTR-targeted siRNA, and cells were EGF and serum starved for 48 h, followed by EGF (2 nM) stimulation (Stim) for 10 min; lysates were then blotted for EGFR, phosphotyrosine (pTyr), EHD1/4, and HSC-70. The major band in the phosphotyrosine blot corresponds to phosphorylated EGFR. **(B)** Densitometric quantification of phosphorylated EGFR bands presented in panel A, normalized to the level of HSC-70 ($n = 3$). **, $P < 0.02$. **(C and D)** Impaired EGF-induced proliferation of 16A5 cells upon EHD1 KD. A total of 1,500 16A5 cells expressing a nontargeting control shRNA or EHD1 shRNA (Seq. 1 or 2) were plated in the inner wells of 96-well plates (60 replicates/time point) and cultured in EGF (2 nM)-containing medium for 5 days in the presence of Dox. Cell proliferation was assessed on each day using a CellTiter-Glo assay (C). 16A5 cells expressing EHD1 shRNA (Seq. 2) were cultured in EGF-containing medium without (−) or with (+) Dox, and a CellTiter-Glo assay was performed on the indicated days (60 replicates per time point) (D). **, $P < 0.02$, by Student's t test.

Figure 2.7

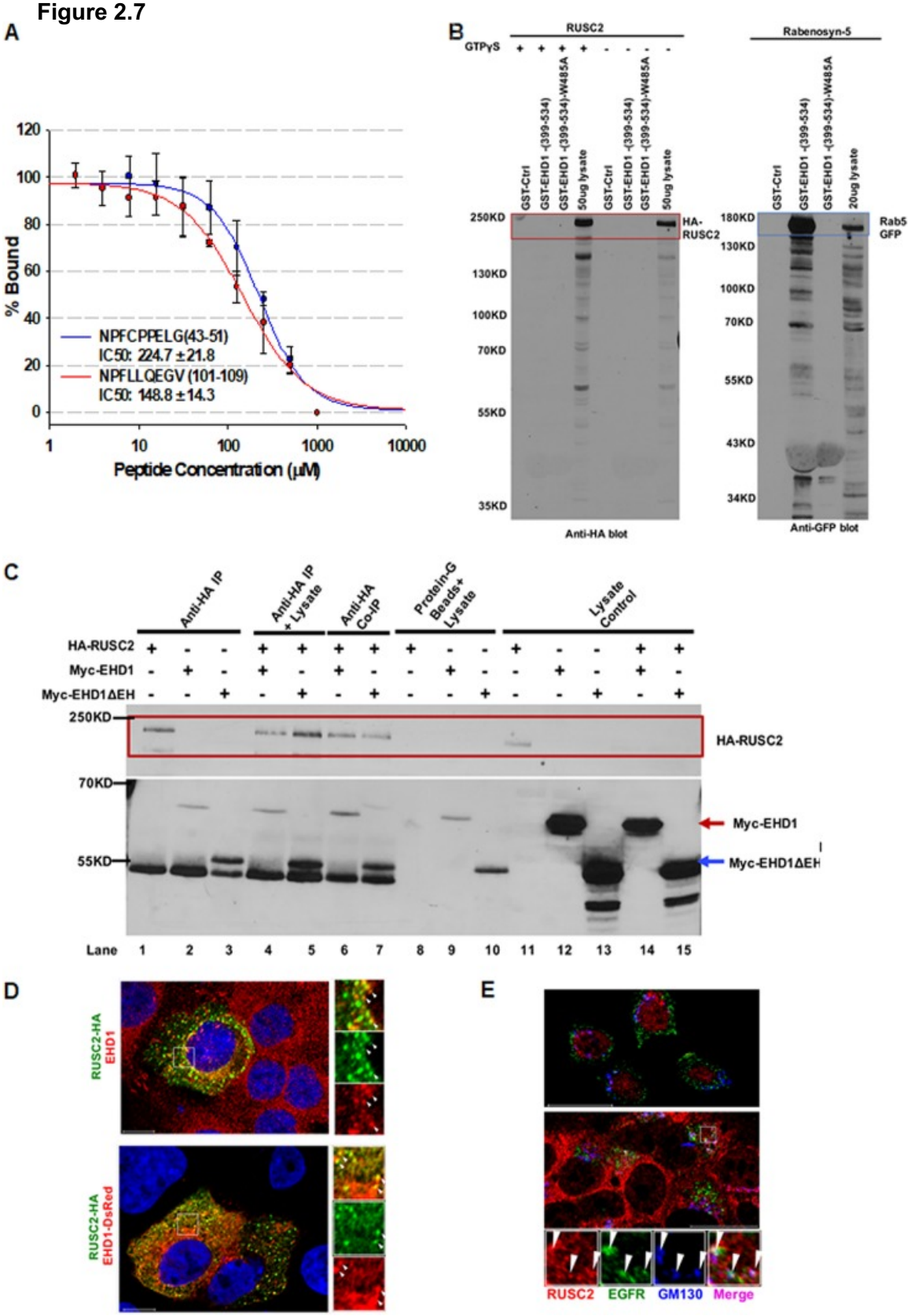
A
% Bound
Peptide Concentration (μM)
NPFCPPELG(43-51)
IC50: 224.7 ±21.8
NPFLLQEGV (101-109)
IC50: 148.8 ±14.3
B
RUSC2
Rabenosyn-5
GTPγS
GST-Ctrl
GST-EHD1 -(399-534)
GST-EHD1 -(399-534)-W485A
50ug lysate
20ug lysate
HA-RUSC2
Rab5 GFP
Anti-HA blot
Anti-GFP blot
C
Anti-HA IP
Anti-HA IP + Lysate
Anti-HA Co-IP
Protein-G Beads+ Lysate
Lysate Control
HA-RUSC2
Myc-EHD1
Myc-EHD1ΔEH
Lane
D
RUSC2-HA EHD1
RUSC2-HA EHD1-DsRed
E
RUSC2
EGFR
GM130
Merge

Figure 2. 7. Identification of RUSC2 as a potential EHD1 partner and its colocalization with EGFR at the Golgi compartment.

(A) EHD1 EH domain binding to RUSC2 NPF-containing motifs in vitro. The binding of two nonameric peptides corresponding to NPF-containing sequences in RUSC2 (amino acids 43-NPFCPPELG-51 and 101-NPFLLQEGV-109) to purified recombinant GST-EHD1 EH domain was assessed in an in vitro fluorescence polarization competition assay using competition binding of a labeled peptide derived from MICAL-like 1 protein (amino acids 425-NPFEEEEED-433). IC50, 50% inhibitory concentration. **(B)** Lack of EHD1 EH domain pulldown of full-length RUSC2 in cell lysates. Five-milligram protein aliquots of lysates of HEK293T cells transiently transfected with HA-RUSC2, supplemented or not supplemented with GTPγS (300 μM), were used for pulldown with 50 μg of purified GST fusion proteins: GST-Ctrl, GST–EHD1-(399–534), and GST–EHD1-(399–534)-W485A (nonbinding point mutant), immobilized on glutathione-Sepharose beads. Binding reactions or lysate control were subjected to anti-HA immunoblotting to detect RUSC2 (left panel). No RUSC2 pulldown with a GST EH domain was seen. Similar analysis of rabenosyn-5-transfected cell lysates (right panel) showed the expected pulldown with the wild-type but not the mutant GST-EHD1 EH fusion protein. **(C)** Lack of binding between full-length RUSC2 and EHD1. HEK293T cells were either separately transfected with HA-RUSC2, Myc-tagged full-length EHD1 (Myc-EHD1), or EH domain-deleted EHD1 (Myc–EHD1-ΔEH) (lanes 1 to 5, 8 to 10, and 11 to 13) or cotransfected with HA-RUSC2 and Myc-EHD1 or Myc–EHD1-ΔEH (lanes 6, 7, 14, and 15). Lysates of cells singly transfected with the indicated proteins were subjected to anti-HA IP from 1-mg aliquots of protein lysate (lanes 1 to 3), or protein G-Sepharose beads containing HA-RUSC2 immunoprecipitated from 1-mg aliquots of protein lysate of HA-RUSC2 singly transfected cells were further incubated with 1-mg lysates of cells transfected with Myc-EHD1 (lane 4) or Myc–EHD1-ΔEH (lane 5). The binding reactions were immunoblotted

with anti-HA (upper) or anti-Myc (lower) antibodies. Anti-HA IPs from lysates of cotransfected cells (lanes 6 and 7) were also subjected to anti-HA and anti-Myc blotting along with whole-cell lysates (lanes 11 to 15). As additional controls, lysates of singly transfected cells without anti-HA IP were incubated with protein G-Sepharose beads and immunoblotted as described for the binding reactions (lanes 8 to 10). HA-RUSC2 is shown in a red box; Myc-EHD1 and Myc–EHD1-ΔEH are indicated by red and blue arrows, respectively. No binding between EHD1 and RUSC2 was seen using the two-step binding approach or co-IP from doubly transfected cells. The Myc-EHD1 and Myc–EHD1-ΔEH bands seen in the binding reaction reflect nonspecific binding to protein G beads, as shown by the presence of these bands in incubations of protein G beads plus lysate. **(D)** Colocalization of EHD1 and RUSC2 in 16A5 cells. 16A5 cells transiently transfected with HA-RUSC2 were either used as such for costaining with anti-HA (green) and anti-EHD1 (endogenous EHD1; red) antibodies or were transiently cotransfected with EHD1-DsRed (bottom panel) and stained with anti-HA (green). Nuclei are visualized with 4′,6′-diamidino-2-phenylindole (blue). **(E)** RUSC2 colocalizes with EGFR. 16A5 cells with a Dox-inducible EHD1 shRNA (Seq. 1) were transiently transfected with HA-RUSC2 and cultured in the presence of Dox for 48 h to induce the EHD1 KD (and thus Golgi retention of EGFR), switched to serum- and EGF-deprived medium for 24 h, and stained with anti-RUSC2 (red), anti-EGFR (green), and anti-GM130 (blue) antibodies. Insets at higher magnification are shown to highlight the colocalization.

Figure 2.8

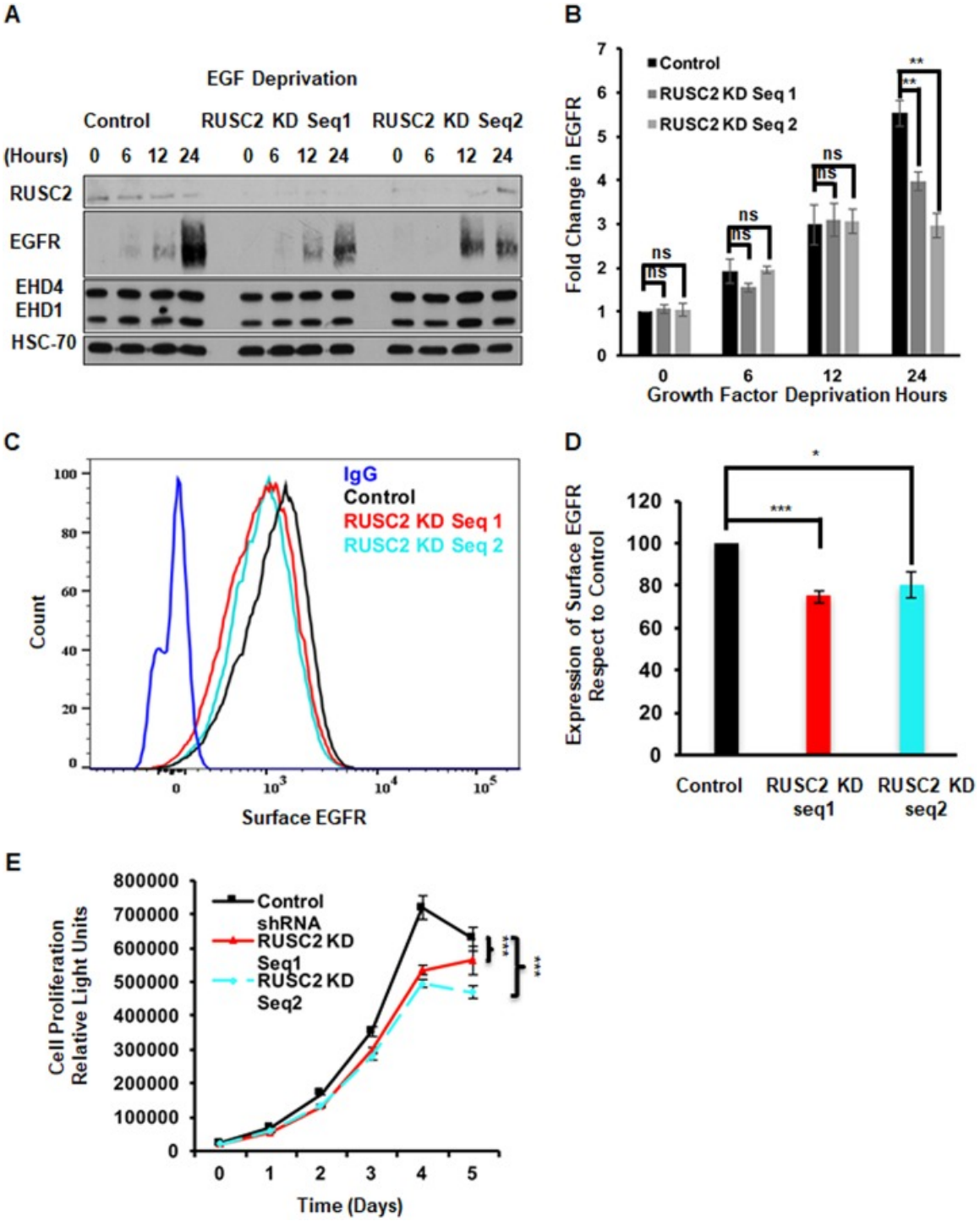
A
EGF Deprivation
Control
RUSC2 KD Seq1
RUSC2 KD Seq2
(Hours) 0 6 12 24 0 6 12 24 0 6 12 24
RUSC2
EGFR
EHD4
EHD1
HSC-70
B
Control
RUSC2 KD Seq 1
RUSC2 KD Seq 2
Fold Change in EGFR
ns
**
Growth Factor Deprivation Hours
C
IgG
Control
RUSC2 KD Seq 1
RUSC2 KD Seq 2
Count
Surface EGFR
D
Expression of Surface EGFR Respect to Control
*
***
Control
RUSC2 KD seq1
RUSC2 KD seq2
E
Control shRNA
RUSC2 KD Seq1
RUSC2 KD Seq2
Cell Proliferation Relative Light Units
Time (Days)

Figure 2.8. RUSC2 knockdown phenocopies the effects of EHD1 depletion on basal, unstimulated EGFR expression.

(A) RUSC2 KD impairs the accumulation of EGFR when cells are switched to EGF-deprived medium. 16A5 cells stably expressing a Dox-inducible nontargeting (control) or RUSC2-targeted (Seq. 1 or 2) shRNA were cultured in the presence of Dox for 3 days before being switched to serum and EGF deprivation medium for the indicated times, followed by analysis of lysates by immunoblotting for EGFR, RUSC2, EHD1/4, and HSC-70 (loading control). RUSC2 KD has no impact on EHD1/4 levels. **(B)** Densitometric quantification of EGFR signals shown in panel A, normalized to the level of HSC-70 (n = 3). **, $P < 0.02$. **(C)** RUSC2 KD reduced the cell surface EGFR levels. Live-cell FACS analysis of surface EGFR levels on 16A5 cells expressing a Dox-inducible nontargeting (Control) or RUSC2-targeted (Seq. 1 or 2) shRNA after 3 days of DOX pretreatment, with the last 24-h culture in serum- and EGF-deprived medium with Dox. **(D)** Quantification of EGFR staining data shown in panel C. Values on the y axis represent MFI data normalized to the level of Ig staining. Control shRNA EGFR levels are set as 100%. Error bars indicate standard errors of the means, and statistical significance was calculated using Student's t test (n = 3). Each experimental condition represents FACS analysis of 100,000 cells. *, $P < 0.05$; ***, $P < 0.001$. **(E)** RUSC2 KD impairs EGF-driven cell proliferation. 16A5 cell lines expressing the Dox-inducible control or RUSC2-targeted (Seq. 1 or 2) shRNA were plated at 1,500 cells per well (60 replicates per time point) and cultured for 5 days in the presence of Dox. Cell proliferation was assessed on each day using a CellTiter-Glo assay ***, $P < 0.001$, by Student's t test.

2.5. Discussion

Growth factor receptor tyrosine kinase activation provides a fundamental mechanism to regulate cellular activities under varied physiological conditions. Expression of a cell-type-dependent level of a given RTK is a prerequisite for the appropriate levels of cellular responses to cognate ligands, and many RTKs are now known to attain oncogenic properties through overexpression, mutations, or aberrant ligand availability. Surface expression of RTKs is indeed a requisite for oncogenesis (Hynes, Lane 2005). Yet relatively little is known about the mechanisms that ensure proper display of activation-ready RTKs on the cell surface to ensure physiological or oncogenic signaling upon ligand-induced activation. Here, we use EGFR, expressed on the nontumorgenic EGF-dependent immortal human mammary epithelial cell line 16A5, to identify a novel role of the endocytic recycling regulator EHD1 and of a little-understood Rab effector protein, RUSC2, in the maintenance of the cell surface display of EGFR by controlling its trafficking at the Golgi compartment. While EHD1 and its family members have emerged as key regulators of intracellular trafficking of internalized cell surface receptors (Naslavsky, Caplan 2011), including in some cases the retrograde trafficking to the Golgi compartment (Zhang, Reiling et al. 2012, McKenzie, Raisley et al. 2012), our studies provide evidence for a novel and functionally important role of EHD1 in the anterograde trafficking of EGFR from the Golgi compartment to the cell surface.

By immunofluorescence analyses, we found that cells deprived of EGFR ligands exhibit EGFR localization to EHD1+ vesicular structures that are also positive for the Golgi marker GM130 (Fig. 2.5B). We demonstrate that EHD1 depletion leads to accumulation of EGFR in this compartment, with concurrent reduction in the trafficking of EGFR to the cell surface (Fig. 2.5A). Since EHD1 is currently thought to work primarily at the endosomes, we tested and found support for the idea that a portion of the Golgi compartment-localized EGFR is derived from the pool internalized from the cell surface

(Fig. 2.5A). However, our results indicate that much of the Golgi compartment-localized EGFR represents the newly synthesized protein on its way to the cell surface (Fig. 2.5C). As our analyses show, the total and cell surface levels of EGFR under steady-state culture in EGF-containing medium are low, as expected from the EGF-induced and Cbl family ubiquitin ligase-dependent lysosomal degradation of activated EGFR (Duan, Raja et al. 2011). We therefore deliberately carried out analyses in which such steady-state cultures were switched to EGF-free medium to allow the newly synthesized EGFR to traffic to, and accumulate at, the cell surface. A block in the transit of EGFR out of the Golgi compartment under EHD1 KD conditions was clear under these conditions (Fig. 5A). Furthermore, the appearance of a fully mature form of the newly synthesized EGFR was delayed in EHD1 KD cells (Fig. 2.5C). The impact of EHD1 depletion was also observed in multiple other cell types, including MEFs in which the endogenous floxed EHD1 was conditionally deleted (Fig. 2.3), albeit the impact was modest in these other cell systems. The differences in the extents to which EGFR levels are impacted by EHD1 depletion may relate to the requirement of EGFR signaling for growth of the immortal MEC line 16A5 used in most of our experiments (Band, Sager 1989), while the other cell systems are not dependent on EGFR signals for in vitro growth. This idea is consistent with a robust reduction in CSF1R expression in EHD1-null murine macrophages (Cypher, Bielecki et al. 2016). Alternatively, other EHD family members may play a more significant redundant role in these other cell types. Notably, EHD4 levels are substantially increased in MEFs with EHD1 depletion, and future analyses using MEFs with double EHD1/EHD4 depletion should be instructive in this regard. Overall, our results support a key role of EHD1 in promoting the exit of unstimulated EGFR out of the Golgi compartment as a mechanism to ensure that optimal EGFR levels are maintained at the cell surface for the physiological activation of cells through this receptor. Indeed, we demonstrate that the reduced levels

and surface display of EGFR in EHD1 KD cells translate into impaired signaling and cell proliferation (Fig. 2.6).

Importantly, since we show that cell surface EGFR (labeled on the cell surface with an antibody) also gains entry into an EHD1+/GM130+ compartment, apparently reflecting its retrograde trafficking to Golgi compartment, and that EHD1 KD caused a more significant Golgi retention of this cohort as well (Fig. 2.5A), it is likely that unstimulated EGFR transported through both anterograde and retrograde mechanisms reaches an EHD1-dependent Golgi compartment and that EHD1 is required for EGFR to be recycled to the cell surface from this compartment. Intermixing of biosynthetic and endocytic cargos of cell surface receptors has been thought to primarily occur in the sorting endosomes, which then direct these receptors to various subcellular destinations (Scott, Vacca et al. 2014). Thus, the control of endocytic as well as biosynthetic pools of a prototype RTK at the Golgi compartment is unprecedented. It is notable that EHD1 knockdown was shown to impair the biosynthetic transport of a vesicular stomatitis virus G protein (VSVG)-GFP fusion protein used as a marker of the transport from the Golgi compartment to the cell surface (Zhang, Reiling et al. 2012), but no further studies along these lines have been reported.

Clearly, the EHD1-dependent control of EGFR trafficking described here is functionally important, as we demonstrate, and it will be of great interest to determine if this mechanism applies broadly to other RTKs and possibly other cell surface receptors. Consistent with a broader role of EHD1 in RTK trafficking, we have recently found that EHD1 also plays a key role in the surface expression of the CSF1R, an RTK, on primary macrophages (Cypher, Bielecki et al. 2016). Notably, however, we did not observe a significant impact of EHD1 depletion on MHC-I cell surface expression when this was examined under the same conditions as we used for analyses of EGFR (ligand-free culture), suggesting that our findings may be more relevant to RTKs whose cell surface

pools are subject to rapid ligand-induced degradation and require efficient surface delivery through new synthesis. Our inability to show an impact of EHD1 depletion on surface MHC-I levels is likely to reflect our methodology (designed to detect the trafficking of newly synthesized RTKs) since endocytic recycling of MHC-I, tracked using antibody binding at the cell surface, is known to be impaired upon EHD1 KD (Caplan, Naslavsky et al. 2002). While our studies have focused on EHD1, it will be important in future studies to assess any roles of the other EHD family members in the Golgi compartment-to-surface exit of EGFR and other RTKs, given their redundant roles that we have observed in other biological systems (George, Rainey et al. 2011, Iseka, Goetz et al. 2018, Sengupta, George et al. 2009).

In addition to demonstrating a novel functional role of EHD1 in EGFR trafficking out of the Golgi compartment, our studies reveal a new potential EHD1 partner, RUSC2, that is involved in this process (Fig. 2.7 and Fig. 2.8). RUSC2 is a little-studied member of a small family of RUN domain-containing proteins that include RUSC1/NESCA (new molecule containing SH3 at the carboxy terminus) with which it displays ~30% overall amino acid sequence identity. RUSC1/NESCA associates with TrkA, an RTK, and regulates dendritic spine dynamics by functioning as an adaptor for SNARE-mediated vesicle fusion events and as a link to molecular motor complexes (MacDonald, Dietrich et al. 2012). A role for RUSC2 in vesicular traffic has been hypothesized based on its interaction with Rab35, Rab1, and GM130 but has not been demonstrated previously (Bayer, Fischer et al. 2005, Fukuda, Kobayashi et al. 2011). Based on the presence of an EH domain-interacting NPF motif in RUSC2 (Fig. 2.7A), which is not present in RUSC1/NESCA, and the isolation of RUSC2 as part of a protein complex associated with unstimulated EGFR (53), we assessed the role of RUSC2 in EGFR trafficking. While RUSC2 did not show a physical interaction with EHD1 in cells (Fig. 2.7B and C), RUSC2 displayed strong colocalization with EHD1 on tubular and vesicular structures, which

included the Golgi compartment (Fig. 2.7D and E). Importantly, RUSC2 KD led to a phenotype that mimicked that of EHD1 KD (Fig. 2.8). Thus, our study provides the first direct evidence for a role of RUSC2 in anterograde EGFR trafficking out of the Golgi compartment and helps describe a novel biochemical duo of EHD1 and RUSC2 that regulates EGFR display on the cell surface. Unlike the recently described EHD1 recruitment to membranes via Rab35 effector MICAL-L1 (Sharma, Giridharan et al. 2009), we did not find any requirement of RUSC2 for EHD1 localization in the Golgi compartment (Fig. 2.5B), suggesting that they function in a common trafficking pathway but independent of an interaction. In this regard, it will also be important to assess in the future if RUSC2, via its apparently functional NPF motifs, might interact with other EH domain-containing proteins to promote EGFR trafficking. The RUSC2 binding partner GM130 was recently shown to play a role in the nucleation of microtubules at the Golgi compartment through sequestration of importin-α and activation of the spindle assembly factor TPX2 (Wei, Zhang et al. 2015). Whether EHD1- and RUSC2-dependent transport of EGFR out of the Golgi compartment might use such a microtubule network will be of considerable future interest, given the proposed role of MICAL-L1 as a link between EHD1+ vesicles and dynein motors through an interaction with the collapsin response mediator protein 2 (CRMP2) at the endocytic recycling compartment (Rahajeng, Caplan et al. 2010).

Notably, several previously known EHD protein interactors have now been recognized to play a role at the Golgi compartment. For example, EHD1 interactor Rab11-FIP1/RCP was recently shown to mediate traffic at the trans-Golgi network through binding to golgin-97 (Jing, Junutula et al. 2010). A GM130-Rab11-mediated pathway for surface expression of the T-cell antigen receptor has been described previously (Onnis, Finetti et al. 2015). Whether these roles involve interactions with EHD proteins will be of significant interest in future studies. Recent studies have also indicated that EHD1 depletion alters the Golgi polarization relevant to cytokinesis, while MICAL-L1 knockdown partially

disrupted the Golgi reorientation toward the direction of a scratch wound (Reinecke, Katafiasz et al. 2015, Reinecke, Katafiasz et al. 2014). Although we have not examined the Golgi dynamics in our studies, we did not observe any gross changes in the Golgi apparatus.

The RUSC2 gene has also been described as an HIV-1 susceptibility gene (Brass, Dykxhoorn et al. 2008), and it will be of great interest in the future to assess if EHD1-RUSC2 complex plays a role in cellular pathology associated with HIV infection. EHD1 expression was recently found to be associated with poor prognosis in non-small cell lung cancer (Lu, H., Meng et al. 2013, Gao, Wang et al. 2014) and breast cancer (Tong, Liang et al. 2017), and EHD1 levels in NSCLC showed a negative correlation with sensitivity to EGFR-targeted kinase inhibitor therapy (Wang, X., Yin et al. 2018). Thus, the new molecular pathway we identify may prove to be of clinical relevance in targeted therapy of cancers driven by aberrations of EGFR or other RTKs.

In conclusion, studies presented here demonstrate a new and functionally important role of EHD1 and a potential novel partner, RUSC2, in the control of Golgi compartment-to-surface transport of a prototype RTK, EGFR under ligand-unstimulated conditions. Using the experimental systems described here, it will be of great interest to use targeted or genome-wide knockdown/KO or ectopic gene expression approaches to identify other novel players that regulate the basal RTK surface expression and their functional roles in physiological and pathological RTK signaling.

ACKNOWLEDGMENTS

We thank the Band Lab members for discussion and the staff of the University of Nebraska Medical Center (UNMC) Cell Analysis and Flow Cytometry Research Facilities for assistance.

Support was provide by the following: NIH grants CA87986 and CA105489 to H.B. and CA96844 and CA144027 to V.B.; Department of Defense grants W81XWH-17-1-0616 (H.B.) and W81XWH-07-1-0351 and W81XWH-11-1-0171 (V.B.); an NE DHHS LB506 (2018-03) grant; University of Nebraska Collaboration Initiative seed grants; pilot grants from the Fred & Pamela Buffett Cancer Center and the Pediatric Cancer Research Program at UNMC (H.B.); Institutional Development Award (IDeA) from the NIGMS of the NIH under grant number P30 GM106397; Nebraska Research Initiative Food for Health seed grant; support to UNMC core facilities from the NCI Cancer Center Support Grant (P30CA036727) to Fred & Pamela Buffett Cancer Center and the Nebraska Research Initiative; and the Raphael Bonita Memorial Fund. T.A.B., B.T.G., and L.R.C. were trainees under an NCI Cancer Biology Training Grant. I.M., N.Z., B.C.M., S.B., and P.A. received UNMC graduate assistantships. H.L. was the recipient of a China Scholarship Council graduate fellowship.

H.B. and V.B. conceived the study and secured the funding. H.B., E.C.T., I.M., B.C.M., A.M.B., N.Z., V.B., C.G., A.N., and P.K.S. designed the experiments. E.C.T., I.M., B.C.M., A.M.B., H.L., N.Z., S.C., N.I., S.B., F.M.I., P.A., T.A.B., L.R.C., B.T.G., and M.D.S. performed experiments. S.K.N. and C.G. performed bioinformatic analysis of NPF motifs. A.B. and G.Y. contributed critical reagents. E.C.T., I.M., B.C.M., H.L., C.G., S.R., A.N., and H.B. analyzed data. E.C.T., I.M., and H.B. wrote and V.B., B.C.M., N.Z., T.A.B., H.L., and L.R.C. edited the manuscript. All authors read the manuscript and provided feedback.

We declare that we have no conflicts of interest in connection with the contents of this article.

Chapter 3: Role of clathrin-mediated endocytosis regulator AAK1 in SARS-CoV-2 entry into cells

3.1. Introduction

The first step in the process of coronavirus infection is the binding of the Spike (S) glycoprotein to cell surface receptors on host cells, ACE2 for SARS-CoV and SARS-CoV-2. The virus/receptor complex must then be internalized into acidic endosomal compartments where host proteases cleave the S protein to release the S2 subunit, which drives viral envelope-host cell membrane fusion (Hoffmann, Kleine-Weber et al. 2020). These sequential steps are essential to deliver the viral genome into the cytosol to initiate viral replication, thus providing potential proximal targets to interrupt infection. The TMPRSS2 protease has emerged as critical for S protein cleavage in endosomes, and an orally administered inhibitor camostat mesylate, clinically used in Japan (Uno 2020), is currently in clinical trials (www.clinicaltrials.gov, NCT04321096). Based on SARS-CoV studies (Inoue, Tanaka et al. 2007), SARS-CoV-2 virus internalization is thought to require clathrin-coated vesicle-mediated endocytosis. AAK1 is required for efficient clathrin-mediated endocytosis by phosphorylating the mu-subunit of AP2 (AP2M1) to promote the internalization process; studies of Hepatitis C (Neveu, Ziv-Av et al. 2015), rabies (Wang, C., Wang et al. 2019), dengue, and Ebola (Bekerman, Neveu et al. 2017) viruses have identified a key role of AAK1 in promoting viral entry and a screen of clinically used drugs identified sunitinib and erlotinib (clinically used anticancer drugs) to possess AAK1 inhibitory activity (besides their known targets) with antiviral activity (Bekerman, Neveu et al. 2017). Clinically-used JAK inhibitor Baricitinib may also inhibit AAK1 (Richardson, Griffin et al. 2020), leading to ongoing clinical trials (NCT04340232; NCT04320277; NCT04280705). However, when the current studies were initiated, the role of AAK1 in SARS-CoV-2 viral entry was unknown and still there is not any study which has elucidated the role of AAK1 in the SARS-CoV-2 life cycle.

We **hypothesized** that AAK1 is essential to promote the early steps of internalizing the SARS-CoV-2/ACE2 complex, independently, and ahead of the later TMPRSS2-mediated S protein cleavage enables viral and host membrane fusion. Thus, targeting AAK1 will allow the inhibition of SARS-CoV-2 entry into host cells. The studies presented here systematically addressed this hypothesis using the isolated SARS-CoV-2 S protein RBD as a fusion protein to drive the internalization of the cellular receptor ACE2.

3.2. Material and Methods

Reagents

Bovine serum albumin (cat. # A7906-100G), paraformaldehyde (cat. # 158127-500G), sodium orthovanadate (Na3VO4, Catalog # S6508-50G), Triton X-100 (Catalog # 93418) were from Sigma-Aldrich (St. Louis, MO). Sodium fluoride (NaF, Catalog # S299-500), sodium chloride (NaCl, Catalog # S271-10), and Tris (Catalog #t BP152-5) were from Fisher Chemicals. BSA for bicinchoninic acid assay (Catalog # 23209) and PMSF (Catalog # 36978) were from Thermo-Scientific. Penicillin/streptomycin (Catalog # 15140-122) and fetal bovine serum (FBS) (Catalog # 10427-028; lot # 1662765A120-01) were from Life Technologies. HEPES (Catalog # SH30237.01) and nonessential amino acids (Catalog # SH30238.01) were from HyClone. Sodium pyruvate was from corning. Alpha-MEM, DMEM, and RPMI were from Gibco. Protein A and G Sepharose beads were from Invitrogen. Mercaptoethanol (2-ME) for cell culture was from gibco and for western from sigma. Vivaspin 20 concentrators were from Sartorius.

Cell lines and medium

Based on the literature and expression data from Human protein atlas the following mentioned cell lines were used to check the expression of proteins of our interest like

ACE2, AAK1, and p-AP2M1 by western blotting and FACS analysis. Some of the cell lines were also used to study binding and endocytosis assays. HEK293T (Human, Embryonic Kidney cell line), HEK293T overexpressing (Myc-ACE2, HA-TMPRSS2, AAK1, GAK), Vero-E6 (Monkey, Kidney) (kindly provided by Drs. Elgamal and Byrareddy, UNMC), Huh7 (Human, Liver Cancer) (Band and Byrareddy labs), Caco2 (Human, colorectal Cancer), A549 (Human, Lung Cancer) (Dr. Bhakat's Lab), JIMT1 (Human, Breast Cancer), Ovcar5 (Human, Ovarian Cancer) were cultured in complete DMEM supplemented with 10% fetal bovine serum, 10 mM HEPES, 1 mM each of sodium pyruvate, nonessential amino acids and glutamine, 50 μM 2-ME, and 1% penicillin/ streptomycin.

HCC1954 (Human, ErbB2+ Breast Cancer), Calu-3 (Human, Lung cancer) (Band, Elgamal and Byrareddy labs), H1666, H3255, and H1650 (Human, Lung Cancer) were cultured in complete alpha MEM, EMEM, and RPMI respectively supplemented with the components as mentioned above.

HEK293T (Human, Embryonic kidney) cells stably expressing either ACE2 only or ACE2 and TMPRSS2 were obtained from Genecopoeia cultured in complete DMEM supplemented with 10% fetal bovine serum, 10 mM HEPES, 1 mM each of sodium pyruvate, nonessential amino acids, and glutamine, 50 μM 2-ME, and 1% penicillin/ streptomycin with 100 ug of Hygromycin for ACE2 only and 100 ug Hygromycin plus 1ug of puromycin for ACE2/TMPRSS2 cell line. FreeStyle 293 cell line was obtained from Genecopoeia and maintained in the medium provided by the vendor.

Plasmids and Transfection Reagents

The recombinant SARS-CoV-2 S protein constructs were used for binding and endocytosis experiments. Also, we obtained plasmids for the ectopic expression or to

generate stable cell lines to be used in our studies. siRNA constructs were for generating the knockdown to study the effect of knockdown on the entry of the virus. pcDNA-SARS-CoV-2-S-RBD-FC (Plasmid #141183), pcDNA3-SARS-CoV-2-S-RBD-sfGFP (Plasmid #141184), pCEP4-Myc-ACE2 (Plasmid #141185), pcDNA.3 CXCL12-sfGFP (Plasmid #98961), pCEP4-Myc-HLA-A2 (Plasmid #135504), Ntn1-Fc-His (Plasmid #72104), pcDNA3.1-SARS2-Spike (Plasmid #145032), pCSDest-HA-TMPRSS2 (Plasmid #154963), pWZL Neo Myr Flag AAK1 (Plasmid #20133), pTwist-EF1alpha-SARS-CoV-2-S-2xstrep (Plasmid #141382), pcDNA3.3-SARS2-Spike (Plasmid #145032) were from Addgene, ON-TARGET plus non-targeting Pool, ON-TARGET plus SMART pool Human AAK1 siRNA, and ON-TARGET plus Human GAK siRNA were from Dharmacon. XtremeGENE 9 transfection reagent was from Roche Applied Science (Indianapolis, IN) DharmaFECT I (Catalog # T-2001-02) transfection reagent was from Dharmacon. 293fectin transfection reagent was from Gibco (Catalog 3 12347-019)

Expression and purification of SARS-CoV-2 RBD

SARS-CoV-2-S-RBD-FC (S-RBD-FC) and SARS-CoV-2-S-RBD-sfGFP (S-RBD-sfGFP) along with controls were transfected either in adherent HEK293T or Suspension FreeStyle 293 cells. In HEK293T cells, the medium was changed the next day of transfection. The supernatant from the cells was collected after 96 hours of transfection. The supernatant containing SARS-CoV-2-S-RBD-FC was applied to Protein A Sepharose beads which were already blocked by 1 % BSA in PBS. After 3 hours of binding, beads were washed, and protein was eluted with glycine buffer (pH 2.3, pH 2.5, and pH 2.7) neutralized with tris buffer pH 8.

Antibodies for Western Blot

The following antibodies were used for immunoblotting: SARS-CoV-2/2019-nCoV Spike/RBD rabbit polyclonal Antibody was from Sino Biological (Catalog # 40592-T62), C9 Tag rabbit Polyclonal Antibody was from MyBioSource(Catalog # MBS430088), SARS-CoV-2 Spike Protein rabbit polyclonal Antibody (Catalog # PA5-114446), SARS-CoV-2 Spike Protein S1 Monoclonal Antibody (Catalog # MA5-36247), SARS-CoV-2 Spike S2 Monoclonal Antibody (Catalog # MA5-36254), Strept-tag Monoclonal Antibody (Catalog # MA517283), AAK1 (Catalog # PA5-20616) and ACE2 Polyclonal Antibody (Catalog # PA5-20046) were from Invitrogen. Human ACE2 Goat polyclonal Ab (R&D Catalog # AF933), SARS-CoV-2 Spike S2 Subunit Mouse Monoclonal antibody (Catalog # MAB10557-100), Mouse ACE2 Antibody (Cat. #AF3437-SP), AAK1 mouse monoclonal Antibody (Catalog # MAB6886) were from R&D. AAK1 Rabbit polyclonal Antibody (Catalog # A302-145A-M) was from Bethyl Laboratories. Inc. AAK1 Rabbit Antibody (Catalog # 79832S) and phospho AP2M1 (Catalog # 7399S) were from Cell Signaling. ACE2 Rabbit monoclonal Antibody (Catalog # ab108252), AP2M1 rabbit polyclonal Antibody (Catalog # ab109397) and phospho AP2M1 rabbit monoclonal Antibody (Catalog # ab137727) were from Abcam. AP2M1 Rabbit polyclonal Antibody was from BIO-RAD (Product code AHP2434), Beta-actin

Secondary reagents used for immunoblotting included horseradish peroxidase (HRP)-conjugated Protein A and Rabbit anti-Mouse HRP (Invitrogen, Carlsbad, CA).

Antibodies for Immunofluorescence:

ACE2 Rabbit polyclonal Antibody was from Bioss Inc. (Catalog # bs-1004r), ACE2 rabbit Monoclonal Antibody was from Novus Biologicals (Catalog # SN0754), ACE2 Rabbit

polyclonal Antibody was from Lifespan biosciences (Catalog # LS-B6672-200), Human ACE2 Goat polyclonal Antibody (Catalog # AF933), and Alexa Fluor 647 Human ACE2 Goat Polyclonal Antibody (Catalog # FAB933R) were from R&D ACE2 Rabbit Antibody was from RockLand (Catalog # 600-401-x60). Rabbit Anti-Human IgG, Fc fragment Specific was from Jackson ImmunoResearch (catalog # 309-001-008), Mouse Anti-Human IgG FC-FITC (catalog # 9042-02) and Fc isotype control Mouse IgG2B-FITC (Catalog # 0104-02) were from SouthernBiotech.

Antibodies for Fluorescence-activated cell sorting (FACS)

In house Myc (9E10), Human ACE2 Goat polyclonal Ab was from R&D (Catalog # AF933)

Inhibitors

LP-935509 (Axon Medchem Cat. ID 2638), LP-922761 (R&D Catalog #: 6229), SGC AAk1-1 (R&D Catalog # 6528/5), Sunitinib Malate (Selleckchem Catalog # S1042), Baricitinib (Selleckchem Catalog # S5754), Erlotinib (LC Laboratories catalog # E-4007 and Sigma Catalog # CDS022564)

Protein lysis and quantification

Cells were lysed with Triton-X-100 lysis buffer (50 mM Tris pH 7.5, 150 mM sodium chloride, 0.5% Triton-X-100), 1 mM PMSF, 10 mM sodium fluoride, and 1 mM sodium orthovanadate. Lysates were rocked at 4°C from 4 hours to overnight, centrifuged at 13,000 rpm for 30 minutes at 4°C in a bench-top micro-centrifuge, and cleared lysates were transferred to fresh tubes. The protein concentration of samples was estimated using the Bicinchoninic acid (BCA) assay kit (Thermo Fisher Scientific, Rockford, IL) using bovine serum albumin (BSA) as a standard.

Immunoblotting

50 µg of protein lysate per sample was resolved by SDS/PAGE and transferred to a PVDF membrane (Millipore, cat. # IPVH00010). The membranes were blocked in TBS-0.1% Tween 20 (BIORAD, cat. # 161-0781) with 5% Bovine Serum Albumin (BSA) with 0.02% sodium azide, incubated with the appropriate primary antibodies diluted in TBS-0.1% Tween 20 or 5% BSA with 0.02% azide either for 2 hours at room temperature or overnight at 4°C. Next, membranes were washed in TBS-0.1% Tween 20 (four times for 5 minutes) followed by 45 minutes incubation with HRP-conjugated secondary antibody at room temperature. The membrane was washed in TBS-0.1% Tween 20 (four times for 5 minutes) and ECL-based detection was performed.

Fluorescence-Activated Cell Sorting (FACS)

To check the surface expression of ACE2 in several cell lines, we did FACS analysis. Cells were plated in a six-well plate, trypsinized, and washed with FACS buffer. Then the cells were incubated with appropriate antibodies in FACS buffer (2% FBS, 25 mM HEPES buffer in PBS) at recommended dilutions/concentrations on ice in the dark for 45 min (depending on the experiment) followed by incubation with secondary antibodies wherever needed. Cells were then washed and suspended in 500 µl of cold FACS buffer. Cells were protected from light until analyses using either the LSR II Green or LSR II cytometer (BD Bioscience). FACS data were analyzed using DIVA (BD FACSDIVA TM Software), FlowJo (FLOWJO, LLC Data Analysis Software, Ashland, OR) and ModFit LT software (Verity Software House, Topsham, ME)

Confocal immunofluorescence microscopy

Confocal microscopy was done for binding and internalization assays to look at surface ACE2 and bound and internalized recombinant S protein. Cells were grown on glass coverslips coated with poly-lysine-D inside in a 24-well tissue culture plate. At the end of the experiment, cells were fixed in 4% paraformaldehyde (PFA) in PBS for 15 minutes. The PFA solution was removed, and the cells were used as either non-permeabilized or were permeabilized for 20 minutes in immunofluorescence (IF) buffer (10% FBS, 0.2% BSA, and 0.05% saponin in PBS). The cells were then stained with primary antibodies overnight at 4 °C, followed by three 10-minute washes in PBS. The cells were then incubated with the appropriate secondary antibodies for 1 hour (diluted 1:500 in the IF buffer), followed by three 10-minute washes in PBS. In preparation for confocal microscopy, PBS was removed, and the coverslips were carefully removed and inverted onto glass microscope slides with Vectashield mounting medium (Vector Laboratories, Burlingame, CA), which contained 4′, 6-diamidino-2-phenylindole (DAPI) to stain DNA in the nucleus of the cell. The coverslips were allowed to adhere to the surface and dry for 5 minutes or more. Then images were acquired using a Zeiss 800 Confocal Laser Scanning Microscope (Carl Zeiss) using 63× objective with a numerical aperture of 1.0 and appropriate filters. Merged fluorescence pictures were generated and analyzed using ZEN® 2012 software from Carl Zeiss.

Statistical analysis

Statistical significance was tested by ANOVA with Dunnett test for endocytosis of S-RBD when Genecopoeia cells were treated with DMSO or inhibitors.

3.3. Results

The system for studying SARS-CoV-2 internalization in Biosafety level I/II Lab.

The recombinant SARS-CoV-2 S protein receptor-binding domain (RBD)-driven ACE2 endocytosis (Hoffmann, Kleine-Weber et al. 2020) provides a simple yet robust system to assess the role of AAK1 and the impact of its inhibition on the first step of SARS-CoV-2 entry into host cells. This system also simplifies the readout and allows studies under BSL1/2 containment as opposed to BSL3 level containment needed for live viral studies. To begin our studies, we developed a cell-based expression system to express the SARS-CoV-2 S protein RBD (amino acids 333-529) (Chan, K. K., Dorosky et al. 2020) fused to the Fc region of human IgG1 or tagged with GFP. HEK293T cells were transiently transfected with these constructs along with CXCL12-GFP, Ntn1-Fc which served as negative control. After 96 hours of transfection, the cell lysates and supernatants were collected. The supernatant containing the SARS-CoV-2-S-RBD-FC was applied to Protein A Sepharose beads pre-blocked by incubation in 1 % BSA in PBS. After 3 hours of binding, beads were washed, and samples were prepared for western blotting. The immunoblotting was done with an RBD-specific antibody (Sino Biological Spike RBD Antibody). We successfully were able to express and purify S-RBD-Fc in HEK293T cells. Ntn1 was included to serve as a negative control (Fig. 3.1A). We also used the HEK293T expression system to express the SARS-CoV-2-S-RBD-sfGFP fusion protein. The GFP tagged construct was chosen to be used while doing binding and internalization immunofluorescence experiments so that we do not have to stain for S-RBD. The supernatant containing the SARS-CoV-2-S-RBD-sfGFP was concentrated using 10,000 MWCO concentrators to get the concentrated protein of interest for further binding/internalization experiments and immunoblotting was done with an RBD-specific

antibody (Sino Biological Spike RBD Antibody). The western blot data shows the successful expression of GFP tagged S-RBD protein and CXCL12-GFP was included as a negative control. 16A5 cell lysates were included to serve as the control for probing with GFP antibody (Fig. 3.1B). The HEK293T expression system gave us non-specific bands (showed by an arrow in the figure) around the same molecular weight size as the protein of our interest, likely a result of immunoglobulins present in serum used to culture the cells. Thus, to avoid non-specific binding of any of the components in our further experiments, we switched to FreeStyle 293 cells. These cells were obtained from Genecopoeia and represent HEK293T cells adapted to grow in a suspension culture in media that is serum- and protein-free.

The FreeStyle 293 cells were transfected with the S-RBD-Fc expression construct. After 96 hours of transfection, the supernatant was collected. To purify protein, SARS-CoV-2 Spike RBD [Fc] supernatant was incubated with Protein A Sepharose beads and eluted with Glycine buffer with different pH (lowering pH helped us in better elution of the protein from the beads). The samples from different conditions were resolved on SDS PAGE and immunoblotted with Sino Biological Spike RBD Antibody. The western blot shows that we successfully were able to express, purify and elute the S-RBD-Fc in FreeStyle 293 cells (Fig. 3.2). In addition to replicating the regular HEK293T expression results of efficient expression of S-RBD-Fc and Protein-A-based purification, no significant contaminating bands were seen. Thus, the FreeStyle 293 system was used to express the S-RBD-Fc for subsequent studies. For endocytosis studies, we used cell supernatant containing S-RBD-Fc directly without purifying the protein. The Fc portion of the chimera provided a suitable tag, and it binds specifically to an anti-human antibody conjugated to a fluorophore. Also, purified protein and crude cell supernatant gave us similar results in the endocytosis experiments.

Characterization of endogenous or ectopically-expressed ACE2 expression levels in various cell lines.

ACE2 is the primary receptor for SARS-CoV-2 (Hoffmann, Kleine-Weber et al. 2020). Therefore, to study the virus internalization process, we established stable 293T cell transfectants expressing Myc-tagged ACE2. We also obtained ACE2 overexpressing HEK293T cell line from Genecopoeia. Using a range of commercial antibodies against ACE2, the Myc-ACE2-expressing 293T generated by band lab, ACE2 overexpressing HEK293T cells from Genecopoeia as well as other cell lines (such as Huh7 and Vero E6) with reported high endogenous ACE2 expression (Hoffmann, Kleine-Weber et al. 2020) were checked for the total and surface expression of ACE2, we validated the use of anti-ACE2 antibodies for Western blotting (WB) as well as FACS staining (Fig. 3.3 and Fig. 3.4). As expected, the 293T-based cell lines expressing ectopic ACE2 showed high levels of total and cell surface ACE2, while lower but detectable levels were seen in Huh7, Vero E6 and some other cell lines (Fig. 3.3 and Fig. 3.4). Given their high ACE2 expression levels, the majority of experiments were undertaken using the 293T-based cell lines made in-house or obtained from Genecopoeia (indicated in each experiment). Some experiments used other cell lines expressing endogenous ACE2.

Specific surface binding of S-RBD to ACE2 on target cells.

We carried out binding assays to establish that the expressed recombinant SARS-CoV-2 S Protein RBD specifically binds to host cells through ACE2. The in-house made Myc-ACE2-expressing 293T cells (with subsets of ACE2-overexpressing and non-expressing cells in it) were grown on coverslips coated with poly-lysine-D. Cells were washed, and the recombinant S-RBD-Fc fusion protein-containing cell supernatants were added for 60 minutes at 4°C, conditions under which no internalization occurred. The cells after binding were washed, fixed, and stained. The S-RBD was visualized by staining with

anti-human IgG-Fc labeled with FITC antibody, while ACE2 was visualized by anti-Myc mouse antibody staining (red). The IF staining results demonstrated binding of S-RBD only to ACE2-overexpressing 293T cells, with no staining of the non-ACE2-expressing cells demonstrating specificity. ACE2 and S-RBD staining signals showed complete co-localization (Fig. 3.5).

Similar analyses were carried out with Huh7 and Vero E6 cell lines which express lower levels of endogenous ACE2 as shown in (Fig. 3.3) to validate the results of HEK293T cells ectopically expressing ACE2. Huh7 and Vero E6 cells were grown on coverslips. Cells were washed, and the recombinant S-RBD-Fc fusion protein-containing cell supernatants were added for 60 minutes at 4°C, conditions under which no internalization occurred. The cells after binding were washed, fixed, and stained. The S-RBD was visualized by staining with anti-human IgG-Fc labeled with FITC antibody, while ACE2 was visualized by goat ACE2 antibody staining (red), for which anti-goat AF647 secondary was used. S-RBD binding and colocalization with ACE2 was also observed in these cell lines (Fig. 3.6). Thus, S-RBD-IgG-Fc fusion protein bound specifically to ACE-2-expressing cells.

Surface-bound SARS-CoV-2 S-RBD is internalized in a time-dependent manner.

To establish an S-RBD-induced ACE2 internalization assay, we added recombinant S-RBD-Fc fusion protein-containing cell supernatants to Myc-ACE2-expressing 293T cells for 60 minutes at 4°C (conditions under which no internalization occurred) as in binding assays above. To demonstrate the S-RBD and ACE2 co-endocytosis, the Myc-ACE2-expressing 293T cells with bound S-RBD-Fc were washed to remove unbound S-RBD protein and further incubated at 37° C for different time points to allow the endocytosis to proceed. Endocytosis of S-RBD was seen based on a reduction

in the cell surface S-RBD and ACE2 signals with concomitant increase in vesicular intracellular signals that accumulated over time; the concurrent accumulation of ACE2 in the same vesicles indicated co-endocytosis of S-RBD and ACE2 (Fig. 3.7). These analyses provided a simple yet robust S-RBD endocytosis and S-RBD/ACE2 co-endocytosis assay for further studies.

The Myc-ACE2-overexpressing 293T stable cell line we generated showed progressive loss of ACE2 expression over time upon passaging. However, a 293T cell line overexpressing untagged ACE2 obtained from Genecopoeia showed more stable ACE2 overexpression over time. When the above time-dependent S-RBD endocytosis assay was repeated with this cell line, results identical to those with in-house generated HEK293T-Myc-ACE2 overexpressing cell line were observed (Fig. 3.8).

AAK1 plays a role in SARS-CoV-2 internalization.

AAK1 is known to play a role in clathrin-mediated endocytosis (Ricotta, Conner et al. 2002) and viral entry like in HCV, Ebola and dengue, therefore, to study the role of this endocytic regulator in the internalization of SARS-CoV-2, we took several cell lines and checked the expression of AAK1 using immunoblotting (Fig. 3.9). All the cell lines, including the HEK cells, which ectopically express ACE2 showed similar levels of AAK1. As all cells have similar levels of AAK1, we used the HEK system from Genecopoeia, which ectopically expresses ACE2 for knocking down AAK1. The purpose of using HEK293T cells ectopically expressing ACE2 from Genecopoeia was because of high total and surface levels of ACE2 as shown by western and FACS analysis (Fig. 3.3 and Fig. 3.4) and also a good staining in case of binding and internalization experiment (Fig. 3.7). We depleted AAK1 in these cells using smart pool small interfering RNA (siRNA). The cells were transfected with siRNA or non-targeting control (NTC) and lysates were collected after 48 hours of transfection. Immunoblotting was done, which showed the

reduction in the levels of AAK1 (Fig. 3.10A and B). Despite a good knockdown of AAK1, we saw a slight effect on the phosphorylation of AP2M1, which could be due to the other molecular players involved in the phosphorylation of AP2M1 (Fig. 3.10C).

It has been previously shown that another member of AAK1 family, cyclin-G associated kinase (GAK) is involved in the phosphorylation of AP2M1 and has a role to play in the entry of HCV virus (Neveu, Ziv-Av et al. 2015). To see the effect of GAK deletion on the levels of AP2M1 phosphorylation, we either depleted AAK1 or GAK or both in HEK293T cells ectopically expressing ACE2 from Genecopoeia. The cells were transfected with siRNAs or NTC and lysates were collected after 48 hours of transfection. Immunoblotting was done, which showed reduction in the levels of AAK1 and GAK. (Fig. 3.11A and B). Like in the case of AAK1 knockdown (Fig. 3.10A and B), we again saw only a slight decrease in the case of single AAK1 or GAK knockdown but combined knockdown of AAK1 and GAK showed a further loss in the phosphorylation of AP2M1 suggesting that in addition to AAK1 other kinases too are involved in the phosphorylation of AP2M1 (Fig. 3.11C).

We then did an S-RBD internalization assay with AAK1 depleted Genecopoeia ACE2 cell line to see the effect of AAK1 KD on the internalization process. After 48 hours of transfection with siRNA or NTC, cells were plated on coverslips to carry out an internalization assay. The recombinant S-RBD-Fc fusion protein-containing cell supernatant was added to cells for 60 minutes at 4°C (conditions under which no internalization occurred). The cells with bound S-RBD-Fc were then washed to remove unbound S-RBD protein and further incubated at 37° C to allow the endocytosis to proceed. Knocking down AAK1 reduced the internalization of S-RBD compared to the control cells suggesting the role of AAK1 in the internalization of SARS-CoV-2 into the target cells (Fig. 3.12). Though in the case of the siRNA KD cell there was a decrease in the internalization compared to the NTC, as can be seen from the representative figure,

this needs to be repeated for quantification purposes to see the significance level between NTC and siRNA cells.

Pharmacological inhibition of AAK1 reduced or inhibited internalization of S-RBD.

AAK1 mediates clathrin-mediated endocytosis by phosphorylating AP2M1 (Ricotta, Conner et al. 2002, Henderson, Conner 2007), so we demonstrated the constitutive phosphorylation of the endocytosis-relevant AAK1 target AP2-mu, using multiple antibodies from independent vendors (Fig. 3.13).

It has been previously shown that some of the kinase inhibitors of AAK1 bind it with high affinities and lead to loss of phosphorylation of AP2M1 subunit, so we established the use of phospho-AP2-mu levels as a readout of AAK1 inhibition by demonstrating loss of phosphorylation signals with low nano-molar to high micro-molar concentrations of 2 AAK1-specific inhibitors LP-922761 and LP-935509 with IC_{50} 2.8 ± 0.4 nM and 7.6 ± 0.7 nM respectively. (Wells, Counago et al. 2019, Kostich, Hamman et al. 2016). Genecopoeia HEK293T ectopically expressing ACE2 cells were treated with AAK1 specific inhibitors for 4 hours. After 4 hours, cells were lysed, and immunoblotting was done using a p-AP2M1 antibody. AAK1 inhibition led to the loss of phosphorylation of AP2M1 by these kinase inhibitors (Fig. 3.14).

Using this assay, we tested the clinically-used drugs that have been shown for their ability to inhibit AAK1 (and other kinases like GAK) and inhibit the entry of viruses (Neveu, Ziv-Av et al. 2015, Bekerman, Neveu et al. 2017, Pu, Xiao et al. 2018). The inhibitors are Sunitinib, Erlotinib and Baricitinib. Sunitinib is multi-targeted receptor tyrosine kinase inhibitor which has been approved by FDA for treating renal cell carcinoma and gastrointestinal stromal tumor resistant to imatinib. The multiple RTK targets of Sunitinib are platelet-derived growth factor receptors, vascular endothelial growth factor

receptors, KIT (CD117), CSF-1r, RET receptor for glial cell line-derived neurotrophic factor (GDNF) family and flt-3. Erlotinib is an inhibitor of EGFR and is used in the treatment of non-small cell lung cancer, pancreatic cancer and several other types of cancer. Recently, it has been shown that Erlotinib also inhibits a mutant of JAK2 tyrosine kinase (JAK2V617F). Baricitinib is a selective Janus Kinase 1 (JAK1) and Janus Kinase 2 (JAK2). Baricitinib in case of rheumatoid arthritis was shown to have significant anti-inflammatory effects. It blocks JAK1/2 and disrupts the activation of downstream signaling molecules and proinflammatory mediators.

Hek293T cells from Genecopoeia ectopically expressing ACE2 after treatment with inhibitors for 4 hours were lysed and immunoblotted with p-AP2M1 antibody. Like AAK1 specific inhibitors, we saw the loss of phosphorylation with Sunitinib and other inhibitors as well (Fig. 3.15). While Sunitinib and SGC-AAK1-1 demonstrated AAK1 inhibitory activity at mid-high nano-molar and low micro-molar concentrations respectively, Erlotinib, and Baricitinib required high micro-molar concentrations at which cell death was apparent (not shown)

To assess the impact of AAK1 inhibition with LP-922761 and LP-935509 (Sunitinib serves as positive control (Wang, P. G., Tang et al. 2020)), on S-RBD/ACE2 co-endocytosis. Based on the inhibition experiment (Fig. 3.13 and Fig. 3.14), we took three concentrations from nM to uM range showing slight to complete loss of phosphorylation of AP2M1. Genecopoeia HEK293T cells ectopically expressing ACE2 were plated on coverslips and pretreated with 625 nM, 2.5 uM, or 10 uM of inhibitors for 2 hours and binding with S-RBD was done in presence of inhibitors at 4°C for 1 hour. After binding cells were washed and endocytosis assay was carried out in the presence of the inhibitors for 8 hours at 37°C. We observed that S-RBD endocytosis is AAK1-dependent and exhibited the dose-dependent manner inhibition of S-RBD internalization. (Fig. 3.16). At

10 uM, we saw a significant difference in the internalization of S-RBD between the control and inhibitor-treated cells (Fig. 3.16C and D).

3.4. Figures

Figure 3.1

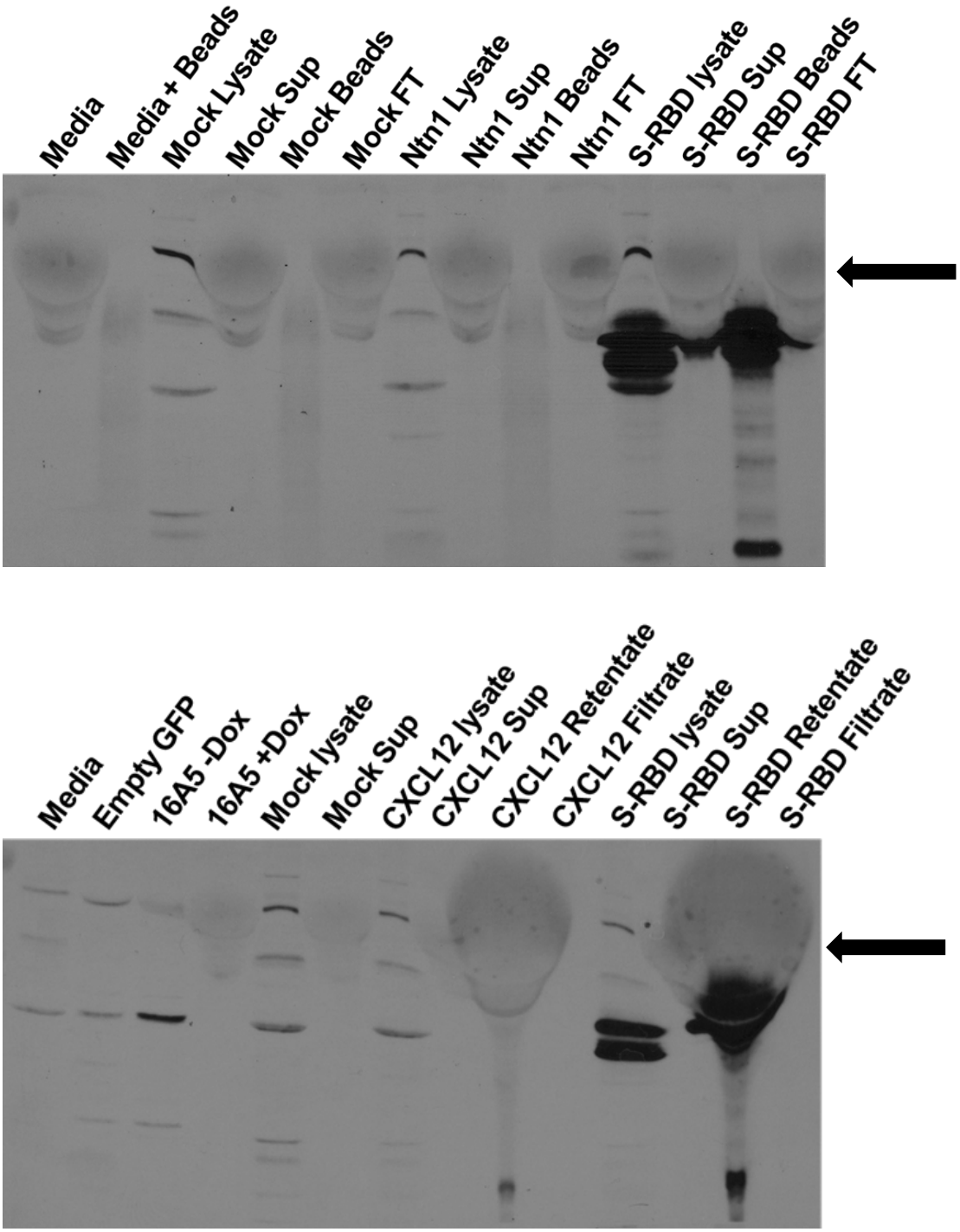
Media
Media + Beads
Mock Lysate
Mock Sup
Mock Beads
Mock FT
Ntn1 Lysate
Ntn1 Sup
Ntn1 Beads
Ntn1 FT
S-RBD lysate
S-RBD Sup
S-RBD Beads
S-RBD FT
Media
Empty GFP
16A5 -Dox
16A5 +Dox
Mock lysate
Mock Sup
CXCL12 lysate
CXCL12 Sup
CXCL12 Retentate
CXCL12 Filtrate
S-RBD lysate
S-RBD Sup
S-RBD Retentate
S-RBD Filtrate

Figure 3.1 Expression and purification of S-RBD-Fc and S-RBD-sfGFP in HEK293T cells.

Upper panel: Western blot analysis of S-RBD-Fc expressed in HEK293T cells after transient transfection and samples taken at various protein A Sepharose purification steps. Immunoblotting was done using commercially available antibody by Sino Biological against RBD of SARS-CoV-2. Ntn1 served as a negative control. The samples prepared for western blot analysis are cell lysates, cell supernatants after 96 hours of transfection, beads which are with bound protein after incubation with cell supernatants (sup) for 3 hours, FT (flow through) are the supernatant samples taken after binding of protein with beads. **Lower panel:** Western blot analysis of S-RBD-sfGFP expressed in HEK293T cells after transient transfection and concentrating the supernatant. Immunoblotting was done using commercially available antibody by Sino Biological against RBD of SARS-CoV-2. CXCl12 served as a negative control. GFP lysates were used for probing with GFP antibody. The samples prepared for western blot analysis are cell lysates, cell supernatants (sup) after 96 hours of transfection, concentrated proteins which is retentate and the filtrate which passes through the concentrator.

Figure 3.2

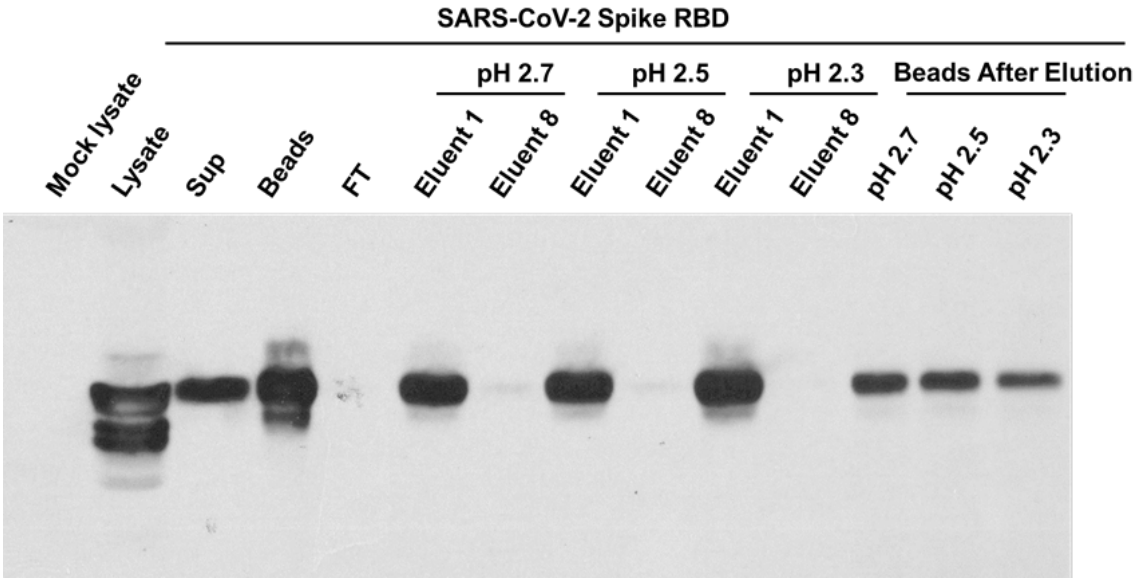
SARS-CoV-2 Spike RBD
pH 2.7
pH 2.5
pH 2.3
Beads After Elution
Mock lysate
Lysate
Sup
Beads
FT
Eluent 1
Eluent 8
Eluent 1
Eluent 8
Eluent 1
Eluent 8
pH 2.7
pH 2.5
pH 2.3

Figure 3.2. Expression and purification of SARS-CoV-2 Spike RBD [Fc].

Western blot analysis of SARS-CoV-2 Spike RBD [Fc] expressed in Freestyle 293 cells after transient transfection and samples were taken at various A Sepharose purification steps and glycine buffer elution. Immunoblotting was done using commercially available antibody by Sino Biological against RBD of SARS-CoV-2. The samples prepared for western blot analysis are cell lysates, cell supernatants (sup) after 96 hours of transfection, beads which are with bound protein after incubation with cell supernatants for 3 hours, FT (flow through) are the supernatant samples taken after binding of protein with beads, several fractions of eluted protein with different pH and beads after eluting the proteins.

Figure 3.3

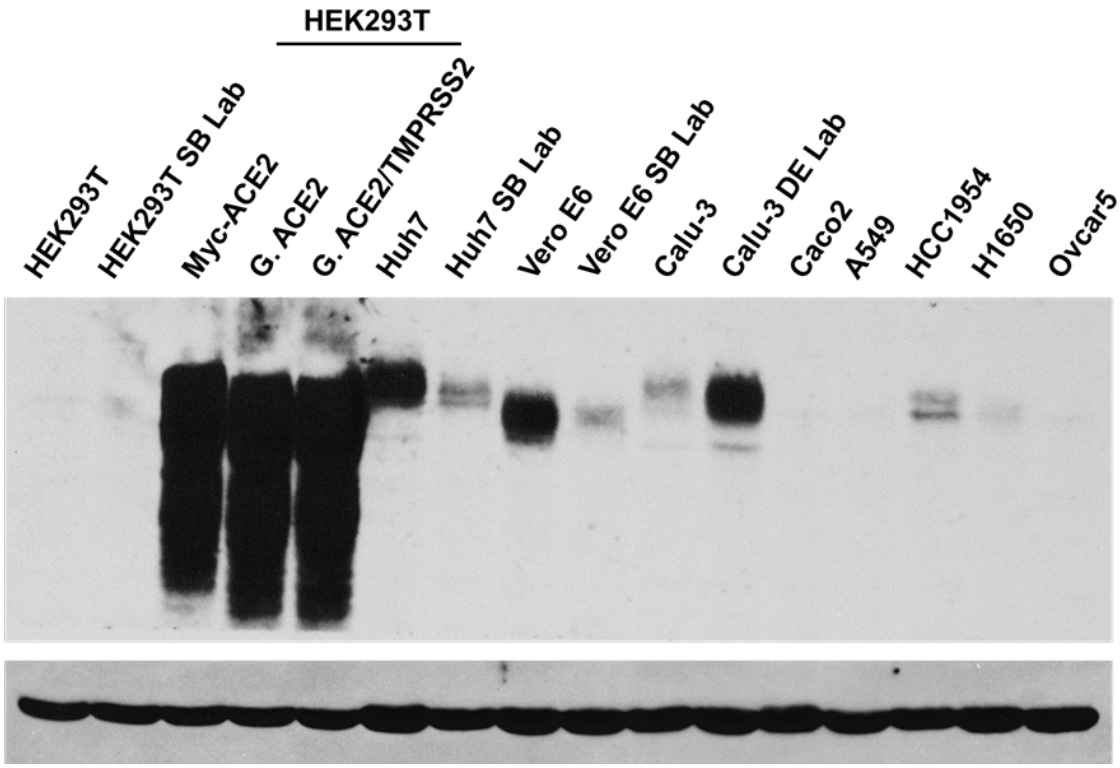
HEK293T
HEK293T
HEK293T SB Lab
Myc-ACE2
G. ACE2
G. ACE2/TMPRSS2
Huh7
Huh7 SB Lab
Vero E6
Vero E6 SB Lab
Calu-3
Calu-3 DE Lab
Caco2
A549
HCC1954
H1650
Ovcar5

Figure 3.3. Relative expression of ACE2.

Western blot analysis of 50ug lysates of HEK293T from our lab or Dr. Sidappa Byrareddy's lab (SB lab), in house generated HEK293T Myc-ACE2, Genecopoeia (G) HEK293T ACE2 or ACE2/TMPRSS2, Huh7 from our lab SB lab, Vero E6 from our lab or SB lab, Calu-3 from our lab or Dr. Dalia Elgamal's lab (DE lab), Caco2, A549, HCC1954, H1650, and Ovcar5 with commercially available ACE2 antibody from abcam at a dilution of 1:1000. Beta-actin as a loading control.

Figure 3.4

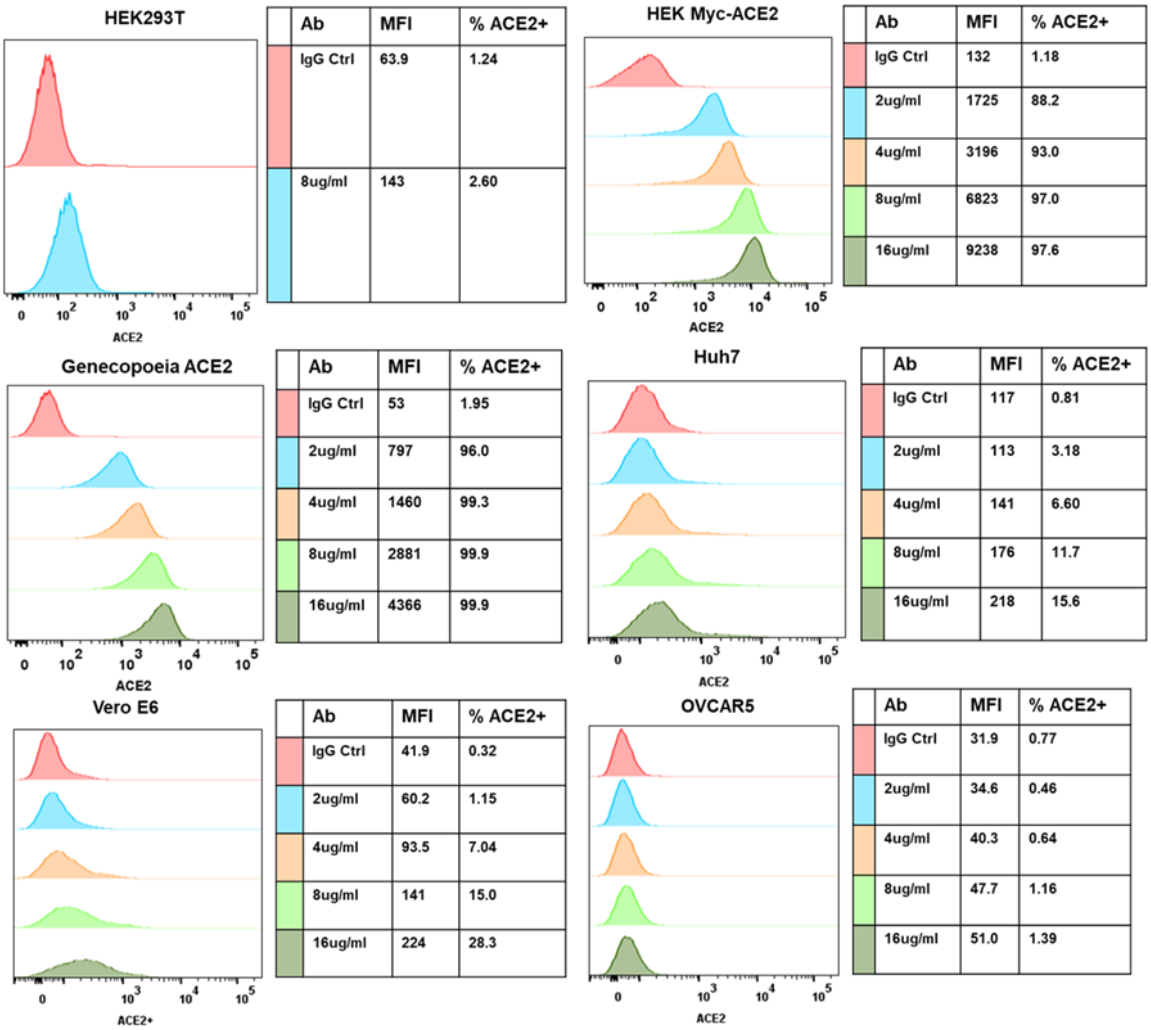

Ab	MFI	% ACE2+
IgG Ctrl	63.9	1.24
8ug/ml	143	2.60

Ab	MFI	% ACE2+
IgG Ctrl	132	1.18
2ug/ml	1725	88.2
4ug/ml	3196	93.0
8ug/ml	6823	97.0
16ug/ml	9238	97.6

Ab	MFI	% ACE2+
IgG Ctrl	53	1.95
2ug/ml	797	96.0
4ug/ml	1460	99.3
8ug/ml	2881	99.9
16ug/ml	4366	99.9

Ab	MFI	% ACE2+
IgG Ctrl	117	0.81
2ug/ml	113	3.18
4ug/ml	141	6.60
8ug/ml	176	11.7
16ug/ml	218	15.6

Ab	MFI	% ACE2+
IgG Ctrl	41.9	0.32
2ug/ml	60.2	1.15
4ug/ml	93.5	7.04
8ug/ml	141	15.0
16ug/ml	224	28.3

Ab	MFI	% ACE2+
IgG Ctrl	31.9	0.77
2ug/ml	34.6	0.46
4ug/ml	40.3	0.64
8ug/ml	47.7	1.16
16ug/ml	51.0	1.39

Figure 3.4 Surface Expression of ACE2.

FACS analysis of ACE2 transfected HEK293T, Genecopoeia ACE2, Huh7, Vero E6 and OVCAR5 (Negative control) cell lines with a control IgG (Goat IgG; R&D Systems #AB-108-C) (2ug/ml) or anti-ACE2 (Goat IgG ACE2; R&D Systems #AF933) antibodies (2-8 ug/ml) followed by (Alexa Fluor 647 donkey anti-goat IgG; Invitrogen #A21447; 2ug/ml). % positive and mean fluorescence intensity (MFI) are indicated in the table.

Figure 3.5

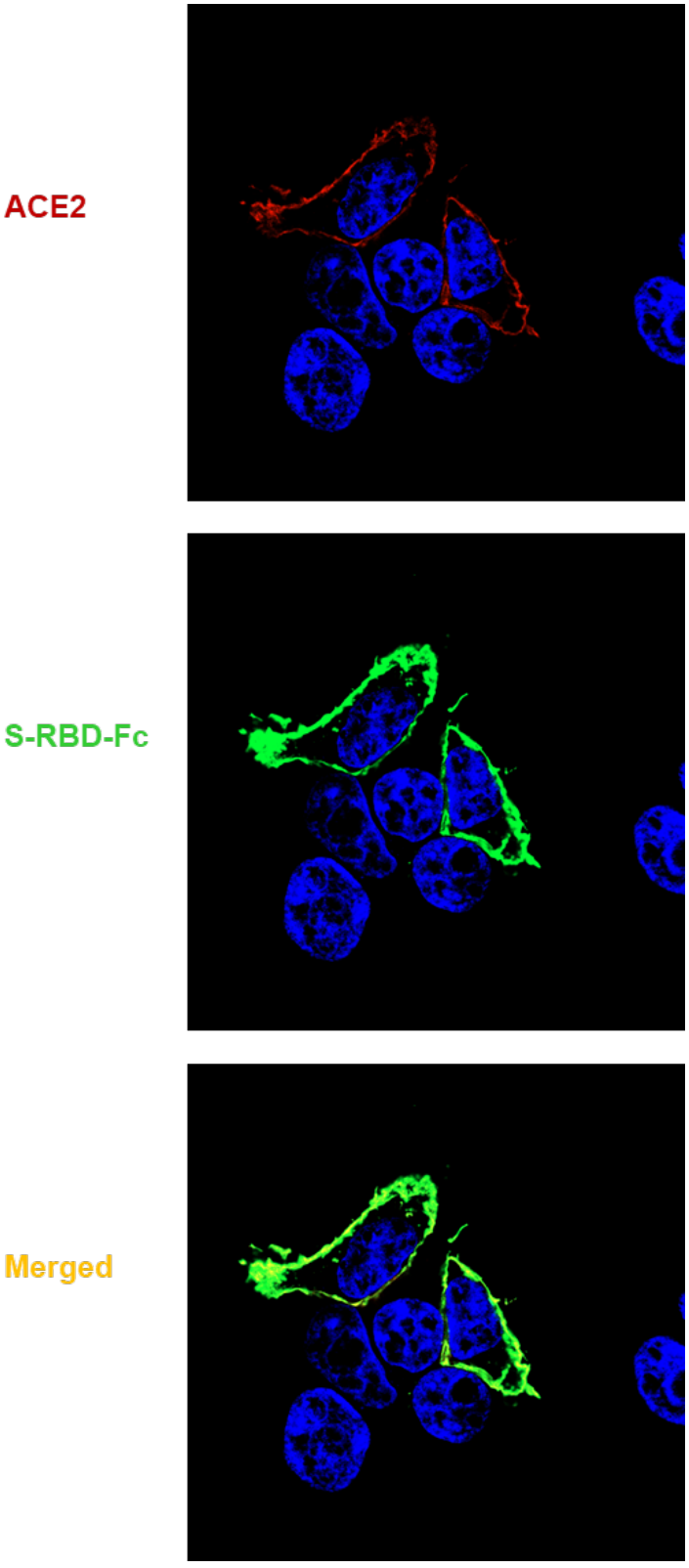

Figure 3.5 Surface Binding of SARS-CoV-2 RBD with receptor ACE2.

HEK293T-ACE2 were grown on coverslips, and after a day of settling, cells were incubated with S-RBD-Fc containing supernatant for 1 hour at 4°C to allow binding. Cells after binding were fixed, permeabilized, and stained with anti-Myc mouse antibody to detect ACE2 (red) and anti-human IgG to detect S-RBD-Fc (green). From the figure, we can see S-RBD binding to ACE2+ cells (no binding to ACE2-negative cells) in green and ACE2 is visualized by staining in red. The IF staining results demonstrated binding of S-RBD only to ACE2-overexpressing 293T cells, with no staining of the non-ACE2-expressing cells demonstrating specificity. ACE2 and S-RBD staining signals showed complete co-localization.

Figure 3.6

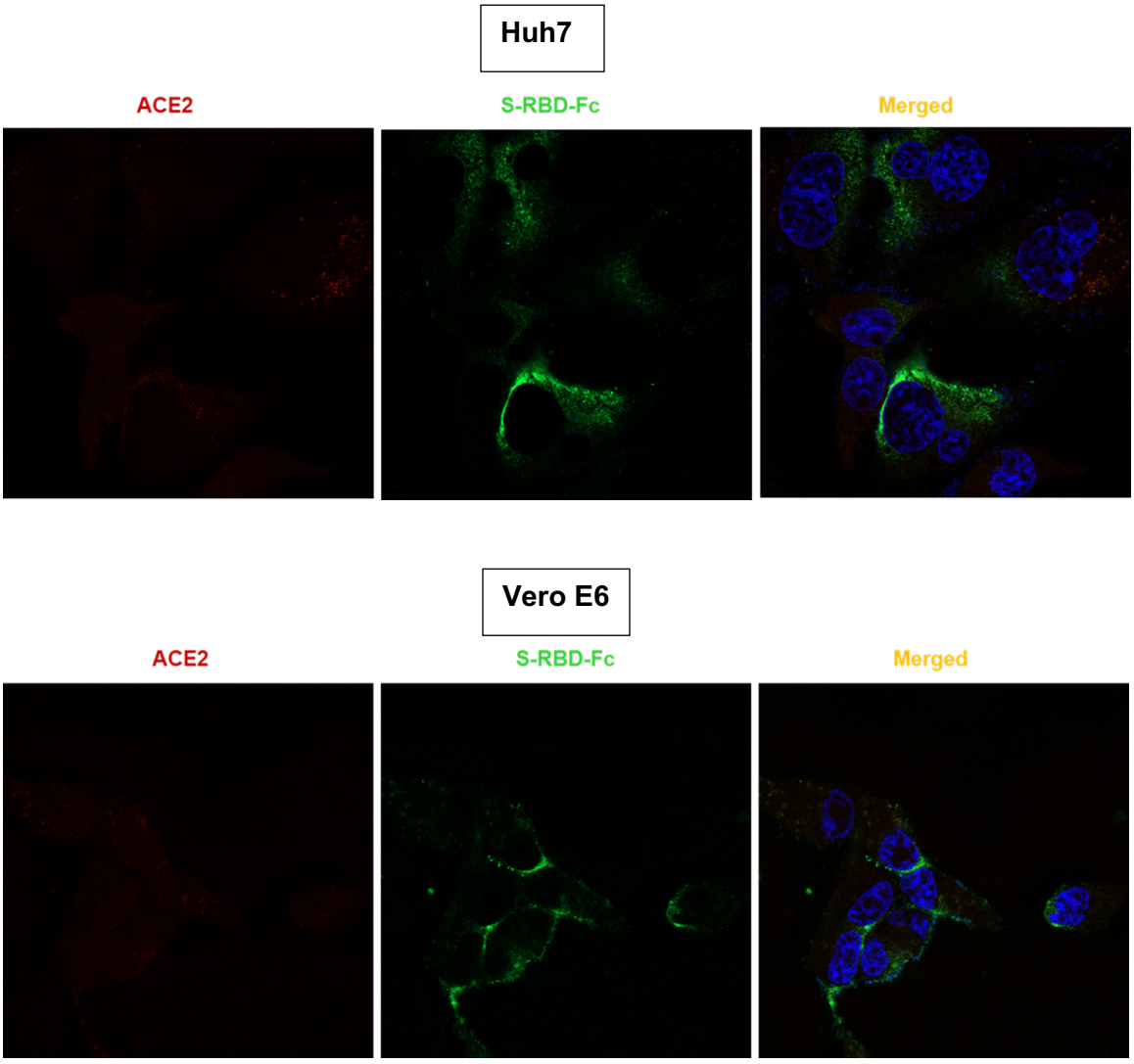

Figure 3.6 Surface Binding of SARS-CoV-2 RBD with receptor ACE2 in Huh7 and Vero E6 cells.

Huh7 (upper panel) and Vero E6 (lower panel) were grown on coverslips. After a day of settling, cells were incubated with S-RBD-Fc containing supernatant for 1 hour at 4°C to allow binding. Cells after binding were washed, fixed, permeabilized, and stained with anti-ACE2 (slight red) and anti-human IgG to detect S-RBD-Fc (green). The staining confirms the specific binding of S-RBD to the ACE2 receptor.

Figure 3.7

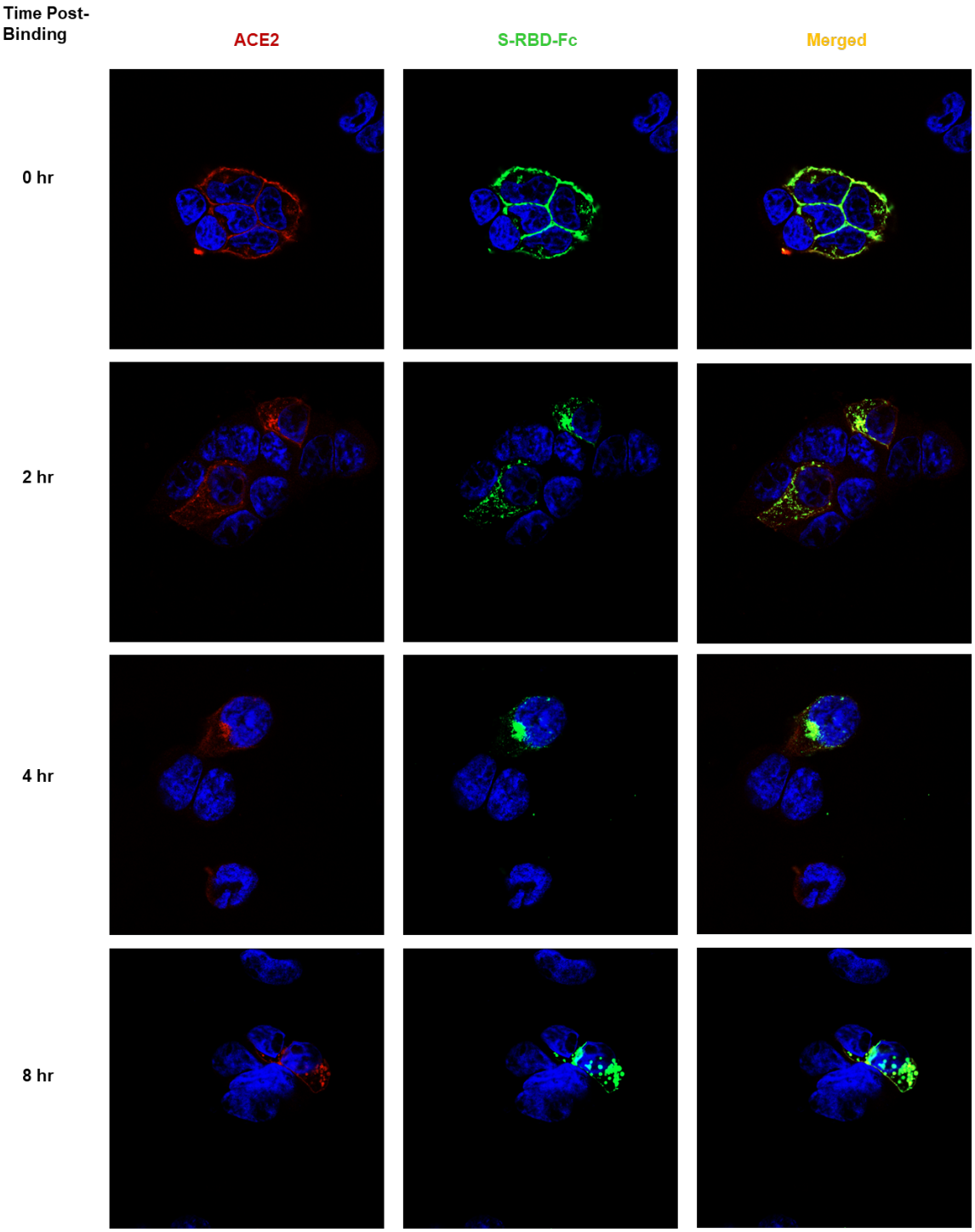

Figure 3.7 SARS-CoV-2 S-RBD and ACE2 Co-endocytosis assay.

HEK293T-ACE2 cells were incubated with S-RBD-Fc containing supernatant for 1 hour at 4°C to allow binding of S-RBD to ACE2+ cells (no binding to ACE2-negative cells) – seen at time 0 hr. Cells were washed and incubated at 37°C for various times to allow endocytosis. Cells were fixed, permeabilized, and stained with anti-Myc mouse antibody to detect ACE2 (red) and anti-human IgG to detect S-RBD-Fc (green). Perfect colocalization of ACE2 and S-RBD-Fc is observed. Note the decrease of surface ACE2/S-RBD over time and accumulation in internalized vesicles, indicating their co-endocytosis.

Figure 3.8

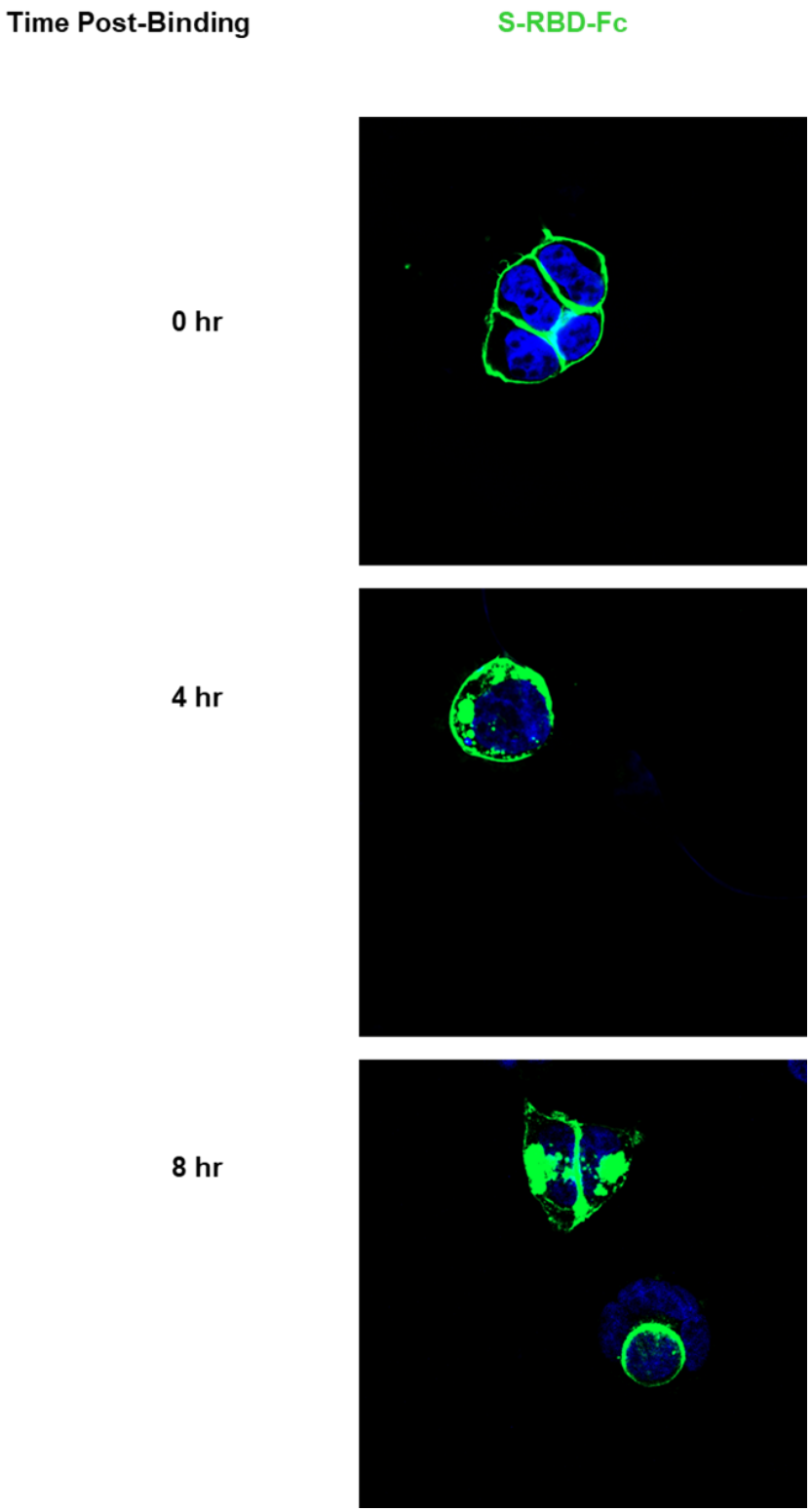

Figure 3.8 SARS-CoV-2 S-RBD endocytosis assay.

Genecopoeia HEK293T cells ectopically expressing ACE2 were incubated with S-RBD-Fc containing supernatant for 1 hour at 4°C to allow binding of S-RBD. Cells were washed and incubated at 37°C for various time points to allow endocytosis. Cells were fixed, permeabilized, and stained with anti- anti-human IgG to detect S-RBD-Fc (green). Endocytosis was seen based on more internalized S-RBD and decreased surface staining over the period.

Figure 3.9

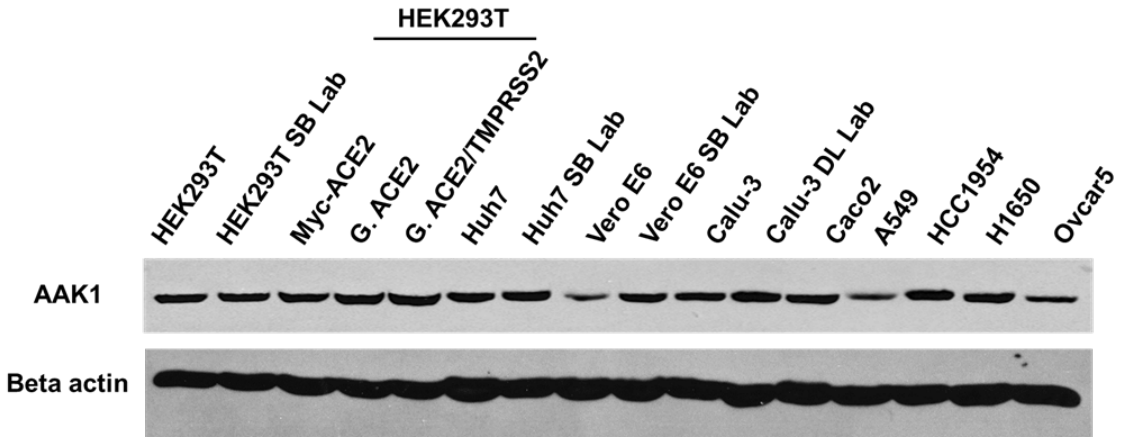
HEK293T
HEK293T
HEK293T SB Lab
Myc-ACE2
G. ACE2
G. ACE2/TMPRSS2
Huh7
Huh7 SB Lab
Vero E6
Vero E6 SB Lab
Calu-3
Calu-3 DL Lab
Caco2
A549
HCC1954
H1650
Ovcar5
AAK1
Beta actin

Figure 3.9 Relative expression of AAK1.

Western blot analysis of 50ug lysates of HEK293T from our lab or Dr. Sidappa Byrareddy's lab (SB lab), in house generated HEK293T Myc-ACE2, Genecopoeia (G) HEK293T ACE2 or ACE2/TMPRSS2, Huh7 from our lab SB lab, Vero E6 from our lab or SB lab , Calu-3 from our lab or Dr. Dalia Elgamal's lab (DE lab), Caco2, A549, HCC1954, H1650, and Ovcar5 with commercially available AAK1 antibody from Bethyl lab at a dilution of 1:1000. Beta-actin as a loading control.

Figure 3.10

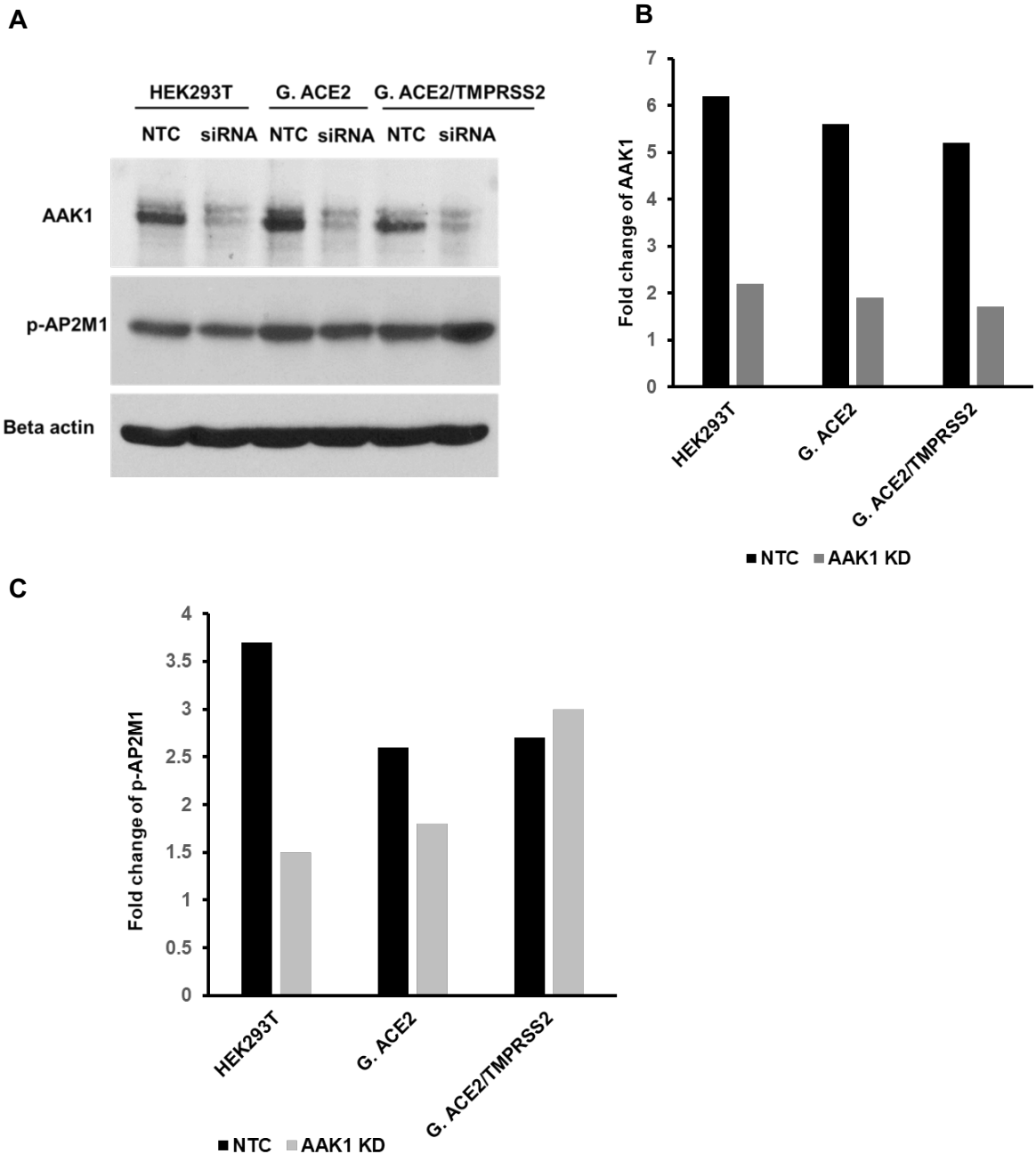
A
HEK293T
G. ACE2
G. ACE2/TMPRSS2
NTC siRNA NTC siRNA NTC siRNA
AAK1
p-AP2M1
Beta actin
B
Fold change of AAK1
0 1 2 3 4 5 6 7
HEK293T
G. ACE2
G. ACE2/TMPRSS2
NTC
AAK1 KD
C
Fold change of p-AP2M1
0 0.5 1 1.5 2 2.5 3 3.5 4
HEK293T
G. ACE2
G. ACE2/TMPRSS2
NTC
AAK1 KD

Figure 3.10. Knockdown of AAK1.

(A). Western blot analysis of siRNA mediated KD of AAK1. Cells were transfected with siRNA targeting AAK1 or with non-targeting control (NTC). After 48 hours of transfection, cells were lysed and immunoblotted with Bethyl- AAK1, CST Phospho-AP2M1, and Beta-actin antibodies. Beta-actin served as a loading control. Upper panel shows knockdown of AAK1 and the middle panel shows reduction of p-AP2M1 levels upon AAK1 knockdown as compared to NTC. **(B)** Densitometric quantification of AAK1 signals presented in panel b normalized to the level of the β-actin loading control. **(C)** Densitometric quantification of p-AP2M1 signals presented in panel c normalized to the level of the β-actin loading control

Figure 3.11

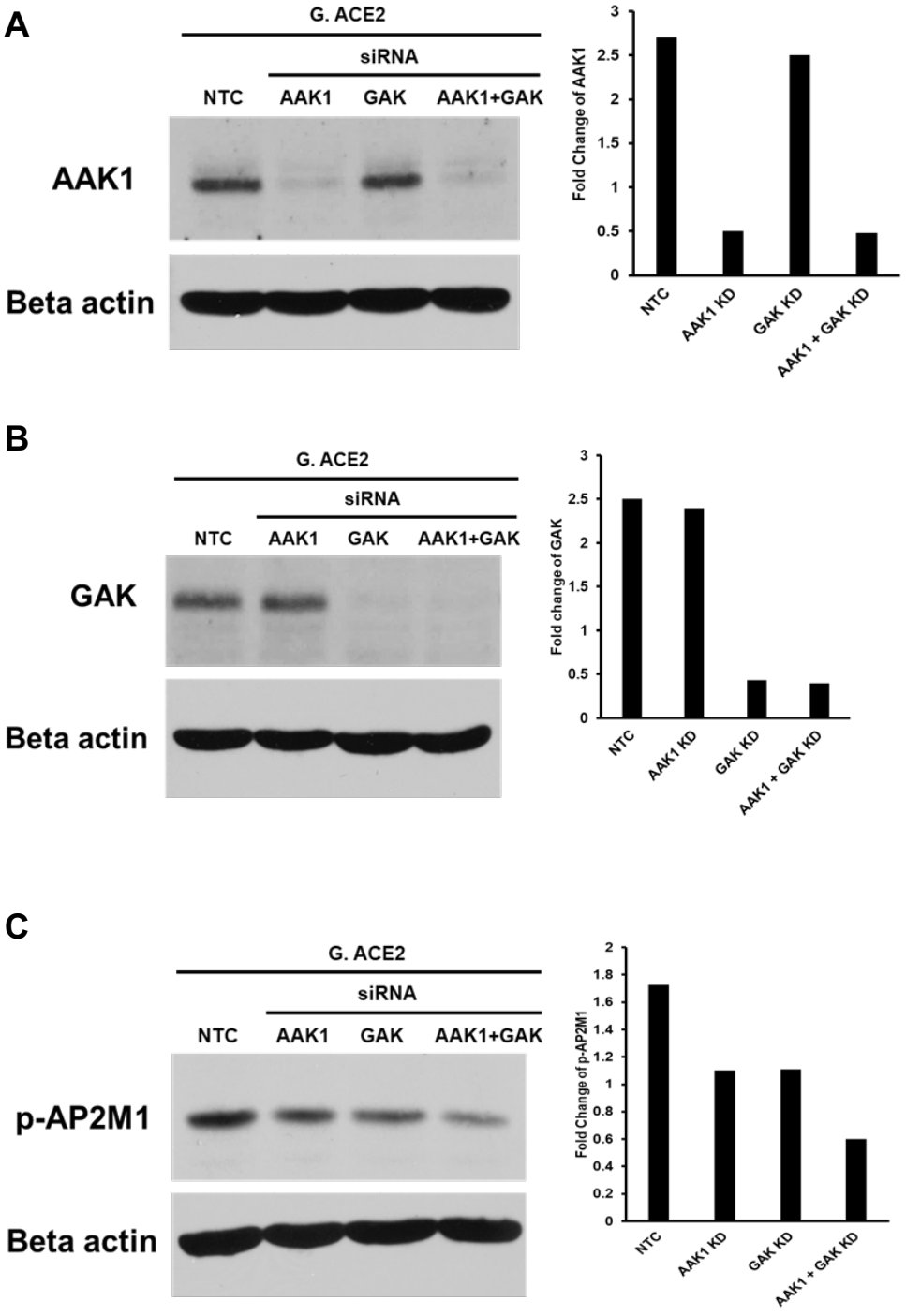
A
G. ACE2
siRNA
NTC
AAK1
GAK
AAK1+GAK
AAK1
Beta actin
Fold Change of AAK1
NTC
AAK1 KD
GAK KD
AAK1 + GAK KD
B
G. ACE2
siRNA
NTC
AAK1
GAK
AAK1+GAK
GAK
Beta actin
Fold change of GAK
NTC
AAK1 KD
GAK KD
AAK1 + GAK KD
C
G. ACE2
siRNA
NTC
AAK1
GAK
AAK1+GAK
p-AP2M1
Beta actin
Fold Change of p-AP2M1
NTC
AAK1 KD
GAK KD
AAK1 + GAK KD

Figure 3.11. Knockdown of AAK1 and GAK

(A) Left Panel: Western blot analysis of siRNA mediated KD of AAK1 or GAK or both. Cells were transfected with siRNA targeting AAK1, GAK, or with non-targeting control (NTC). Cells were lysed after 48 hours of transfection and immunoblotted with Bethyl- AAK1 and Beta-actin antibodies. Beta-actin serves as a loading control. **Right panel**: Densitometric quantification of AAK1 signals presented in panel b normalized to the level of the β-actin loading control. **(B) Left Panel**: Western blot analysis of siRNA mediated KD of AAK1 or GAK or both. Cells were transfected with siRNA targeting AAK1, GAK, or with a non-targeting control (NTC). Cells were lysed after 48 hours of transfection and immunoblotted with R&D GAK and Beta-actin antibodies. Beta-actin serves as a loading control. **Right panel**: Densitometric quantification of GAK signals presented in panel b normalized to the level of the β-actin loading control. **(C) Left Panel**: Western blot analysis of siRNA mediated KD of AAK1 or GAK or both. Cells were transfected with siRNA targeting AAK1, GAK, or with non-targeting control (NTC). Cells were lysed after 48 hours of transfection and immunoblotted with CST Phospho-AP2M1 and Beta-actin antibodies. Beta-actin serves as a loading control. **Right panel**: Densitometric quantification of p-AP2M1 signals presented in panel b normalized to the level of the β-actin loading control.

Figure 3.12

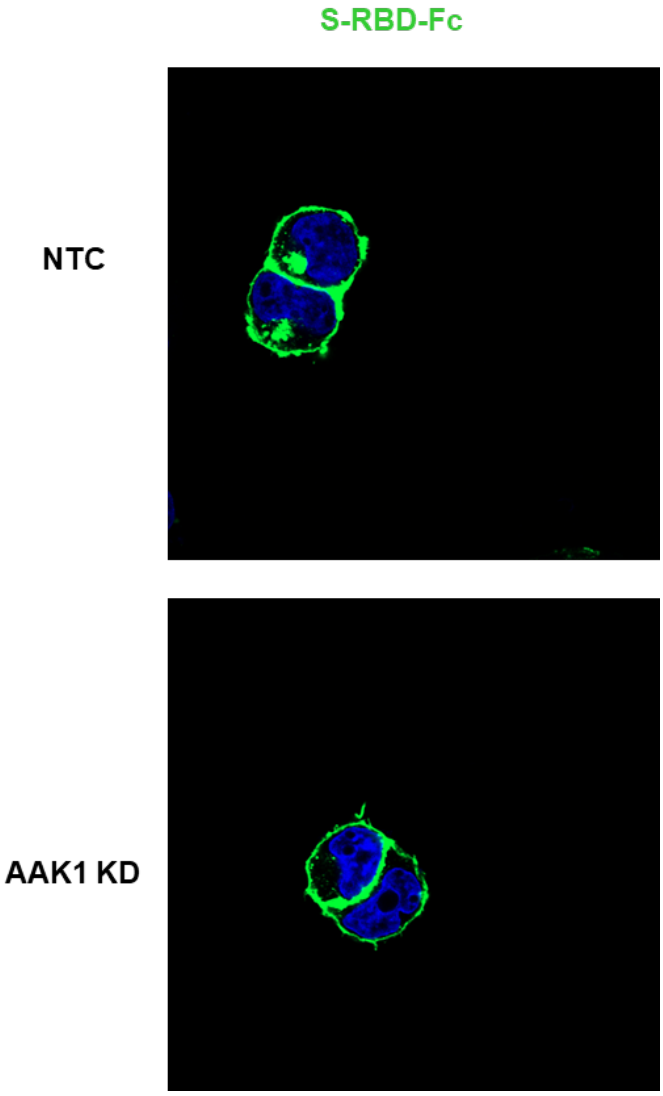

Figure 3.12 SARS-CoV-2 S-RBD endocytosis in AAK1 control and KD cells

Genecopoeia cells were transfected with either NTC or smartpool AAK1 siRNA. After 48 hours, cells were trypsinized and re-plated on coverslips. After a day of attachment, cells were incubated with S-RBD-Fc containing supernatant for 1 hour at 4°C to allow binding of S-RBD to ACE2+ cells. Cells were washed and incubated at 37°C for 4 hours to allow endocytosis. Cells were fixed, permeabilized, and stained with anti-human IgG to detect S-RBD-Fc (green). Lower panel knocking down AAK1 reduced the internalization as compared to the control cells in the upper panel.

Figure 3.13

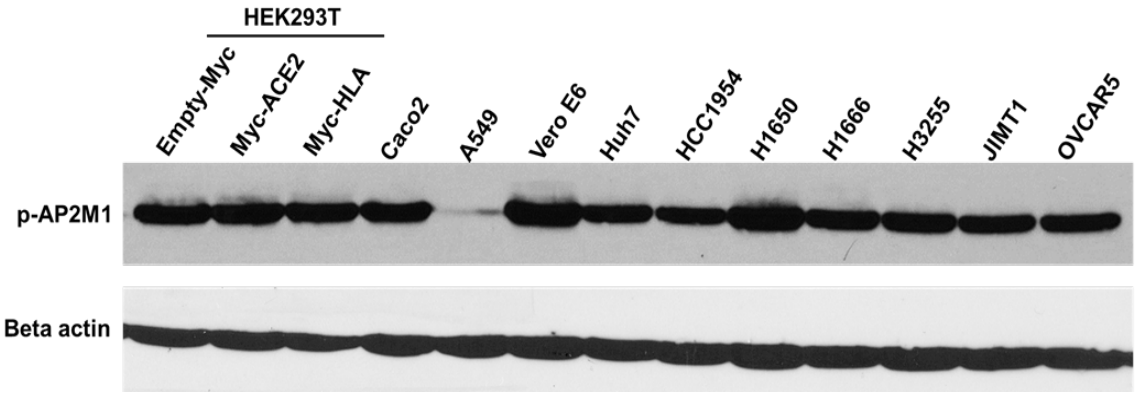
HEK293T
Empty-Myc
Myc-ACE2
Myc-HLA
Caco2
A549
Vero E6
Huh7
HCC1954
H1650
H1666
H3255
JIMT1
OVCAR5
p-AP2M1
Beta actin

Figure 3.13. Relative expression of p-AP2M1.

Western blot analysis of 50 ug lysates of HEK293T mock and transfected cell lines and additional lines (Caco2, A549, Vero-E6, Huh7, HCC1954, H1666, H3255, JIMT1, and Ovcar5) with CST p-AP2M1 antibody at a dilution of 1:1000. Beta-actin (loading control).

Figure 3.14

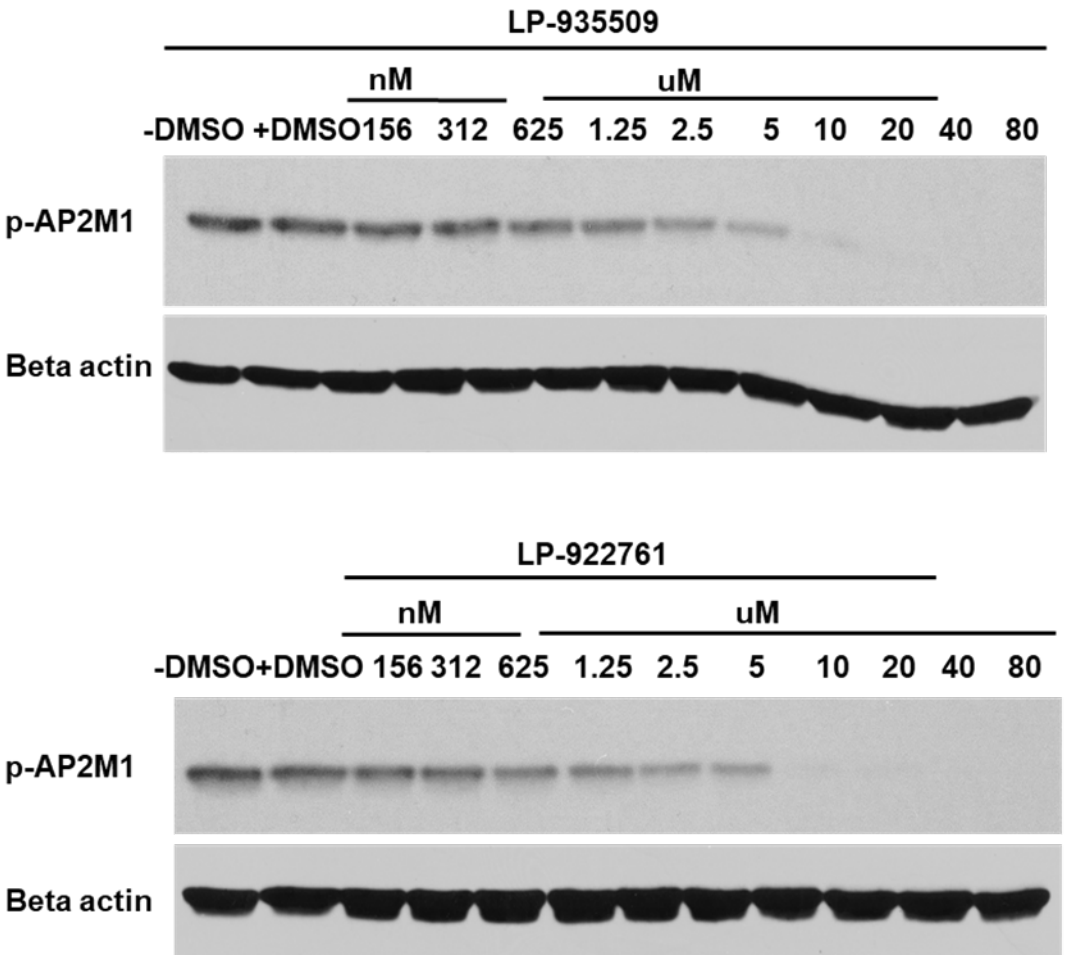
LP-935509
nM
uM
-DMSO +DMSO156 312 625 1.25 2.5 5 10 20 40 80
p-AP2M1
Beta actin
LP-922761
nM
uM
-DMSO+DMSO 156 312 625 1.25 2.5 5 10 20 40 80
p-AP2M1
Beta actin

Figure 3.14. Inhibition of AAK1-by-AAK1 specific inhibitors

Genecopoeia HEK293T cells ectopically expressing ACE2 were incubated with the indicated concentrations of AAK1 specific inhibitors (or DMSO) for 4 hours. 50 ug of cell lysates were run on a run Western blot and probed for AAK1 activity for the phosphorylation levels of AP2M1 (an endogenous substrate of AAK1) using CST p-AP2M1 antibody. Beta-actin as a loading control. AAK1 inhibition led to the loss of phosphorylation of AP2M1 by these kinase inhibitors.

Figure 3.15

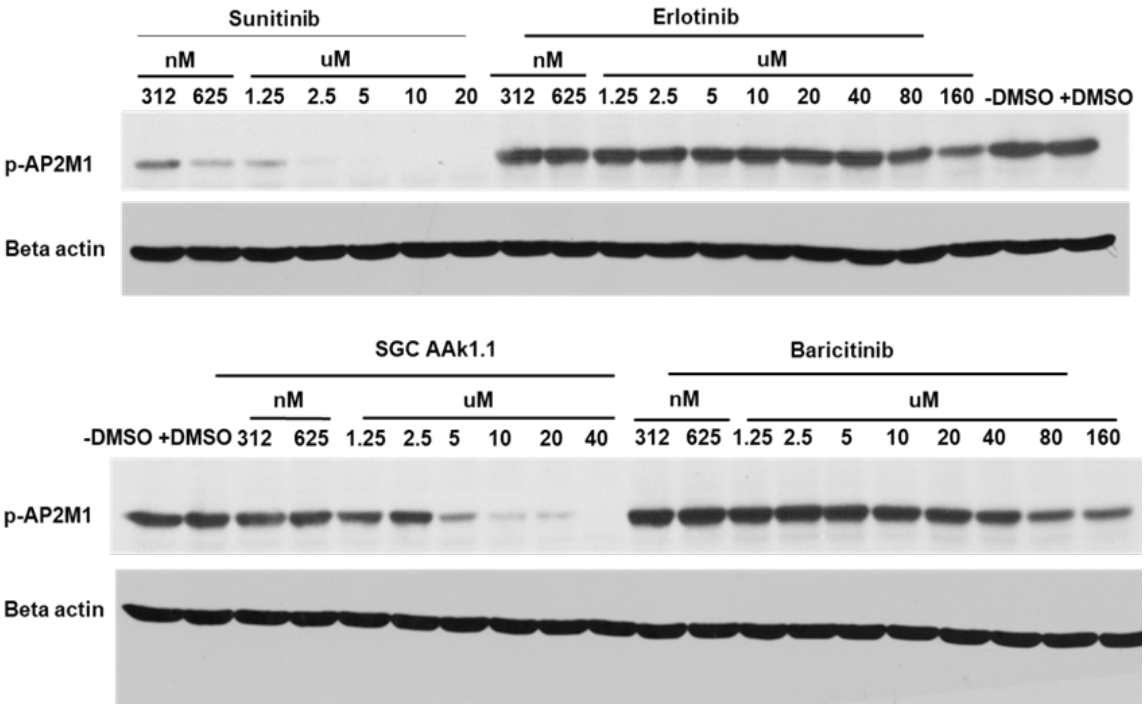
Sunitinib
Erlotinib
nM
uM
nM
uM
312 625 1.25 2.5 5 10 20 312 625 1.25 2.5 5 10 20 40 80 160 -DMSO +DMSO
p-AP2M1
Beta actin
SGC AAk1.1
Baricitinib
nM
uM
nM
uM
-DMSO +DMSO 312 625 1.25 2.5 5 10 20 40 312 625 1.25 2.5 5 10 20 40 80 160
p-AP2M1
Beta actin

Figure 3.15. Inhibition of AAK1 by Sunitinib, Erlotinib, SGC-AAK1-1, and Baricitinib.

Genecopoeia HEK293T cells ectopically expressing ACE2 were incubated with the indicated concentrations of clinically used inhibitors (or DMSO) for 4 hours. 50 ug of cell lysates were run on a run Western blot and probed for AAK1 activity for the phosphorylation levels of AP2M1 (an endogenous substrate of AAK1) using CST p-AP2M1 antibody. Beta-actin as a loading control. AAK1 inhibition led to the loss of phosphorylation of AP2M1 by these kinase inhibitors. While Sunitinib and SGC-AAK1-1 demonstrated AAK1 inhibitory activity at mid-high nano-molar and low micro-molar concentrations respectively, Erlotinib and Baricitinib required high micro-molar concentrations.

Figure 3.16

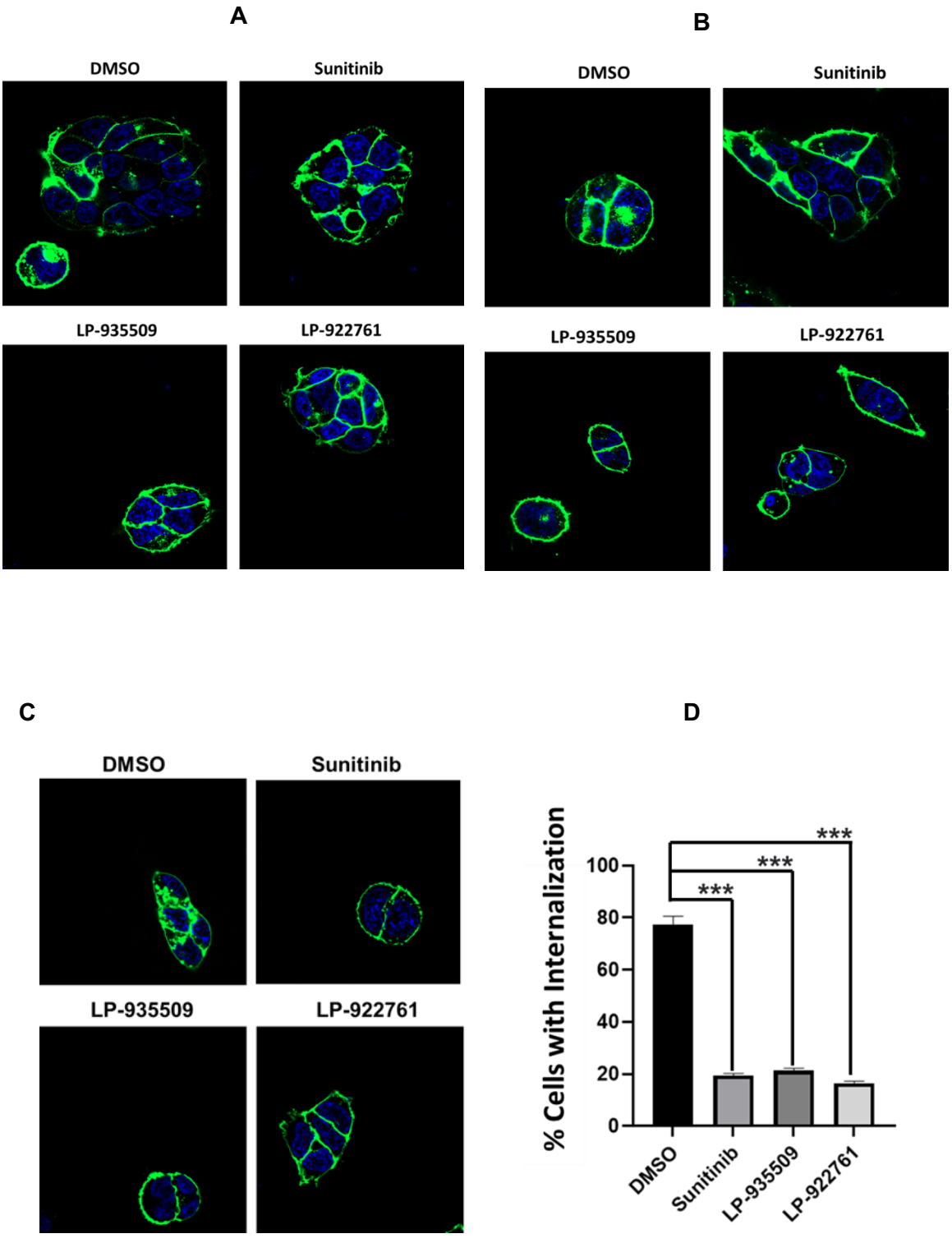
A
DMSO
Sunitinib
LP-935509
LP-922761
B
DMSO
Sunitinib
LP-935509
LP-922761
C
DMSO
Sunitinib
LP-935509
LP-922761
D
% Cells with Internalization
100
80
60
40
20
0
***
***
***
DMSO
Sunitinib
LP-935509
LP-922761

Figure 3.16 SARS-CoV-2 S-RBD endocytosis in Genecopoeia ACE2 cells treated with AAK1 inhibitors or DMSO

(A and B) Genecopoeia ACE2 cells were pre-treated with 625 nM (**Upper Left**) or 2.5 uM (**Upper Right)** of inhibitors or DMSO and incubated with S-RBD-Fc containing supernatant for 1 hour at 4°C to allow binding of S-RBD along with the inhibitors. Cells were washed and incubated at 37°C for 8 hours to allow endocytosis. Inhibitor treatment was continued during the internalization step. Cells were fixed, permeabilized, and stained with anti- anti-human IgG to detect S-RBD-Fc (green). **(C)** Genecopoeia ACE2 cells were pre-treated with 10 uM of inhibitors or DMSO and incubated with S-RBD-Fc containing supernatant for 1 hour at 4°C to allow binding of S-RBD along with the inhibitors. Cells were washed and incubated at 37°C for 8 hours to allow endocytosis. Inhibitor treatment was continued during the internalization step. Cells were fixed, permeabilized, and stained with anti- anti-human IgG to detect S-RBD-Fc (green). **(D)** Quantification of internalization when cells were treated with 10 uM of inhibitors. The average of three independent experiments conducted in triplicate samples Error bars indicate Standard error means. Cells with DMSO served as a control for the inhibitor-treated cells. $P < 0.001$ ***.

3.5. Discussion

The immune system of human populations is naïve towards the newly-emerged SARS-CoV-2. Combined with the high transmission rate and a huge burden of morbidity and mortality among patients, COVID-19 has led to enormous healthcare and economic emergency worldwide. The urgency to reduce the impact of COVID-19 has led to numerous ongoing efforts to develop vaccines and repurpose existing drugs that may target host factors used by SARS-CoV-2 for host cell infection and/or pathogenesis, some with moderate success (e.g., dexamethasone) (Bai, Chotirmall et al. 2020). The first step in viral infection is its entry into the target cell to reach the subcellular location where replication and assembly of the virus can take place. The mechanisms used by viruses to enter the host cells are unique to viruses and highly variable (Pelkmans, Helenius 2003). However, most viruses use the endocytic pathways to deliver viral contents into the host cell (Yamauchi, Helenius 2013). Among them, the most used pathway is clathrin-mediated endocytosis (Helenius, Kartenbeck et al. 1980). The strategic entry of viruses into host cells using clathrin-mediated endocytosis helps them multiply efficiently and evade immune surveillance. It has been shown for SARS-CoV that one of the pathways for endocytic entry is a clathrin-mediated pathway (Inoue, Tanaka et al. 2007). Since SARS-CoV-2 bears many similarities to SARS-CoV, it might also utilize the same mechanism to enter the host cells. In this regard, studies were conducted which showed that SARS-CoV-2 uses this mode of endocytosis to enter into mammalian cells by using ACE2 as the receptor. Still, the complete elucidation of the pathways and the molecular players involved in the entry of SARS-CoV-2 remain to be fully established (Hoffmann, Kleine-Weber et al. 2020, Owczarek, Szczepanski et al. 2018, Bayati, Kumar et al. 2021). The studies and information about the host molecular players involved in the clathrin-mediated endocytosis of viruses are limited. Previously it has been shown that AAK1 plays a role in the entry of several viruses (Bekerman, Neveu et al. 2017, Pu, Xiao et al. 2018, Neveu,

Ziv-Av et al. 2015), but no role of AAK1 in the entry of SARS-CoV-2 was elucidated when the current studies were initiated in May of 2020 and still there hasn't been any study published which will primarily talk about role of AAK1 in the entry of SARS-CoV-2, providing an impetus for the studies presented in this chapter. These studies establish a role for AAK1 (and potentially related kinases), via AP2M1 phosphorylation, in facilitating the entry of SARS-CoV-2 as modeled by the S-RBD. Our studies also define clinically-used candidate drugs with an ability to inhibit the phosphorylation of AP2M1 as well as AAK1-specific early-stage inhibitors as potential therapeutic agents to inhibit SARS-CoV-2 entry into host cells and thereby reduce the impact of COVID-19.

Our use of the recombinant S protein receptor-binding domain (S-RBD) to study the role of AAK1 in the entry of SARS-CoV-2 is based on multiple studies where researchers have attempted to examine the mechanisms of SARS-CoV-2 entry (Chan, K. K., Dorosky et al. 2020) as such studies are not easy to carry out with the live virus infection. The latter requires a BSL-3 containment facility, making it impractical to examine molecular mechanisms. However, further studies to extend our findings using live viral infection will be required prior to considering our findings for further translational studies. However, the use of recombinant system limits us in studying the whole life cycle of virus. In order to study the steps beyond entry like replication, assembly, and release of virus, we will have to have to setup experiments using the live virus to see the impact of deletion and inhibition of AAK1.

The role of AAK1 in the entry of viruses has been shown with a small number of viruses like hepatitis C, dengue, and ebola (Neveu, Ziv-Av et al. 2015, Bekerman, Neveu et al. 2017). We used a combination of genetic and pharmacological approaches to test our hypothesis that AAK1 regulates the endocytosis of SARS-CoV-2. We found that genetic knockdown of AAK1 with a siRNA pool (smartpool siRNA) reduced the

internalization of S-RBD, suggesting a role for AAK1 in the entry of SARS-CoV-2 into host cells (Fig. 3.12). AP2M1 phosphorylation on T156 residue serves as a surrogate marker of AAK1 (and related kinase) activity (Ricotta, Conner et al. 2002). Notably, genetic depletion did not impair the phosphorylation of AP2M1 significantly, while combined knockdown of AAK1 and GAK reduced it more significantly. The fact that AAK1 knockdown appeared to reduce the internalization of the S-RBD/ACE2 complex despite incomplete inhibition of AP2M1 phosphorylation suggests that additional targets of AAK1 besides AP2M1 may be important for the SARS-CoV-2 internalization process. Future studies to examine the impact of concurrent knockdown of AAK1 and family members on S-RBD internalization, as well as proteomic approaches to identify other targets of AAK1 and related kinases, should be of interest in this regard. Approaches such as global phospho-proteomics of control and AAK1 knockdown cell systems should provide such clues. Similarly, affinity purification of AAK1-associated proteins using tagged AAK1, or its kinase-dead mutant could reveal additional relevant players. Recently it has been shown that there are other host endocytic traffic regulators like RAB7 involved in the SARS-CoV-2 infection, RAB7A loss resulted in areduced cell surface expression and an increased endosomal accumulation of ACE2 (Daniloski, Jordan et al. 2021) so Including AAK1 which is the regulator of clathrin-mediated endocytosis we would like to know the role of other regulators involved in the endocytosis and infection of SARS-CoV-2.

Towards a chemical inhibitor approach to determine the role of AAK1 (and potentially related kinases) in SARS-CoV-2 entry into host cells, we employed two types of inhibitors. First, we used AAK1 inhibitors LP-935509 and LP-922761 that have been reported and used as tool compounds to inhibit AAK1 (Kostich, Hamman et al. 2016). Secondly, we used clinically-used drugs that have merged to have an AAK1 inhibitory activity in addition to their activities for which they have been approved for clinical use.

These included the JAK kinase targeting inhibitor baricitinib, the multi-receptor tyrosine kinase inhibitor (whose main known targets are PDGF receptors and VEGF receptors), and EGF receptor tyrosine kinase inhibitor Erlotinib (Lupberger, Zeisel et al. 2011). These clinically approved anti-cancer drugs were identified in screens for viral entry inhibition against dengue virus (Pu, Xiao et al. 2018) and also shown to inhibit the entry of Hepatitis C viruses into host cells (Neveu, Ziv-Av et al. 2015, Neveu, Barouch-Bentov et al. 2012). While AAK1 inhibition is one of the multiple activities, these drugs exhibit, their successful clinical use with tolerable side effects during prolonged use makes their AAK1 inhibitory activity of great interest since these could be rapidly translated into short-term clinical use a strategy to mitigate COVID-19 without significant side effects.

In all cases using chemical inhibitors, we used their ability to reduce AP2M1 phosphorylation as a readout of AAK1 inhibitory activity to build dose responses. These dose-response analyses showed that while all of the inhibitors we tested had AAK1 inhibitory activity, only the specific AAK1 inhibitors LP-935509 and LP-922761, and Sunitinib among the clinically-used drugs displayed AAK1 inhibitory activity at low concentrations (Fig. 3.15 and Fig. 3.15). Accordingly, sunitinib and the AAK1 specific inhibitors LP-935509 and LP-922761 exhibited a dose-dependent inhibition of the SARS-CoV-2 S-RBD internalization into host cells (Fig. 3.16). In fact, baricitinib and erlotinib treatment of cells at concentrations that effectively inhibited AP2M1 phosphorylation reduced growth and induced other signs of ill-health, suggesting that these drugs may not be suitable for use based on their AAK1 inhibitory activities. Recent studies suggest that baricitinib has positive effects on the disease course in COVID-19 patients (Weisberg, Parent et al. 2020). We speculate that such benefit is likely to reflect its JAK kinase inhibitory activity since cytokine-dependent organ pathogenesis is now recognized as a key component of COVID-19 disease.

These genetic and pharmacological approaches suggest the requirement of AAK1 (and potentially related kinases) in the entry of SARS-CoV-2 and provide an insight into the mechanism of viral entry by regulating the clathrin-mediated endocytic machinery.

Thus far, the strategies employed to control COVID-19 infection have primarily focused on preventive strategies (social distancing, etc.) and antiviral drugs. Indeed, remdesivir and an oral antiviral clinical candidate developed by Pfizer (PF-07321332, which is in clinical trials) have exhibited moderate effectiveness, while vaccines have shown dramatic effectiveness. However, there is a clear need to target SARS-CoV-2 using alternate strategies. It is already clear that social distancing measures, while highly effective, are not practical in most cases due to the social and economic burden they entail. Vaccines, while effective, suffer from huge logistical issues of rapid, effective, and universal distribution and acceptance by populations. Importantly, the emergence of variants of SARS-CoV-2 with increased ability for transmission and pathogenesis already suggests the likelihood of vaccine-escape variants requiring newer vaccines to be administered regularly. The development of resistance to antiviral drugs directed at viral enzymes is well established as a mechanism and will likely manifest for SARS-CoV-2 over time. Thus, alternate approaches to target SARS-CoV-2 infection that might be less susceptible to the constraints above and could function against emerging variants as well will be of great interest. Targeting host factors involved in viral entry represents one such approach.

At present, no agents targeting the host mechanisms of viral entry are in clinical practice against COVID-19. Thus, identifying clinically used drugs as efficient at inhibiting the first step of endocytosis could represent a significant step forward. In this regard, a recent study showed that sunitinib exhibited an inhibitory effect against SARS-CoV-2 by targeting the crucial host factor AP2M1 (Wang, P. G., Tang et al. 2020). The use of drugs

targeting the host mechanisms involved in the viral entry is unlikely to face a high resistance rate. Besides SARS-CoV-2, experimental studies have shown the viral entry inhibition by sunitinib against HCV, rabies virus, dengue virus, and Ebola virus, indicating that this drug might have broader antiviral application by targeting the host system components involved in viral entry. Finally, since viral entry is a multi-step process, it is feasible to develop combinatorial approaches to inhibit SARS-CoV-2 and other viral entry. For example, the requirement of S-protein cleavage by host proteases for viral penetration (e.g., targeting TMPRSS2 with camostat mesylate, or inhibition of other cleavage enzymes) and a requirement for acidic endosomal pH (e.g., targeting proton pump with inhibitors such as chloroquine or hydroxychloroquine) could provide strategies to develop effective combination approaches with clinically-used drugs.

Since our studies have only been carried out at a cell biological level by examining the inhibition of S-RBD internalization, future studies are needed to validate S-RBD inhibition by AAK1 inhibitors sunitinib in actual virus infection experiments. While the expansion of such studies to an in vivo model may be required to fully establish a rationale to advance the AAK1-specific inhibitors into clinical trials for COVID-19, sunitinib is already in such trials. Hence, the development of additional combinations of sunitinib with other clinically used drugs targeting additional viral entry steps may proceed quickly into clinical trials. Therefore, cell biological studies to establish a rationale for such combinations are urgently needed as a future direction.

Chapter 4: Bibliography

1. DOHERTY, G.J. and MCMAHON, H.T., 2009. Mechanisms of endocytosis. *Annual Review of Biochemistry,* **78**, pp. 857-902.

2. FLANNAGAN, R.S., JAUMOUILLE, V. and GRINSTEIN, S., 2012. The cell biology of phagocytosis. *Annual review of pathology,* **7**, pp. 61-98.

3. LIM, J.P. and GLEESON, P.A., 2011. Macropinocytosis: an endocytic pathway for internalising large gulps. *Immunology and cell biology,* **89**(8), pp. 836-843.

4. PELKMANS, L. and HELENIUS, A., 2002. Endocytosis via caveolae. *Traffic (Copenhagen, Denmark),* **3**(5), pp. 311-320.

5. MCMAHON, H.T. and BOUCROT, E., 2011. Molecular mechanism and physiological functions of clathrin-mediated endocytosis. *Nature reviews.Molecular cell biology,* **12**(8), pp. 517-533.

6. MUKHERJEE, S., GHOSH, R.N. and MAXFIELD, F.R., 1997. Endocytosis. *Physiological Reviews,* **77**(3), pp. 759-803.

7. MARSH, M. and MCMAHON, H.T., 1999. The structural era of endocytosis. *Science (New York, N.Y.),* **285**(5425), pp. 215-220.

8. GUICHET, A., WUCHERPFENNIG, T., DUDU, V., ETTER, S., WILSCH-BRAUNIGER, M., HELLWIG, A., GONZALEZ-GAITAN, M., HUTTNER, W.B. and SCHMIDT, A.A., 2002. Essential role of endophilin A in synaptic vesicle budding at the Drosophila neuromuscular junction. *The EMBO journal,* **21**(7), pp. 1661-1672.

9. OVED, S. and YARDEN, Y., 2002. Signal transduction: molecular ticket to enter cells. *Nature,* **416**(6877), pp. 133-136.

10. SORKIN, A. and VON ZASTROW, M., 2002. Signal transduction and endocytosis: close encounters of many kinds. *Nature reviews.Molecular cell biology,* **3**(8), pp. 600-614.

11. VANLANDINGHAM, P.A. and CERESA, B.P., 2009. Rab7 regulates late endocytic trafficking downstream of multivesicular body biogenesis and cargo sequestration. *The Journal of biological chemistry,* **284**(18), pp. 12110-12124.

12. MERESSE, S., GORVEL, J.P. and CHAVRIER, P., 1995. The rab7 GTPase resides on a vesicular compartment connected to lysosomes. *Journal of cell science,* **108 (Pt 11)**(Pt 11), pp. 3349-3358.

13. ULLRICH, O., REINSCH, S., URBE, S., ZERIAL, M. and PARTON, R.G., 1996. Rab11 regulates recycling through the pericentriolar recycling endosome. *The Journal of cell biology,* **135**(4), pp. 913-924.

14. DARO, E., VAN DER SLUIJS, P., GALLI, T. and MELLMAN, I., 1996. Rab4 and cellubrevin define different early endosome populations on the pathway of

transferrin receptor recycling. *Proceedings of the National Academy of Sciences of the United States of America,* **93**(18), pp. 9559-9564.

15. VAN DER SLUIJS, P., HULL, M., WEBSTER, P., MALE, P., GOUD, B. and MELLMAN, I., 1992. The small GTP-binding protein rab4 controls an early sorting event on the endocytic pathway. *Cell,* **70**(5), pp. 729-740.

16. BUCCI, C., PARTON, R.G., MATHER, I.H., STUNNENBERG, H., SIMONS, K., HOFLACK, B. and ZERIAL, M., 1992. The small GTPase rab5 functions as a regulatory factor in the early endocytic pathway. *Cell,* **70**(5), pp. 715-728.

17. GORVEL, J.P., CHAVRIER, P., ZERIAL, M. and GRUENBERG, J., 1991. Rab5 Controls Early Endosome Fusion in Vitro. *Cell,* **64**(5), pp. 915-925.

18. SALMINEN, A. and NOVICK, P.J., 1987. A ras-like protein is required for a post-Golgi event in yeast secretion. *Cell,* **49**(4), pp. 527-538.

19. SCHMITT, H.D., WAGNER, P., PFAFF, E. and GALLWITZ, D., 1986. The ras-related YPT1 gene product in yeast: a GTP-binding protein that might be involved in microtubule organization. *Cell,* **47**(3), pp. 401-412.

20. TOUCHOT, N., CHARDIN, P. and TAVITIAN, A., 1987. Four additional members of the ras gene superfamily isolated by an oligonucleotide strategy: molecular cloning of YPT-related cDNAs from a rat brain library. *Proceedings of the National Academy of Sciences of the United States of America,* **84**(23), pp. 8210-8214.

21. MILIARAS, N.B. and WENDLAND, B., 2004. EH proteins: multivalent regulators of endocytosis (and other pathways). *Cell biochemistry and biophysics,* **41**(2), pp. 295-318.

22. GRANT, B., ZHANG, Y., PAUPARD, M.C., LIN, S.X., HALL, D.H. and HIRSH, D., 2001. Evidence that RME-1, a conserved C. elegans EH-domain protein, functions in endocytic recycling. *Nature cell biology,* **3**(6), pp. 573-579.

23. LIN, S.X., GRANT, B., HIRSH, D. and MAXFIELD, F.R., 2001. Rme-1 regulates the distribution and function of the endocytic recycling compartment in mammalian cells. *Nature cell biology,* **3**(6), pp. 567-572.

24. NASLAVSKY, N. and CAPLAN, S., 2011. EHD proteins: key conductors of endocytic transport. *Trends in cell biology,* **21**(2), pp. 122-131.

25. BAHL, K., NASLAVSKY, N. and CAPLAN, S., 2015. Role of the EHD2 unstructured loop in dimerization, protein binding and subcellular localization. *PloS one,* **10**(4), pp. e0123710.

26. DAUMKE, O., LUNDMARK, R., VALLIS, Y., MARTENS, S., BUTLER, P.J. and MCMAHO, 2007. Architectural and mechanistic insights into an EHD ATPase involved in membrane remodelling. *Nature,* **449**(7164), pp. 923-927.

27. JAKOBSSON, J., ACKERMANN, F., ANDERSSON, F., LARHAMMAR, D., LOW, P. and BRODIN, L., 2011. Regulation of synaptic vesicle budding and dynamin function by an EHD ATPase. *The Journal of neuroscience : the official journal of the Society for Neuroscience,* **31**(39), pp. 13972-13980.

28. WONG, W.T., SCHUMACHER, C., SALCINI, A.E., ROMANO, A., CASTAGNINO, P., PELICCI, P.G. and DI FIORE, P.P., 1995. A protein-binding domain, EH, identified in the receptor tyrosine kinase substrate Eps15 and conserved in evolution. *Proceedings of the National Academy of Sciences of the United States of America,* **92**(21), pp. 9530-9534.

29. SANTOLINI, E., SALCINI, A.E., KAY, B.K., YAMABHAI, M. and DI FIORE, P.P., 1999. The EH network. *Experimental cell research,* **253**(1), pp. 186-209.

30. GIRAO, H., CATARINO, S. and PEREIRA, P., 2009. Eps15 interacts with ubiquitinated Cx43 and mediates its internalization. *Experimental cell research,* **315**(20), pp. 3587-3597.

31. LIN, A. and MAN, H.Y., 2014. Endocytic adaptor epidermal growth factor receptor substrate 15 (Eps15) is involved in the trafficking of ubiquitinated alpha-amino-3-hydroxy-5-methyl-4-isoxazolepropionic acid receptors. *The Journal of biological chemistry,* **289**(35), pp. 24652-24664.

32. CARBONE, R., FRE, S., IANNOLO, G., BELLEUDI, F., MANCINI, P., PELICCI, P.G., TORRISI, M.R. and DI FIORE, P.P., 1997. eps15 and eps15R are essential components of the endocytic pathway. *Cancer research,* **57**(24), pp. 5498-5504.

33. VAN DELFT, S., SCHUMACHER, C., HAGE, W., VERKLEIJ, A.J. and VAN BERGEN EN HENEGOUWEN, P.M., 1997. Association and colocalization of Eps15 with adaptor protein-2 and clathrin. *The Journal of cell biology,* **136**(4), pp. 811-821.

34. FAZIOLI, F., MINICHIELLO, L., MATOSKOVA, B., WONG, W.T. and DI FIORE, P.P., 1993. Eps15, a Novel Tyrosine Kinase Substrate, Exhibits Transforming Activity. *Molecular and cellular biology,* **13**(9), pp. 5814-5828.

35. SIGISMUND, S., WOELK, T., PURI, C., MASPERO, E., TACCHETTI, C., TRANSIDICO, P., DI FIORE, P.P. and POLO, S., 2005. Clathrin-independent endocytosis of ubiquitinated cargos. *Proceedings of the National Academy of Sciences of the United States of America,* **102**(8), pp. 2760-2765.

36. CHI, S., CAO, H., WANG, Y. and MCNIVEN, M.A., 2011. Recycling of the epidermal growth factor receptor is mediated by a novel form of the clathrin adaptor protein Eps15. *The Journal of biological chemistry,* **286**(40), pp. 35196-35208.

37. NASLAVSKY, N., RAHAJENG, J., CHENAVAS, S., SORGEN, P.L. and CAPLAN, S., 2007. EHD1 and Eps15 interact with phosphatidylinositols via their Eps15 homology domains. *The Journal of biological chemistry,* **282**(22), pp. 16612-16622.

38. ROTEM-YEHUDAR, R., GALPERIN, E. and HOROWITZ, M., 2001. Association of insulin-like growth factor 1 receptor with EHD1 and SNAP29. *The Journal of biological chemistry,* **276**(35), pp. 33054-33060.

39. JOVIC, M., NASLAVSKY, N., RAPAPORT, D., HOROWITZ, M. and CAPLAN, S., 2007. EHD1 regulates beta1 integrin endosomal transport: effects on focal adhesions, cell spreading and migration. *Journal of cell science,* **120**(Pt 5), pp. 802-814.

40. ALLAIRE, P.D., MARAT, A.L., DALL'ARMI, C., DI PAOLO, G., MCPHERSON, P.S. and RITTER, B., 2010. The Connecdenn DENN domain: a GEF for Rab35 mediating cargo-specific exit from early endosomes. *Molecular cell,* **37**(3), pp. 370-382.

41. WALSENG, E., BAKKE, O. and ROCHE, P.A., 2008. Major histocompatibility complex class II-peptide complexes internalize using a clathrin- and dynamin-independent endocytosis pathway. *The Journal of biological chemistry,* **283**(21), pp. 14717-14727.

42. SATO, M., SATO, K., LIOU, W., PANT, S., HARADA, A. and GRANT, B.D., 2008. Regulation of endocytic recycling by C. elegans Rab35 and its regulator RME-4, a coated-pit protein. *The EMBO journal,* **27**(8), pp. 1183-1196.

43. MARI, M., BUJNY, M.V., ZEUSCHNER, D., GEERTS, W.J., GRIFFITH, J., PETERSEN, C.M., CULLEN, P.J., KLUMPERMAN, J. and GEUZE, H.J., 2008. SNX1 defines an early endosomal recycling exit for sortilin and mannose 6-phosphate receptors. *Traffic (Copenhagen, Denmark),* **9**(3), pp. 380-393.

44. GOKOOL, S., TATTERSALL, D. and SEAMAN, M.N., 2007. EHD1 interacts with retromer to stabilize SNX1 tubules and facilitate endosome-to-Golgi retrieval. *Traffic (Copenhagen, Denmark),* **8**(12), pp. 1873-1886.

45. ZHANG, J., REILING, C., REINECKE, J.B., PRISLAN, I., MARKY, L.A., SORGEN, P.L., NASLAVSKY, N. and CAPLAN, S., 2012. Rabankyrin-5 interacts with EHD1 and Vps26 to regulate endocytic trafficking and retromer function. *Traffic (Copenhagen, Denmark),* **13**(5), pp. 745-757.

46. MCKENZIE, J.E., RAISLEY, B., ZHOU, X., NASLAVSKY, N., TAGUCHI, T., CAPLAN, S. and SHEFF, D., 2012. Retromer guides STxB and CD8-M6PR from early to recycling endosomes, EHD1 guides STxB from recycling endosome to Golgi. *Traffic (Copenhagen, Denmark),* **13**(8), pp. 1140-1159.

47. GUILHERME, A., SORIANO, N.A., BOSE, S., HOLIK, J., BOSE, A., POMERLEAU, D.P., FURCINITTI, P., LESZYK, J., CORVERA, S. and CZECH, M.P., 2004. EHD2 and the novel EH domain binding protein EHBP1 couple endocytosis to the actin cytoskeleton. *The Journal of biological chemistry,* **279**(11), pp. 10593-10605.

48. PARK, S.Y., HA, B.G., CHOI, G.H., RYU, J., KIM, B., JUNG, C.Y. and LEE, W., 2004. EHD2 interacts with the insulin-responsive glucose transporter (GLUT4) in rat adipocytes and may participate in insulin-induced GLUT4 recruitment. *Biochemistry,* **43**(23), pp. 7552-7562.

49. PEKAR, O., BENJAMIN, S., WEIDBERG, H., SMALDONE, S., RAMIREZ, F. and HOROWITZ, M., 2012. EHD2 shuttles to the nucleus and represses transcription. *The Biochemical journal,* **444**(3), pp. 383-394.

50. CABASSO, O., PEKAR, O. and HOROWITZ, M., 2015. SUMOylation of EHD3 Modulates Tubulation of the Endocytic Recycling Compartment. *PloS one,* **10**(7), pp. e0134053.

51. NASLAVSKY, N., RAHAJENG, J., SHARMA, M., JOVIC, M. and CAPLAN, S., 2006. Interactions between EHD proteins and Rab11-FIP2: a role for EHD3 in early endosomal transport. *Molecular biology of the cell,* **17**(1), pp. 163-177.

52. SHARMA, M., NASLAVSKY, N. and CAPLAN, S., 2008. A role for EHD4 in the regulation of early endosomal transport. *Traffic (Copenhagen, Denmark),* **9**(6), pp. 995-1018.

53. WATSON, F.L., HEERSSEN, H.M., BHATTACHARYYA, A., KLESSE, L., LIN, M.Z. and SEGAL, R.A., 2001. Neurotrophins use the Erk5 pathway to mediate a retrograde survival response. *Nature neuroscience,* **4**(10), pp. 981-988.

54. VALDEZ, G., PHILIPPIDOU, P., ROSENBAUM, J., AKMENTIN, W., SHAO, Y. and HALEGOUA, S., 2007. Trk-signaling endosomes are generated by Rac-dependent macroendocytosis. *Proceedings of the National Academy of Sciences of the United States of America,* **104**(30), pp. 12270-12275.

55. SHAO, Y., AKMENTIN, W., TOLEDO-ARAL, J.J., ROSENBAUM, J., VALDEZ, G., CABOT, J.B., HILBUSH, B.S. and HALEGOUA, S., 2002. Pincher, a pinocytic chaperone for nerve growth factor/TrkA signaling endosomes. *The Journal of cell biology,* **157**(4), pp. 679-691.

56. VALDEZ, G., AKMENTIN, W., PHILIPPIDOU, P., KURUVILLA, R., GINTY, D.D. and HALEGOUA, S., 2005. Pincher-mediated macroendocytosis underlies retrograde signaling by neurotrophin receptors. *The Journal of neuroscience : the official journal of the Society for Neuroscience,* **25**(21), pp. 5236-5247.

57. RAINEY, M.A., GEORGE, M., YING, G., AKAKURA, R., BURGESS, D.J., SIEFKER, E., BARGAR, T., DOGLIO, L., CRAWFORD, S.E., TODD, G.L., GOVINDARAJAN, V., HESS, R.A., BAND, V., NARAMURA, M. and BAND, H., 2010. The endocytic recycling regulator EHD1 is essential for spermatogenesis and male fertility in mice. *BMC developmental biology,* **10**, pp. 37-213X-10-37.

58. ARYA, P., RAINEY, M.A., BHATTACHARYYA, S., MOHAPATRA, B.C., GEORGE, M., KURACHA, M.R., STORCK, M.D., BAND, V., GOVINDARAJAN, V. and BAND, H., 2015. The endocytic recycling regulatory protein EHD1 Is required for ocular lens development. *Developmental biology,* **408**(1), pp. 41-55.

59. GEORGE, M., YING, G., RAINEY, M.A., SOLOMON, A., PARIKH, P.T., GAO, Q., BAND, V. and BAND, H., 2007. Shared as well as distinct roles of EHD proteins revealed by biochemical and functional comparisons in mammalian cells and C. elegans. *BMC cell biology,* **8**, pp. 3-2121-8-3.

60. MATTHAEUS, C., LAHMANN, I., KUNZ, S., JONAS, W., MELO, A.A., LEHMANN, M., LARSSON, E., LUNDMARK, R., KERN, M., BLUHER, M., OLSCHOWSKI, H., KOMPA, J., BRUGGER, B., MULLER, D.N., HAUCKE, V., SCHURMANN, A., BIRCHMEIER, C. and DAUMKE, O., 2020. EHD2-mediated restriction of caveolar dynamics regulates cellular fatty acid uptake. *Proceedings of the National Academy of Sciences of the United States of America,* **117**(13), pp. 7471-7481.

61. MATTHAEUS, C., LIAN, X., KUNZ, S., LEHMANN, M., ZHONG, C., BERNERT, C., LAHMANN, I., MULLER, D.N., GOLLASCH, M. and DAUMKE, O., 2019. eNOS-NO-induced small blood vessel relaxation requires EHD2-dependent caveolae stabilization. *PloS one,* **14**(10), pp. e0223620.

62. GUDMUNDSSON, H., CURRAN, J., KASHEF, F., SNYDER, J.S., SMITH, S.A., VARGAS-PINTO, P., BONILLA, I.M., WEISS, R.M., ANDERSON, M.E., BINKLEY, P., FELDER, R.B., CARNES, C.A., BAND, H., HUND, T.J. and MOHLER, P.J., 2012. Differential regulation of EHD3 in human and mammalian heart failure. *Journal of Molecular and Cellular Cardiology,* **52**(5), pp. 1183-1190.

63. CURRAN, J., MAKARA, M.A., LITTLE, S.C., MUSA, H., LIU, B., WU, X., POLINA, I., ALECUSAN, J.S., WRIGHT, P., LI, J., BILLMAN, G.E., BOYDEN, P.A., GYORKE, S., BAND, H., HUND, T.J. and MOHLER, P.J., 2014. EHD3-dependent endosome pathway regulates cardiac membrane excitability and physiology. *Circulation research,* **115**(1), pp. 68-78.

64. GEORGE, M., RAINEY, M.A., NARAMURA, M., FOSTER, K.W., HOLZAPFEL, M.S., WILLOUGHBY, L.L., YING, G., GOSWAMI, R.M., GURUMURTHY, C.B., BAND, V., SATCHELL, S.C. and BAND, H., 2011. Renal thrombotic microangiopathy in mice with combined deletion of endocytic recycling regulators EHD3 and EHD4. *PloS one,* **6**(3), pp. e17838.

65. GEORGE, M., RAINEY, M.A., NARAMURA, M., YING, G., HARMS, D.W., VITATERNA, M.H., DOGLIO, L., CRAWFORD, S.E., HESS, R.A., BAND, V. and BAND, H., 2010. Ehd4 is required to attain normal prepubertal testis size but dispensable for fertility in male mice. *Genesis (New York, N.Y.: 2000),* **48**(5), pp. 328-342.

66. COSSART, P. and HELENIUS, A., 2014. Endocytosis of viruses and bacteria. *Cold Spring Harbor perspectives in biology,* **6**(8), pp. 10.1101/cshperspect.a016972.

67. HELENIUS, A., KARTENBECK, J., SIMONS, K. and FRIES, E., 1980. On the entry of Semliki forest virus into BHK-21 cells. *The Journal of cell biology,* **84**(2), pp. 404-420.

68. DANTHI, P., GUGLIELMI, K.M., KIRCHNER, E., MAINOU, B., STEHLE, T. and DERMODY, T.S., 2010. From touchdown to transcription: the reovirus cell entry pathway. *Current topics in microbiology and immunology,* **343**, pp. 91-119.

69. HUNT, C.L., LENNEMANN, N.J. and MAURY, W., 2012. Filovirus entry: a novelty in the viral fusion world. *Viruses,* **4**(2), pp. 258-275.

70. KUBO, Y., HAYASHI, H., MATSUYAMA, T., SATO, H. and YAMAMOTO, N., 2012. Retrovirus entry by endocytosis and cathepsin proteases. *Advances in virology,* **2012**, pp. 640894.

71. GILBERT, J.M., GOLDBERG, I.G. and BENJAMIN, T.L., 2003. Cell penetration and trafficking of polyomavirus. *Journal of virology,* **77**(4), pp. 2615-2622.

72. DAMM, E.M., PELKMANS, L., KARTENBECK, J., MEZZACASA, A., KURZCHALIA, T. and HELENIUS, A., 2005. Clathrin- and caveolin-1-independent endocytosis: entry of simian virus 40 into cells devoid of caveolae. *The Journal of cell biology,* **168**(3), pp. 477-488.

73. ANDERSON, H.A., CHEN, Y. and NORKIN, L.C., 1996. Bound simian virus 40 translocates to caveolin-enriched membrane domains, and its entry is inhibited by drugs that selectively disrupt caveolae. *Molecular biology of the cell,* **7**(11), pp. 1825-1834.

74. STANG, E. and BAKKE, O., 1997. MHC class II-associated invariant chain-induced enlarged endosomal structures: a morphological study. *Experimental cell research,* **235**(1), pp. 79-92.

75. SWANSON, J.A. and WATTS, C., 1995. Macropinocytosis. *Trends in cell biology,* **5**(11), pp. 424-428.

76. MATLIN, K.S., REGGIO, H., HELENIUS, A. and SIMONS, K., 1981. Infectious entry pathway of influenza virus in a canine kidney cell line. *The Journal of cell biology,* **91**(3 Pt 1), pp. 601-613.

77. DETULLEO, L. and KIRCHHAUSEN, T., 1998. The clathrin endocytic pathway in viral infection. *The EMBO journal,* **17**(16), pp. 4585-4593.

78. SUN, E., HE, J. and ZHUANG, X., 2013. Live cell imaging of viral entry. *Current opinion in virology,* **3**(1), pp. 34-43.

79. EHRLICH, M., BOLL, W., VAN OIJEN, A., HARIHARAN, R., CHANDRAN, K., NIBERT, M.L. and KIRCHHAUSEN, T., 2004. Endocytosis by random initiation and stabilization of clathrin-coated pits. *Cell,* **118**(5), pp. 591-605.

80. RICOTTA, D., CONNER, S.D., SCHMID, S.L., VON FIGURA, K. and HONING, S., 2002. Phosphorylation of the AP2 mu subunit by AAK1 mediates high affinity binding to membrane protein sorting signals. *The Journal of cell biology,* **156**(5), pp. 791-795.

81. CONNER, S.D. and SCHMID, S.L., 2003a. Regulated portals of entry into the cell. *Nature,* **422**(6927), pp. 37-44.

82. CONNER, S.D. and SCHMID, S.L., 2003b. Differential requirements for AP-2 in clathrin-mediated endocytosis. *The Journal of cell biology,* **162**(5), pp. 773-779.

83. BRODSKY, F.M., 2012. Diversity of clathrin function: new tricks for an old protein. *Annual Review of Cell and Developmental Biology,* **28**, pp. 309-336.

84. OWEN, D.J., COLLINS, B.M. and EVANS, P.R., 2004. Adaptors for clathrin coats: structure and function. *Annual Review of Cell and Developmental Biology,* **20**, pp. 153-191.

85. OHNO, H., 2006. Clathrin-associated adaptor protein complexes. *Journal of cell science,* **119**(Pt 18), pp. 3719-3721.

86. OHNO, H., STEWART, J., FOURNIER, M.C., BOSSHART, H., RHEE, I., MIYATAKE, S., SAITO, T., GALLUSSER, A., KIRCHHAUSEN, T. and BONIFACINO, J.S., 1995. Interaction of tyrosine-based sorting signals with clathrin-associated proteins. *Science (New York, N.Y.),* **269**(5232), pp. 1872-1875.

87. PEARSE, B.M., 1988. Receptors compete for adaptors found in plasma membrane coated pits. *The EMBO journal,* **7**(11), pp. 3331-3336.

88. BOLL, W., OHNO, H., SONGYANG, Z., RAPOPORT, I., CANTLEY, L.C., BONIFACINO, J.S. and KIRCHHAUSEN, T., 1996. Sequence requirements for the recognition of tyrosine-based endocytic signals by clathrin AP-2 complexes. *The EMBO journal,* **15**(21), pp. 5789-5795.

89. SMYTHE, E. and AYSCOUGH, K.R., 2003. The Ark1/Prk1 family of protein kinases. Regulators of endocytosis and the actin skeleton. *EMBO reports,* **4**(3), pp. 246-251.

90. HENDERSON, D.M. and CONNER, S.D., 2007. A novel AAK1 splice variant functions at multiple steps of the endocytic pathway. *Molecular biology of the cell,* **18**(7), pp. 2698-2706.

91. CONNER, S.D. and SCHMID, S.L., 2002. Identification of an adaptor-associated kinase, AAK1, as a regulator of clathrin-mediated endocytosis. *The Journal of cell biology,* **156**(5), pp. 921-929.

92. SEKIYA-KAWASAKI, M., GROEN, A.C., COPE, M.J., KAKSONEN, M., WATSON, H.A., ZHANG, C., SHOKAT, K.M., WENDLAND, B., MCDONALD, K.L., MCCAFFERY, J.M. and DRUBIN, D.G., 2003. Dynamic phosphoregulation of the cortical actin cytoskeleton and endocytic machinery revealed by real-time chemical genetic analysis. *The Journal of cell biology,* **162**(5), pp. 765-772.

93. GUPTA-ROSSI, N., ORTICA, S., MEAS-YEDID, V., HEUSS, S., MORETTI, J., OLIVO-MARIN, J.C. and ISRAEL, A., 2011. The adaptor-associated kinase 1, AAK1, is a positive regulator of the Notch pathway. *The Journal of biological chemistry,* **286**(21), pp. 18720-18730.

94. SORENSEN, E.B. and CONNER, S.D., 2008. AAK1 regulates Numb function at an early step in clathrin-mediated endocytosis. *Traffic (Copenhagen, Denmark),* **9**(10), pp. 1791-1800.

95. WAXMONSKY, N.C. and CONNER, S.D., 2013. Alphavbeta3-integrin-mediated adhesion is regulated through an AAK1L- and EHD3-dependent rapid-recycling pathway. *Journal of cell science,* **126**(Pt 16), pp. 3593-3601.

96. KUAI, L., ONG, S.E., MADISON, J.M., WANG, X., DUVALL, J.R., LEWIS, T.A., LUCE, C.J., CONNER, S.D., PEARLMAN, D.A., WOOD, J.L., SCHREIBER, S.L., CARR, S.A., SCOLNICK, E.M. and HAGGARTY, S.J., 2011. AAK1 identified as an inhibitor of neuregulin-1/ErbB4-dependent neurotrophic factor signaling using integrative chemical genomics and proteomics. *Chemistry & biology,* **18**(7), pp. 891-906.

97. ULTANIR, S.K., HERTZ, N.T., LI, G., GE, W.P., BURLINGAME, A.L., PLEASURE, S.J., SHOKAT, K.M., JAN, L.Y. and JAN, Y.N., 2012. Chemical genetic identification of NDR1/2 kinase substrates AAK1 and Rabin8 Uncovers their roles in dendrite arborization and spine development. *Neuron,* **73**(6), pp. 1127-1142.

98. KOSTICH, W., HAMMAN, B.D., LI, Y.W., NAIDU, S., DANDAPANI, K., FENG, J., EASTON, A., BOURIN, C., BAKER, K., ALLEN, J., SAVELIEVA, K., LOUIS, J.V., DOKANIA, M., ELAVAZHAGAN, S., VATTIKUNDALA, P., SHARMA, V., DAS, M.L., SHANKAR, G., KUMAR, A., HOLENARSIPUR, V.K., GULIANELLO, M., MOLSKI, T., BROWN, J.M., LEWIS, M., HUANG, Y., LU, Y., PIESCHL, R., O'MALLEY, K., LIPPY, J., NOURALDEEN, A., LANTHORN, T.H., YE, G., WILSON, A., BALAKRISHNAN, A., DENTON, R., GRACE, J.E., LENTZ, K.A., SANTONE, K.S., BI, Y., MAIN, A., SWAFFIELD, J., CARSON, K., MANDLEKAR, S., VIKRAMADITHYAN, R.K., NARA, S.J., DZIERBA, C., BRONSON, J., MACOR, J.E., ZACZEK, R., WESTPHAL, R., KISS, L., BRISTOW, L., CONWAY, C.M., ZAMBROWICZ, B. and ALBRIGHT, C.F., 2016. Inhibition of AAK1 Kinase as a Novel Therapeutic Approach to Treat Neuropathic Pain. *The Journal of pharmacology and experimental therapeutics,* **358**(3), pp. 371-386.

99. FU, X., KE, M., YU, W., WANG, X., XIAO, Q., GU, M. and LU, Y., 2018. Periodic Variation of AAK1 in an Abeta1-42-Induced Mouse Model of Alzheimer's Disease. *Journal of molecular neuroscience : MN,* **65**(2), pp. 179-189.

100. ABDEL-MAGID, A.F., 2017. Inhibitors of Adaptor-Associated Kinase 1 (AAK1) May Treat Neuropathic Pain, Schizophrenia, Parkinson's Disease, and Other Disorders. *ACS medicinal chemistry letters,* **8**(6), pp. 595-597.

101. LATOURELLE, J.C., PANKRATZ, N., DUMITRIU, A., WILK, J.B., GOLDWURM, S., PEZZOLI, G., MARIANI, C.B., DESTEFANO, A.L., HALTER, C., GUSELLA, J.F., NICHOLS, W.C., MYERS, R.H., FOROUD, T., PROGENI INVESTIGATORS, COORDINATORS AND MOLECULAR GENETIC LABORATORIES and GENEPD INVESTIGATORS, COORDINATORS AND MOLECULAR GENETIC LABORATORIES, 2009. Genomewide association study for onset age in Parkinson disease. *BMC medical genetics,* **10**, pp. 98-2350-10-98.

102. AGAJANIAN, M.J., WALKER, M.P., AXTMAN, A.D., RUELA-DE-SOUSA, R.R., SERAFIN, D.S., RABINOWITZ, A.D., GRAHAM, D.M., RYAN, M.B., TAMIR, T., NAKAMICHI, Y., GAMMONS, M.V., BENNETT, J.M., COUNAGO, R.M., DREWRY, D.H., ELKINS, J.M., GILEADI, C., GILEADI, O., GODOI, P.H., KAPADIA, N., MULLER, S., SANTIAGO, A.S., SORRELL, F.J., WELLS, C.I., FEDOROV, O., WILLSON, T.M., ZUERCHER, W.J. and MAJOR, M.B., 2019. WNT Activates the AAK1 Kinase to

Promote Clathrin-Mediated Endocytosis of LRP6 and Establish a Negative Feedback Loop. *Cell reports,* **26**(1), pp. 79-93.e8.

103. TAKAHASHI, T., FURUCHI, T. and NAGANUMA, A., 2006. Endocytic Ark/Prk kinases play a critical role in adriamycin resistance in both yeast and mammalian cells. *Cancer research,* **66**(24), pp. 11932-11937.

104. PU, S.Y., XIAO, F., SCHOR, S., BEKERMAN, E., ZANINI, F., BAROUCH-BENTOV, R., NAGAMINE, C.M. and EINAV, S., 2018. Feasibility and biological rationale of repurposing sunitinib and erlotinib for dengue treatment. *Antiviral Research,* **155**, pp. 67-75.

105. NEVEU, G., ZIV-AV, A., BAROUCH-BENTOV, R., BERKERMAN, E., MULHOLLAND, J. and EINAV, S., 2015. AP-2-associated protein kinase 1 and cyclin G-associated kinase regulate hepatitis C virus entry and are potential drug targets. *Journal of virology,* **89**(8), pp. 4387-4404.

106. NEVEU, G., BAROUCH-BENTOV, R., ZIV-AV, A., GERBER, D., JACOB, Y. and EINAV, S., 2012. Identification and targeting of an interaction between a tyrosine motif within hepatitis C virus core protein and AP2M1 essential for viral assembly. *PLoS pathogens,* **8**(8), pp. e1002845.

107. XIAO, F., WANG, S., BAROUCH-BENTOV, R., NEVEU, G., PU, S., BEER, M., SCHOR, S., KUMAR, S., NICOLAESCU, V., LINDENBACH, B.D., RANDALL, G. and EINAV, S., 2018. Interactions between the Hepatitis C Virus Nonstructural 2 Protein and Host Adaptor Proteins 1 and 4 Orchestrate Virus Release. *mBio,* **9**(2), pp. 10.1128/mBio.02233-17.

108. WANG, C., WANG, J., SHUAI, L., MA, X., ZHANG, H., LIU, R., CHEN, W., WANG, X., GE, J., WEN, Z. and BU, Z., 2019. The Serine/Threonine Kinase AP2-Associated Kinase 1 Plays an Important Role in Rabies Virus Entry. *Viruses,* **12**(1), pp. 10.3390/v12010045.

109. BEKERMAN, E., NEVEU, G., SHULLA, A., BRANNAN, J., PU, S.Y., WANG, S., XIAO, F., BAROUCH-BENTOV, R., BAKKEN, R.R., MATEO, R., GOVERO, J., NAGAMINE, C.M., DIAMOND, M.S., DE JONGHE, S., HERDEWIJN, P., DYE, J.M., RANDALL, G. and EINAV, S., 2017. Anticancer kinase inhibitors impair intracellular viral trafficking and exert broad-spectrum antiviral effects. *The Journal of clinical investigation,* **127**(4), pp. 1338-1352.

110. LOI, M., MULLER, A., STEINBACH, K., NIVEN, J., BARREIRA DA SILVA, R., PAUL, P., LIGEON, L.A., CARUSO, A., ALBRECHT, R.A., BECKER, A.C., ANNAHEIM, N., NOWAG, H., DENGJEL, J., GARCIA-SASTRE, A., MERKLER, D., MUNZ, C. and GANNAGE, M., 2016. Macroautophagy Proteins Control MHC Class I Levels on Dendritic Cells and Shape Anti-viral CD8(+) T Cell Responses. *Cell reports,* **15**(5), pp. 1076-1087.

111. LI, F., 2016. Structure, Function, and Evolution of Coronavirus Spike Proteins. *Annual review of virology,* **3**(1), pp. 237-261.

112. WOO, P.C., LAU, S.K., LAM, C.S., LAU, C.C., TSANG, A.K., LAU, J.H., BAI, R., TENG, J.L., TSANG, C.C., WANG, M., ZHENG, B.J., CHAN, K.H. and YUEN, K.Y., 2012. Discovery of seven novel Mammalian and avian coronaviruses in the genus deltacoronavirus supports bat coronaviruses as the gene source of alphacoronavirus and betacoronavirus and avian coronaviruses as the gene source of gammacoronavirus and deltacoronavirus. *Journal of virology,* **86**(7), pp. 3995-4008.

113. CUI, J., LI, F. and SHI, Z.L., 2019. Origin and evolution of pathogenic coronaviruses. *Nature reviews.Microbiology,* **17**(3), pp. 181-192.

114. FOUCHIER, R.A., HARTWIG, N.G., BESTEBROER, T.M., NIEMEYER, B., DE JONG, J.C., SIMON, J.H. and OSTERHAUS, A.D., 2004. A previously undescribed coronavirus associated with respiratory disease in humans. *Proceedings of the National Academy of Sciences of the United States of America,* **101**(16), pp. 6212-6216.

115. VAN DER HOEK, L., PYRC, K., JEBBINK, M.F., VERMEULEN-OOST, W., BERKHOUT, R.J., WOLTHERS, K.C., WERTHEIM-VAN DILLEN, P.M., KAANDORP, J., SPAARGAREN, J. and BERKHOUT, B., 2004. Identification of a new human coronavirus. *Nature medicine,* **10**(4), pp. 368-373.

116. HOLMES, K.V., 2003. SARS-associated coronavirus. *The New England journal of medicine,* **348**(20), pp. 1948-1951.

117. ZAKI, A.M., VAN BOHEEMEN, S., BESTEBROER, T.M., OSTERHAUS, A.D. and FOUCHIER, R.A., 2012. Isolation of a novel coronavirus from a man with pneumonia in Saudi Arabia. *The New England journal of medicine,* **367**(19), pp. 1814-1820.

118. ZHOU, P., YANG, X.L., WANG, X.G., HU, B., ZHANG, L., ZHANG, W., SI, H.R., ZHU, Y., LI, B., HUANG, C.L., CHEN, H.D., CHEN, J., LUO, Y., GUO, H., JIANG, R.D., LIU, M.Q., CHEN, Y., SHEN, X.R., WANG, X., ZHENG, X.S., ZHAO, K., CHEN, Q.J., DENG, F., LIU, L.L., YAN, B., ZHAN, F.X., WANG, Y.Y., XIAO, G.F. and SHI, Z.L., 2020. A pneumonia outbreak associated with a new coronavirus of probable bat origin. *Nature,* **579**(7798), pp. 270-273.

119. CHAN, J.F., KOK, K.H., ZHU, Z., CHU, H., TO, K.K., YUAN, S. and YUEN, K.Y., 2020. Genomic characterization of the 2019 novel human-pathogenic coronavirus isolated from a patient with atypical pneumonia after visiting Wuhan. *Emerging microbes & infections,* **9**(1), pp. 221-236.

120. LU, R., ZHAO, X., LI, J., NIU, P., YANG, B., WU, H., WANG, W., SONG, H., HUANG, B., ZHU, N., BI, Y., MA, X., ZHAN, F., WANG, L., HU, T., ZHOU, H., HU, Z., ZHOU, W., ZHAO, L., CHEN, J., MENG, Y., WANG, J., LIN, Y., YUAN, J., XIE, Z., MA, J., LIU, W.J., WANG, D., XU, W., HOLMES, E.C., GAO, G.F., WU, G., CHEN, W., SHI, W. and TAN, W., 2020. Genomic characterisation and epidemiology of 2019 novel coronavirus: implications for virus origins and receptor binding. *Lancet (London, England),* **395**(10224), pp. 565-574.

121. PECK, K.M., BURCH, C.L., HEISE, M.T. and BARIC, R.S., 2015. Coronavirus Host Range Expansion and Middle East Respiratory Syndrome Coronavirus

Emergence: Biochemical Mechanisms and Evolutionary Perspectives. *Annual review of virology,* **2**(1), pp. 95-117.

122. ZHU, N., ZHANG, D., WANG, W., LI, X., YANG, B., SONG, J., ZHAO, X., HUANG, B., SHI, W., LU, R., NIU, P., ZHAN, F., MA, X., WANG, D., XU, W., WU, G., GAO, G.F., TAN, W. and CHINA NOVEL CORONAVIRUS INVESTIGATING AND RESEARCH TEAM, 2020. A Novel Coronavirus from Patients with Pneumonia in China, 2019. *The New England journal of medicine,* **382**(8), pp. 727-733.

123. CHEN, L., LIU, W., ZHANG, Q., XU, K., YE, G., WU, W., SUN, Z., LIU, F., WU, K., ZHONG, B., MEI, Y., ZHANG, W., CHEN, Y., LI, Y., SHI, M., LAN, K. and LIU, Y., 2020. RNA based mNGS approach identifies a novel human coronavirus from two individual pneumonia cases in 2019 Wuhan outbreak. *Emerging microbes & infections,* **9**(1), pp. 313-319.

124. WANG, C., LIU, Z., CHEN, Z., HUANG, X., XU, M., HE, T. and ZHANG, Z., 2020. The establishment of reference sequence for SARS-CoV-2 and variation analysis. *Journal of medical virology,* **92**(6), pp. 667-674.

125. WU, A., PENG, Y., HUANG, B., DING, X., WANG, X., NIU, P., MENG, J., ZHU, Z., ZHANG, Z., WANG, J., SHENG, J., QUAN, L., XIA, Z., TAN, W., CHENG, G. and JIANG, T., 2020. Genome Composition and Divergence of the Novel Coronavirus (2019-nCoV) Originating in China. *Cell host & microbe,* **27**(3), pp. 325-328.

126. HARCOURT, B.H., JUKNELIENE, D., KANJANAHALUETHAI, A., BECHILL, J., SEVERSON, K.M., SMITH, C.M., ROTA, P.A. and BAKER, S.C., 2004. Identification of severe acute respiratory syndrome coronavirus replicase products and characterization of papain-like protease activity. *Journal of virology,* **78**(24), pp. 13600-13612.

127. NIETO-TORRES, J.L., DEDIEGO, M.L., ALVAREZ, E., JIMENEZ-GUARDENO, J.M., REGLA-NAVA, J.A., LLORENTE, M., KREMER, L., SHUO, S. and ENJUANES, L., 2011. Subcellular location and topology of severe acute respiratory syndrome coronavirus envelope protein. *Virology,* **415**(2), pp. 69-82.

128. SIU, Y.L., TEOH, K.T., LO, J., CHAN, C.M., KIEN, F., ESCRIOU, N., TSAO, S.W., NICHOLLS, J.M., ALTMEYER, R., PEIRIS, J.S., BRUZZONE, R. and NAL, B., 2008. The M, E, and N structural proteins of the severe acute respiratory syndrome coronavirus are required for efficient assembly, trafficking, and release of virus-like particles. *Journal of virology,* **82**(22), pp. 11318-11330.

129. VENNEMA, H., GODEKE, G.J., ROSSEN, J.W., VOORHOUT, W.F., HORZINEK, M.C., OPSTELTEN, D.J. and ROTTIER, P.J., 1996. Nucleocapsid-independent assembly of coronavirus-like particles by co-expression of viral envelope protein genes. *The EMBO journal,* **15**(8), pp. 2020-2028.

130. VOSS, D., KERN, A., TRAGGIAI, E., EICKMANN, M., STADLER, K., LANZAVECCHIA, A. and BECKER, S., 2006. Characterization of severe acute respiratory syndrome coronavirus membrane protein. *FEBS letters,* **580**(3), pp. 968-973.

131. BOSCH, B.J., VAN DER ZEE, R., DE HAAN, C.A. and ROTTIER, P.J., 2003. The coronavirus spike protein is a class I virus fusion protein: structural and functional characterization of the fusion core complex. *Journal of virology,* **77**(16), pp. 8801-8811.

132. WATANABE, Y., ALLEN, J.D., WRAPP, D., MCLELLAN, J.S. and CRISPIN, M., 2020. Site-specific glycan analysis of the SARS-CoV-2 spike. *Science (New York, N.Y.),* **369**(6501), pp. 330-333.

133. XIA, S., ZHU, Y., LIU, M., LAN, Q., XU, W., WU, Y., YING, T., LIU, S., SHI, Z., JIANG, S. and LU, L., 2020. Fusion mechanism of 2019-nCoV and fusion inhibitors targeting HR1 domain in spike protein. *Cellular & molecular immunology,* **17**(7), pp. 765-767.

134. WRAPP, D., WANG, N., CORBETT, K.S., GOLDSMITH, J.A., HSIEH, C.L., ABIONA, O., GRAHAM, B.S. and MCLELLAN, J.S., 2020. Cryo-EM structure of the 2019-nCoV spike in the prefusion conformation. *Science (New York, N.Y.),* **367**(6483), pp. 1260-1263.

135. WALLS, A.C., PARK, Y.J., TORTORICI, M.A., WALL, A., MCGUIRE, A.T. and VEESLER, D., 2020. Structure, Function, and Antigenicity of the SARS-CoV-2 Spike Glycoprotein. *Cell,* **181**(2), pp. 281-292.e6.

136. BERTRAM, S., DIJKMAN, R., HABJAN, M., HEURICH, A., GIERER, S., GLOWACKA, I., WELSCH, K., WINKLER, M., SCHNEIDER, H., HOFMANN-WINKLER, H., THIEL, V. and POHLMANN, S., 2013. TMPRSS2 activates the human coronavirus 229E for cathepsin-independent host cell entry and is expressed in viral target cells in the respiratory epithelium. *Journal of virology,* **87**(11), pp. 6150-6160.

137. HOFFMANN, M., KLEINE-WEBER, H., SCHROEDER, S., KRUGER, N., HERRLER, T., ERICHSEN, S., SCHIERGENS, T.S., HERRLER, G., WU, N.H., NITSCHE, A., MULLER, M.A., DROSTEN, C. and POHLMANN, S., 2020. SARS-CoV-2 Cell Entry Depends on ACE2 and TMPRSS2 and Is Blocked by a Clinically Proven Protease Inhibitor. *Cell,* **181**(2), pp. 271-280.e8.

138. WANG, Q., ZHANG, Y., WU, L., NIU, S., SONG, C., ZHANG, Z., LU, G., QIAO, C., HU, Y., YUEN, K.Y., WANG, Q., ZHOU, H., YAN, J. and QI, J., 2020. Structural and Functional Basis of SARS-CoV-2 Entry by Using Human ACE2. *Cell,* **181**(4), pp. 894-904.e9.

139. LAN, J., GE, J., YU, J., SHAN, S., ZHOU, H., FAN, S., ZHANG, Q., SHI, X., WANG, Q., ZHANG, L. and WANG, X., 2020. Structure of the SARS-CoV-2 spike receptor-binding domain bound to the ACE2 receptor. *Nature,* **581**(7807), pp. 215-220.

140. MILLET, J.K. and WHITTAKER, G.R., 2018. Physiological and molecular triggers for SARS-CoV membrane fusion and entry into host cells. *Virology,* **517**, pp. 3-8.

141. ROBSON, B., 2020. Computers and viral diseases. Preliminary bioinformatics studies on the design of a synthetic vaccine and a preventative

peptidomimetic antagonist against the SARS-CoV-2 (2019-nCoV, COVID-19) coronavirus. *Computers in biology and medicine,* **119**, pp. 103670.

142. TANG, T., BIDON, M., JAIMES, J.A., WHITTAKER, G.R. and DANIEL, S., 2020. Coronavirus membrane fusion mechanism offers a potential target for antiviral development. *Antiviral Research,* **178**, pp. 104792.

143. XIA, S., XU, W., WANG, Q., WANG, C., HUA, C., LI, W., LU, L. and JIANG, S., 2018. Peptide-Based Membrane Fusion Inhibitors Targeting HCoV-229E Spike Protein HR1 and HR2 Domains. *International journal of molecular sciences,* **19**(2), pp. 10.3390/ijms19020487.

144. COUTARD, B., VALLE, C., DE LAMBALLERIE, X., CANARD, B., SEIDAH, N.G. and DECROLY, E., 2020. The spike glycoprotein of the new coronavirus 2019-nCoV contains a furin-like cleavage site absent in CoV of the same clade. *Antiviral Research,* **176**, pp. 104742.

145. ANDERSEN, K.G., RAMBAUT, A., LIPKIN, W.I., HOLMES, E.C. and GARRY, R.F., 2020. The proximal origin of SARS-CoV-2. *Nature medicine,* **26**(4), pp. 450-452.

146. HAMMING, I., TIMENS, W., BULTHUIS, M.L., LELY, A.T., NAVIS, G. and VAN GOOR, H., 2004. Tissue distribution of ACE2 protein, the functional receptor for SARS coronavirus. A first step in understanding SARS pathogenesis. *The Journal of pathology,* **203**(2), pp. 631-637.

147. DONOGHUE, M., HSIEH, F., BARONAS, E., GODBOUT, K., GOSSELIN, M., STAGLIANO, N., DONOVAN, M., WOOLF, B., ROBISON, K., JEYASEELAN, R., BREITBART, R.E. and ACTON, S., 2000. A novel angiotensin-converting enzyme-related carboxypeptidase (ACE2) converts angiotensin I to angiotensin 1-9. *Circulation research,* **87**(5), pp. E1-9.

148. RIORDAN, J.F., 2003. Angiotensin-I-converting enzyme and its relatives. *Genome biology,* **4**(8), pp. 225-2003-4-8-225. Epub 2003 Jul 25.

149. KUBA, K., IMAI, Y., OHTO-NAKANISHI, T. and PENNINGER, J.M., 2010. Trilogy of ACE2: a peptidase in the renin-angiotensin system, a SARS receptor, and a partner for amino acid transporters. *Pharmacology & therapeutics,* **128**(1), pp. 119-128.

150. TIKELLIS, C. and THOMAS, M.C., 2012. Angiotensin-Converting Enzyme 2 (ACE2) Is a Key Modulator of the Renin Angiotensin System in Health and Disease. *International journal of peptides,* **2012**, pp. 256294.

151. KSIAZEK, T.G., ERDMAN, D., GOLDSMITH, C.S., ZAKI, S.R., PERET, T., EMERY, S., TONG, S., URBANI, C., COMER, J.A., LIM, W., ROLLIN, P.E., DOWELL, S.F., LING, A.E., HUMPHREY, C.D., SHIEH, W.J., GUARNER, J., PADDOCK, C.D., ROTA, P., FIELDS, B., DERISI, J., YANG, J.Y., COX, N., HUGHES, J.M., LEDUC, J.W., BELLINI, W.J., ANDERSON, L.J. and SARS WORKING GROUP, 2003. A novel coronavirus associated with severe acute respiratory syndrome. *The New England journal of medicine,* **348**(20), pp. 1953-1966.

152. HARMER, D., GILBERT, M., BORMAN, R. and CLARK, K.L., 2002. Quantitative mRNA expression profiling of ACE 2, a novel homologue of angiotensin converting enzyme. *FEBS letters,* **532**(1-2), pp. 107-110.

153. LEUNG, W.K., TO, K.F., CHAN, P.K., CHAN, H.L., WU, A.K., LEE, N., YUEN, K.Y. and SUNG, J.J., 2003. Enteric involvement of severe acute respiratory syndrome-associated coronavirus infection. *Gastroenterology,* **125**(4), pp. 1011-1017.

154. REGAD, T., 2015. Targeting RTK Signaling Pathways in Cancer. *Cancers,* **7**(3), pp. 1758-1784.

155. SIGISMUND, S., CONFALONIERI, S., CILIBERTO, A., POLO, S., SCITA, G. and DI FIORE, P.P., 2012. Endocytosis and signaling: cell logistics shape the eukaryotic cell plan. *Physiological Reviews,* **92**(1), pp. 273-366.

156. SORKIN, A. and GOH, L.K., 2009. Endocytosis and intracellular trafficking of ErbBs. *Experimental cell research,* **315**(4), pp. 683-696.

157. MISHRA, R., HANKER, A.B. and GARRETT, J.T., 2017. Genomic alterations of ERBB receptors in cancer: clinical implications. *Oncotarget,* **8**(69), pp. 114371-114392.

158. HERBST, R.S., 2004. Review of epidermal growth factor receptor biology. *International journal of radiation oncology, biology, physics,* **59**(2 Suppl), pp. 21-26.

159. ROWINSKY, E.K., 2004. The erbB family: targets for therapeutic development against cancer and therapeutic strategies using monoclonal antibodies and tyrosine kinase inhibitors. *Annual Review of Medicine,* **55**, pp. 433-457.

160. GSCHWIND, A., FISCHER, O.M. and ULLRICH, A., 2004. The discovery of receptor tyrosine kinases: targets for cancer therapy. *Nature reviews.Cancer,* **4**(5), pp. 361-370.

161. SANTARIUS, T., SHIPLEY, J., BREWER, D., STRATTON, M.R. and COOPER, C.S., 2010. A census of amplified and overexpressed human cancer genes. *Nature reviews.Cancer,* **10**(1), pp. 59-64.

162. RAKHA, E.A., REIS-FILHO, J.S. and ELLIS, I.O., 2008. Basal-like breast cancer: a critical review. *Journal of clinical oncology : official journal of the American Society of Clinical Oncology,* **26**(15), pp. 2568-2581.

163. ROEPSTORFF, K., GRANDAL, M.V., HENRIKSEN, L., KNUDSEN, S.L., LERDRUP, M., GROVDAL, L., WILLUMSEN, B.M. and VAN DEURS, B., 2009. Differential effects of EGFR ligands on endocytic sorting of the receptor. *Traffic (Copenhagen, Denmark),* **10**(8), pp. 1115-1127.

164. MOSESSON, Y., MILLS, G.B. and YARDEN, Y., 2008. Derailed endocytosis: an emerging feature of cancer. *Nature reviews.Cancer,* **8**(11), pp. 835-850.

165. TOMAS, A., FUTTER, C.E. and EDEN, E.R., 2014. EGF receptor trafficking: consequences for signaling and cancer. *Trends in cell biology,* **24**(1), pp. 26-34.

166. CHUNG, B.M., TOM, E., ZUTSHI, N., BIELECKI, T.A., BAND, V. and BAND, H., 2014. Nexus of signaling and endocytosis in oncogenesis driven by non-small cell lung cancer-associated epidermal growth factor receptor mutants. *World journal of clinical oncology,* **5**(5), pp. 806-823.

167. MOHAPATRA, B., AHMAD, G., NADEAU, S., ZUTSHI, N., AN, W., SCHEFFE, S., DONG, L., FENG, D., GOETZ, B., ARYA, P., BAILEY, T.A., PALERMO, N., BORGSTAHL, G.E., NATARAJAN, A., RAJA, S.M., NARAMURA, M., BAND, V. and BAND, H., 2013. Protein tyrosine kinase regulation by ubiquitination: critical roles of Cbl-family ubiquitin ligases. *Biochimica et biophysica acta,* **1833**(1), pp. 122-139.

168. NADEAU, S.A., AN, W., MOHAPATRA, B.C., MUSHTAQ, I., BIELECKI, T.A., LUAN, H., ZUTSHI, N., AHMAD, G., STORCK, M.D., SANADA, M., OGAWA, S., BAND, V. and BAND, H., 2017. Structural Determinants of the Gain-of-Function Phenotype of Human Leukemia-associated Mutant CBL Oncogene. *The Journal of biological chemistry,* **292**(9), pp. 3666-3682.

169. WATERMAN, H., SABANAI, I., GEIGER, B. and YARDEN, Y., 1998. Alternative intracellular routing of ErbB receptors may determine signaling potency. *The Journal of biological chemistry,* **273**(22), pp. 13819-13827.

170. WILEY, H.S., 2003. Trafficking of the ErbB receptors and its influence on signaling. *Experimental cell research,* **284**(1), pp. 78-88.

171. HERBST, J.J., OPRESKO, L.K., WALSH, B.J., LAUFFENBURGER, D.A. and WILEY, H.S., 1994. Regulation of postendocytic trafficking of the epidermal growth factor receptor through endosomal retention. *The Journal of biological chemistry,* **269**(17), pp. 12865-12873.

172. GOMEZ, T.S., GORMAN, J.A., DE NARVAJAS, A.A., KOENIG, A.O. and BILLADEAU, D.D., 2012. Trafficking defects in WASH-knockout fibroblasts originate from collapsed endosomal and lysosomal networks. *Molecular biology of the cell,* **23**(16), pp. 3215-3228.

173. SEAMAN, M.N., GAUTREAU, A. and BILLADEAU, D.D., 2013. Retromer-mediated endosomal protein sorting: all WASHed up! *Trends in cell biology,* **23**(11), pp. 522-528.

174. GULLAPALLI, A., GARRETT, T.A., PAING, M.M., GRIFFIN, C.T., YANG, Y. and TREJO, J., 2004. A role for sorting nexin 2 in epidermal growth factor receptor down-regulation: evidence for distinct functions of sorting nexin 1 and 2 in protein trafficking. *Molecular biology of the cell,* **15**(5), pp. 2143-2155.

175. CAPLAN, S., NASLAVSKY, N., HARTNELL, L.M., LODGE, R., POLISHCHUK, R.S., DONALDSON, J.G. and BONIFACINO, J.S., 2002. A tubular EHD1-containing compartment involved in the recycling of major histocompatibility

complex class I molecules to the plasma membrane. *The EMBO journal,* **21**(11), pp. 2557-2567.

176. BRAUN, A., PINYOL, R., DAHLHAUS, R., KOCH, D., FONAREV, P., GRANT, B.D., KESSELS, M.M. and QUALMANN, B., 2005. EHD proteins associate with syndapin I and II and such interactions play a crucial role in endosomal recycling. *Molecular biology of the cell,* **16**(8), pp. 3642-3658.

177. NASLAVSKY, N., MCKENZIE, J., ALTAN-BONNET, N., SHEFF, D. and CAPLAN, S., 2009. EHD3 regulates early-endosome-to-Golgi transport and preserves Golgi morphology. *Journal of cell science,* **122**(Pt 3), pp. 389-400.

178. PHILIPPIDOU, P., VALDEZ, G., AKMENTIN, W., BOWERS, W.J., FEDEROFF, H.J. and HALEGOUA, S., 2011. Trk retrograde signaling requires persistent, Pincher-directed endosomes. *Proceedings of the National Academy of Sciences of the United States of America,* **108**(2), pp. 852-857.

179. GUILHERME, A., SORIANO, N.A., FURCINITTI, P.S. and CZECH, M.P., 2004. Role of EHD1 and EHBP1 in perinuclear sorting and insulin-regulated GLUT4 recycling in 3T3-L1 adipocytes. *The Journal of biological chemistry,* **279**(38), pp. 40062-40075.

180. GUDMUNDSSON, H., HUND, T.J., WRIGHT, P.J., KLINE, C.F., SNYDER, J.S., QIAN, L., KOVAL, O.M., CUNHA, S.R., GEORGE, M., RAINEY, M.A., KASHEF, F.E., DUN, W., BOYDEN, P.A., ANDERSON, M.E., BAND, H. and MOHLER, P.J., 2010. EH domain proteins regulate cardiac membrane protein targeting. *Circulation research,* **107**(1), pp. 84-95.

181. CURRAN, J., MUSA, H., KLINE, C.F., MAKARA, M.A., LITTLE, S.C., HIGGINS, J.D., HUND, T.J., BAND, H. and MOHLER, P.J., 2015. Eps15 Homology Domain-containing Protein 3 Regulates Cardiac T-type Ca2+ Channel Targeting and Function in the Atria. *The Journal of biological chemistry,* **290**(19), pp. 12210-12221.

182. POSEY, A.D.,Jr, PYTEL, P., GARDIKIOTES, K., DEMONBREUN, A.R., RAINEY, M., GEORGE, M., BAND, H. and MCNALLY, E.M., 2011. Endocytic recycling proteins EHD1 and EHD2 interact with fer-1-like-5 (Fer1L5) and mediate myoblast fusion. *The Journal of biological chemistry,* **286**(9), pp. 7379-7388.

183. POSEY, A.D.,Jr, SWANSON, K.E., ALVAREZ, M.G., KRISHNAN, S., EARLEY, J.U., BAND, H., PYTEL, P., MCNALLY, E.M. and DEMONBREUN, A.R., 2014. EHD1 mediates vesicle trafficking required for normal muscle growth and transverse tubule development. *Developmental biology,* **387**(2), pp. 179-190.

184. CYPHER, L.R., BIELECKI, T.A., HUANG, L., AN, W., ISEKA, F., TOM, E., STORCK, M.D., HOPPE, A.D., BAND, V. and BAND, H., 2016. Corrigendum to CSF-1 receptor signalling is governed by pre-requisite EHD1 mediated receptor display on the macrophage cell surface [Cell Signalling 2016 Sep.; 28(9): 1325-35. *Cellular signalling,* **28**(12), pp. 1933.

185. CHUNG, B.M., RAJA, S.M., CLUBB, R.J., TU, C., GEORGE, M., BAND, V. and BAND, H., 2009. Aberrant trafficking of NSCLC-associated EGFR mutants through the endocytic recycling pathway promotes interaction with Src. *BMC cell biology,* **10**, pp. 84-2121-10-84.

186. LU, H., MENG, Q., WEN, Y., HU, J., ZHAO, Y. and CAI, L., 2013. Increased EHD1 in non-small cell lung cancer predicts poor survival. *Thoracic cancer,* **4**(4), pp. 422-432.

187. GAO, Y., WANG, Y., SUN, L., MENG, Q., CAI, L. and DONG, X., 2014. Expression of TGFbeta-1 and EHD1 correlated with survival of non-small cell lung cancer. *Tumour biology : the journal of the International Society for Oncodevelopmental Biology and Medicine,* **35**(9), pp. 9371-9380.

188. TONG, D., LIANG, Y.N., STEPANOVA, A.A., LIU, Y., LI, X., WANG, L., ZHANG, F. and VASILYEVA, N.V., 2017. Increased Eps15 homology domain 1 and RAB11FIP3 expression regulate breast cancer progression via promoting epithelial growth factor receptor recycling. *Tumour biology : the journal of the International Society for Oncodevelopmental Biology and Medicine,* **39**(2), pp. 1010428317691010.

189. LIU, Y., LIANG, Y., LI, M., LIU, D., TANG, J., YANG, W., TONG, D. and JIN, X., 2018. Eps15 homology domain 1 promotes the evolution of papillary thyroid cancer by regulating endocytotic recycling of epidermal growth factor receptor. *Oncology letters,* **16**(4), pp. 4263-4270.

190. WANG, X., YIN, H., ZHANG, H., HU, J., LU, H., LI, C., CAO, M., YAN, S. and CAI, L., 2018. NF-kappaB-driven improvement of EHD1 contributes to erlotinib resistance in EGFR-mutant lung cancers. *Cell death & disease,* **9**(4), pp. 418-018-0447-7.

191. AMESSOU, M., EBRAHIM, A.S., DILLY, A., JOSEPH, M., TABOLINA, M., CHUKKAPALLI, S., MEROUEH, L., SYED, J.T., LIDDANE, A., LANG, S.L., AL-KATIB, A. and KANDOUZ, M., 2016. Spatio-temporal regulation of EGFR signaling by the Eps15 homology domain-containing protein 3 (EHD3). *Oncotarget,* **7**(48), pp. 79203-79216.

192. CHUKKAPALLI, S., AMESSOU, M., DEKHIL, H., DILLY, A.K., LIU, Q., BANDYOPADHYAY, S., THOMAS, R.D., BEJNA, A., BATIST, G. and KANDOUZ, M., 2014. Ehd3, a regulator of vesicular trafficking, is silenced in gliomas and functions as a tumor suppressor by controlling cell cycle arrest and apoptosis. *Carcinogenesis,* **35**(4), pp. 877-885.

193. BAYER, M., FISCHER, J., KREMERSKOTHEN, J., OSSENDORF, E., MATANIS, T., KONCZAL, M., WEIDE, T. and BARNEKOW, A., 2005. Identification and characterization of Iporin as a novel interaction partner for rab1. *BMC cell biology,* **6**(1), pp. 15-2121-6-15.

194. FUKUDA, M., KOBAYASHI, H., ISHIBASHI, K. and OHBAYASHI, N., 2011. Genome-wide investigation of the Rab binding activity of RUN domains: development of

a novel tool that specifically traps GTP-Rab35. *Cell structure and function,* **36**(2), pp. 155-170.

195. DERIBE, Y.L., WILD, P., CHANDRASHAKER, A., CURAK, J., SCHMIDT, M.H.H., KALAIDZIDIS, Y., MILUTINOVIC, N., KRATCHMAROVA, I., BUERKLE, L., FETCHKO, M.J., SCHMIDT, P., KITTANAKOM, S., BROWN, K.R., JURISICA, I., BLAGOEV, B., ZERIAL, M., STAGLJAR, I. and DIKIC, I., 2009. Regulation of epidermal growth factor receptor trafficking by lysine deacetylase HDAC6. *Science signaling,* **2**(102), pp. ra84.

196. BAND, V. and SAGER, R., 1989. Distinctive traits of normal and tumor-derived human mammary epithelial cells expressed in a medium that supports long-term growth of both cell types. *Proceedings of the National Academy of Sciences of the United States of America,* **86**(4), pp. 1249-1253.

197. BHATTACHARYYA, S., RAINEY, M.A., ARYA, P., MOHAPATRA, B.C., MUSHTAQ, I., DUTTA, S., GEORGE, M., STORCK, M.D., MCCOMB, R.D., MUIRHEAD, D., TODD, G.L., GOULD, K., DATTA, K., GELINEAU-VAN WAES, J., BAND, V. and BAND, H., 2016. Endocytic recycling protein EHD1 regulates primary cilia morphogenesis and SHH signaling during neural tube development. *Scientific reports,* **6**, pp. 20727.

198. ZHAO, X., GOSWAMI, M., POKHRIYAL, N., MA, H., DU, H., YAO, J., VICTOR, T.A., POLYAK, K., STURGIS, C.D., BAND, H. and BAND, V., 2008. Cyclooxygenase-2 expression during immortalization and breast cancer progression. *Cancer research,* **68**(2), pp. 467-475.

199. AHMAD, G., MOHAPATRA, B.C., SCHULTE, N.A., NADEAU, S.A., LUAN, H., ZUTSHI, N., TOM, E., ORTEGA-CAVA, C., TU, C., SANADA, M., OGAWA, S., TOEWS, M.L., BAND, V. and BAND, H., 2014. Cbl-family ubiquitin ligases and their recruitment of CIN85 are largely dispensable for epidermal growth factor receptor endocytosis. *The international journal of biochemistry & cell biology,* **57**, pp. 123-134.

200. GOH, L.K., HUANG, F., KIM, W., GYGI, S. and SORKIN, A., 2010. Multiple mechanisms collectively regulate clathrin-mediated endocytosis of the epidermal growth factor receptor. *The Journal of cell biology,* **189**(5), pp. 871-883.

201. FUKAZAWA, T., MIYAKE, S., BAND, V. and BAND, H., 1996. Tyrosine phosphorylation of Cbl upon epidermal growth factor (EGF) stimulation and its association with EGF receptor and downstream signaling proteins. *The Journal of biological chemistry,* **271**(24), pp. 14554-14559.

202. DUAN, L., MIURA, Y., DIMRI, M., MAJUMDER, B., DODGE, I.L., REDDI, A.L., GHOSH, A., FERNANDES, N., ZHOU, P., MULLANE-ROBINSON, K., RAO, N., DONOGHUE, S., ROGERS, R.A., BOWTELL, D., NARAMURA, M., GU, H., BAND, V. and BAND, H., 2003. Cbl-mediated ubiquitinylation is required for lysosomal sorting of epidermal growth factor receptor but is dispensable for endocytosis. *The Journal of biological chemistry,* **278**(31), pp. 28950-28960.

203. DUAN, L., CHEN, G., VIRMANI, S., YING, G., RAJA, S.M., CHUNG, B.M., RAINEY, M.A., DIMRI, M., ORTEGA-CAVA, C.F., ZHAO, X., CLUBB, R.J., TU, C., REDDI, A.L., NARAMURA, M., BAND, V. and BAND, H., 2010. Distinct roles for Rho versus Rac/Cdc42 GTPases downstream of Vav2 in regulating mammary epithelial acinar architecture. *The Journal of biological chemistry,* **285**(2), pp. 1555-1568.

204. DIMRI, M., NARAMURA, M., DUAN, L., CHEN, J., ORTEGA-CAVA, C., CHEN, G., GOSWAMI, R., FERNANDES, N., GAO, Q., DIMRI, G.P., BAND, V. and BAND, H., 2007. Modeling breast cancer-associated c-Src and EGFR overexpression in human MECs: c-Src and EGFR cooperatively promote aberrant three-dimensional acinar structure and invasive behavior. *Cancer research,* **67**(9), pp. 4164-4172.

205. DUAN, L., RAJA, S.M., CHEN, G., VIRMANI, S., WILLIAMS, S.H., CLUBB, R.J., MUKHOPADHYAY, C., RAINEY, M.A., YING, G., DIMRI, M., CHEN, J., REDDI, A.L., NARAMURA, M., BAND, V. and BAND, H., 2011. Negative regulation of EGFR-Vav2 signaling axis by Cbl ubiquitin ligase controls EGF receptor-mediated epithelial cell adherens junction dynamics and cell migration. *The Journal of biological chemistry,* **286**(1), pp. 620-633.

206. ALEXANDER, A., 1998. Endocytosis and intracellular sorting of receptor tyrosine kinases. *Frontiers in bioscience : a journal and virtual library,* **3**, pp. d729-38.

207. BARZILAY, E., BEN-CALIFA, N., HIRSCHBERG, K. and NEUMANN, D., 2005. Uncoupling of brefeldin a-mediated coatomer protein complex-I dissociation from Golgi redistribution. *Traffic (Copenhagen, Denmark),* **6**(9), pp. 794-802.

208. JOHNS, T.G., MELLMAN, I., CARTWRIGHT, G.A., RITTER, G., OLD, L.J., BURGESS, A.W. and SCOTT, A.M., 2005. The antitumor monoclonal antibody 806 recognizes a high-mannose form of the EGF receptor that reaches the cell surface when cells over-express the receptor. *FASEB journal : official publication of the Federation of American Societies for Experimental Biology,* **19**(7), pp. 780-782.

209. FRANOVIC, A., GUNARATNAM, L., SMITH, K., ROBERT, I., PATTEN, D. and LEE, S., 2007. Translational up-regulation of the EGFR by tumor hypoxia provides a nonmutational explanation for its overexpression in human cancer. *Proceedings of the National Academy of Sciences of the United States of America,* **104**(32), pp. 13092-13097.

210. GAMOU, S. and SHIMIZU, N., 1987. Change in metabolic turnover is an alternate mechanism increasing cell surface epidermal growth factor receptor levels in tumor cells. *The Journal of biological chemistry,* **262**(14), pp. 6708-6713.

211. WANG, Y.N., WANG, H., YAMAGUCHI, H., LEE, H.J., LEE, H.H. and HUNG, M.C., 2010. COPI-mediated retrograde trafficking from the Golgi to the ER regulates EGFR nuclear transport. *Biochemical and biophysical research communications,* **399**(4), pp. 498-504.

212. CALHOUN, B.C. and GOLDENRING, J.R., 1996. Rab proteins in gastric parietal cells: evidence for the membrane recycling hypothesis. *The Yale journal of biology and medicine,* **69**(1), pp. 1-8.

213. ALLAN, B.B., MOYER, B.D. and BALCH, W.E., 2000. Rab1 recruitment of p115 into a cis-SNARE complex: programming budding COPII vesicles for fusion. *Science (New York, N.Y.),* **289**(5478), pp. 444-448.

214. MUKHOPADHYAY, A., QUIROZ, J.A. and WOLKOFF, A.W., 2014. Rab1a regulates sorting of early endocytic vesicles. *American journal of physiology.Gastrointestinal and liver physiology,* **306**(5), pp. G412-24.

215. HYNES, N.E. and LANE, H.A., 2005. ERBB receptors and cancer: the complexity of targeted inhibitors. *Nature reviews.Cancer,* **5**(5), pp. 341-354.

216. SCOTT, C.C., VACCA, F. and GRUENBERG, J., 2014. Endosome maturation, transport and functions. *Seminars in cell & developmental biology,* **31**, pp. 2-10.

217. ISEKA, F.M., GOETZ, B.T., MUSHTAQ, I., AN, W., CYPHER, L.R., BIELECKI, T.A., TOM, E.C., ARYA, P., BHATTACHARYYA, S., STORCK, M.D., SEMERAD, C.L., TALMADGE, J.E., MOSLEY, R.L., BAND, V. and BAND, H., 2018. Role of the EHD Family of Endocytic Recycling Regulators for TCR Recycling and T Cell Function. *Journal of immunology (Baltimore, Md.: 1950),* **200**(2), pp. 483-499.

218. SENGUPTA, S., GEORGE, M., MILLER, K.K., NAIK, K., CHOU, J., CHEATHAM, M.A., DALLOS, P., NARAMURA, M., BAND, H. and ZHENG, J., 2009. EHD4 and CDH23 are interacting partners in cochlear hair cells. *The Journal of biological chemistry,* **284**(30), pp. 20121-20129.

219. MACDONALD, J.I., DIETRICH, A., GAMBLE, S., HRYCIW, T., GRANT, R.I. and MEAKIN, S.O., 2012. Nesca, a novel neuronal adapter protein, links the molecular motor kinesin with the pre-synaptic membrane protein, syntaxin-1, in hippocampal neurons. *Journal of neurochemistry,* **121**(6), pp. 861-880.

220. SHARMA, M., GIRIDHARAN, S.S., RAHAJENG, J., NASLAVSKY, N. and CAPLAN, S., 2009. MICAL-L1 links EHD1 to tubular recycling endosomes and regulates receptor recycling. *Molecular biology of the cell,* **20**(24), pp. 5181-5194.

221. WEI, J.H., ZHANG, Z.C., WYNN, R.M. and SEEMANN, J., 2015. GM130 Regulates Golgi-Derived Spindle Assembly by Activating TPX2 and Capturing Microtubules. *Cell,* **162**(2), pp. 287-299.

222. RAHAJENG, J., CAPLAN, S. and NASLAVSKY, N., 2010. Common and distinct roles for the binding partners Rabenosyn-5 and Vps45 in the regulation of endocytic trafficking in mammalian cells. *Experimental cell research,* **316**(5), pp. 859-874.

223. JING, J., JUNUTULA, J.R., WU, C., BURDEN, J., MATERN, H., PEDEN, A.A. and PREKERIS, R., 2010. FIP1/RCP binding to Golgin-97 regulates retrograde transport from recycling endosomes to the trans-Golgi network. *Molecular biology of the cell,* **21**(17), pp. 3041-3053.

224. ONNIS, A., FINETTI, F., PATRUSSI, L., GOTTARDO, M., CASSIOLI, C., SPANO, S. and BALDARI, C.T., 2015. The small GTPase Rab29 is a common regulator of immune synapse assembly and ciliogenesis. *Cell death and differentiation,* **22**(10), pp. 1687-1699.

225. REINECKE, J.B., KATAFIASZ, D., NASLAVSKY, N. and CAPLAN, S., 2015. Novel functions for the endocytic regulatory proteins MICAL-L1 and EHD1 in mitosis. *Traffic (Copenhagen, Denmark),* **16**(1), pp. 48-67.

226. REINECKE, J.B., KATAFIASZ, D., NASLAVSKY, N. and CAPLAN, S., 2014. Regulation of Src trafficking and activation by the endocytic regulatory proteins MICAL-L1 and EHD1. *Journal of cell science,* **127**(Pt 8), pp. 1684-1698.

227. BRASS, A.L., DYKXHOORN, D.M., BENITA, Y., YAN, N., ENGELMAN, A., XAVIER, R.J., LIEBERMAN, J. and ELLEDGE, S.J., 2008. Identification of host proteins required for HIV infection through a functional genomic screen. *Science (New York, N.Y.),* **319**(5865), pp. 921-926.

228. UNO, Y., 2020. Camostat mesilate therapy for COVID-19. *Internal and emergency medicine,* .

229. INOUE, Y., TANAKA, N., TANAKA, Y., INOUE, S., MORITA, K., ZHUANG, M., HATTORI, T. and SUGAMURA, K., 2007. Clathrin-dependent entry of severe acute respiratory syndrome coronavirus into target cells expressing ACE2 with the cytoplasmic tail deleted. *Journal of virology,* **81**(16), pp. 8722-8729.

230. RICHARDSON, P., GRIFFIN, I., TUCKER, C., SMITH, D., OECHSLE, O., PHELAN, A., RAWLING, M., SAVORY, E. and STEBBING, J., 2020. Baricitinib as potential treatment for 2019-nCoV acute respiratory disease. *Lancet (London, England),* **395**(10223), pp. e30-e31.

231. CHAN, K.K., DOROSKY, D., SHARMA, P., ABBASI, S.A., DYE, J.M., KRANZ, D.M., HERBERT, A.S. and PROCKO, E., 2020. Engineering human ACE2 to optimize binding to the spike protein of SARS coronavirus 2. *Science (New York, N.Y.),* **369**(6508), pp. 1261-1265.

232. WELLS, C., COUNAGO, R.M., LIMAS, J.C., ALMEIDA, T.L., COOK, J.G., DREWRY, D.H., ELKINS, J.M., GILEADI, O., KAPADIA, N.R., LORENTE-MACIAS, A., PICKETT, J.E., RIEMEN, A., RUELA-DE-SOUSA, R.R., WILLSON, T.M., ZHANG, C., ZUERCHER, W.J., ZUTSHI, R. and AXTMAN, A.D., 2019. SGC-AAK1-1: A Chemical Probe Targeting AAK1 and BMP2K. *ACS medicinal chemistry letters,* **11**(3), pp. 340-345.

233. WANG, P.G., TANG, D.J., HUA, Z., WANG, Z. and AN, J., 2020. Sunitinib reduces the infection of SARS-CoV, MERS-CoV and SARS-CoV-2 partially by inhibiting AP2M1 phosphorylation. *Cell discovery,* **6**, pp. 71-020-00217-2. eCollection 2020.

234. BAI, C., CHOTIRMALL, S.H., RELLO, J., ALBA, G.A., GINNS, L.C., KRISHNAN, J.A., ROGERS, R., BENDSTRUP, E., BURGEL, P.R., CHALMERS, J.D., CHUA, A., CROTHERS, K.A., DUGGAL, A., KIM, Y.W., LAFFEY, J.G., LUNA, C.M.,

NIEDERMAN, M.S., RAGHU, G., RAMIREZ, J.A., RIERA, J., ROCA, O., TAMAE-KAKAZU, M., TORRES, A., WATKINS, R.R., BARRECHEGUREN, M., BELLIATO, M., CHAMI, H.A., CHEN, R., CORTES-PUENTES, G.A., DELACRUZ, C., HAYES, M.M., HEUNKS, L.M.A., HOLETS, S.R., HOUGH, C.L., JAGPAL, S., JEON, K., JOHKOH, T., LEE, M.M., LIEBLER, J., MCELVANEY, G.N., MOSKOWITZ, A., OECKLER, R.A., OJANGUREN, I., O'REGAN, A., PLETZ, M.W., RHEE, C.K., SCHULTZ, M.J., STORTI, E., STRANGE, C., THOMSON, C.C., TORRIANI, F.J., WANG, X., WUYTS, W., XU, T., YANG, D., ZHANG, Z. and WILSON, K.C., 2020. Updated guidance on the management of COVID-19: from an American Thoracic Society/European Respiratory Society coordinated International Task Force (29 July 2020). *European respiratory review : an official journal of the European Respiratory Society,* **29**(157), pp. 10.1183/16000617.0287-2020. Print 2020 Sep 30.

235. PELKMANS, L. and HELENIUS, A., 2003. Insider information: what viruses tell us about endocytosis. *Current opinion in cell biology,* **15**(4), pp. 414-422.

236. YAMAUCHI, Y. and HELENIUS, A., 2013. Virus entry at a glance. *Journal of cell science,* **126**(Pt 6), pp. 1289-1295.

237. OWCZAREK, K., SZCZEPANSKI, A., MILEWSKA, A., BASTER, Z., RAJFUR, Z., SARNA, M. and PYRC, K., 2018. Early events during human coronavirus OC43 entry to the cell. *Scientific reports,* **8**(1), pp. 7124-018-25640-0.

238. BAYATI, A., KUMAR, R., FRANCIS, V. and MCPHERSON, P.S., 2021. SARS-CoV-2 infects cells following viral entry via clathrin-mediated endocytosis. *The Journal of biological chemistry,* , pp. 100306.

239. DANILOSKI, Z., JORDAN, T.X., WESSELS, H.H., HOAGLAND, D.A., KASELA, S., LEGUT, M., MANIATIS, S., MIMITOU, E.P., LU, L., GELLER, E., DANZIGER, O., ROSENBERG, B.R., PHATNANI, H., SMIBERT, P., LAPPALAINEN, T., TENOEVER, B.R. and SANJANA, N.E., 2021. Identification of Required Host Factors for SARS-CoV-2 Infection in Human Cells. *Cell,* **184**(1), pp. 92-105.e16.

240. LUPBERGER, J., ZEISEL, M.B., XIAO, F., THUMANN, C., FOFANA, I., ZONA, L., DAVIS, C., MEE, C.J., TUREK, M., GORKE, S., ROYER, C., FISCHER, B., ZAHID, M.N., LAVILLETTE, D., FRESQUET, J., COSSET, F.L., ROTHENBERG, S.M., PIETSCHMANN, T., PATEL, A.H., PESSAUX, P., DOFFOEL, M., RAFFELSBERGER, W., POCH, O., MCKEATING, J.A., BRINO, L. and BAUMERT, T.F., 2011. EGFR and EphA2 are host factors for hepatitis C virus entry and possible targets for antiviral therapy. *Nature medicine,* **17**(5), pp. 589-595.

241. WEISBERG, E., PARENT, A., YANG, P.L., SATTLER, M., LIU, Q., LIU, Q., WANG, J., MENG, C., BUHRLAGE, S.J., GRAY, N. and GRIFFIN, J.D., 2020. Repurposing of Kinase Inhibitors for Treatment of COVID-19. *Pharmaceutical research,* **37**(9), pp. 167-020-02851-7.